TURUN
YLIOPISTO
UNIVERSITY
OF TURKU

BIOMECHANICS OF CANCER CELL MOTILITY

Aleksi Isomursu

TURUN YLIOPISTON JULKAISUJA – ANNALES UNIVERSITATIS TURKUENSIS
SARJA – SER. F OSA – TOM. 37 | TECHNICA – INFORMATICA | TURKU 2024

TURUN
YLIOPISTO
UNIVERSITY
OF TURKU

BIOMECHANICS OF CANCER CELL MOTILITY

Aleksi Isomursu

TURUN YLIOPISTON JULKAISUJA – ANNALES UNIVERSITATIS TURKUENSIS
SARJA – SER. F OSA – TOM. 37 | TECHNICA – INFORMATICA | TURKU 2024

University of Turku

Faculty of Technology
Department of Life Technologies
Biochemistry
Doctoral Programme in Technology

Supervised by

Professor Johanna Ivaska, PhD
Turku Bioscience Center
University of Turku and Åbo Akademi
Turku, Finland

Camilo Guzmán, PhD
Euro-BioImaging ERIC
Turku, Finland

Reviewed by

Anna Taubenberger, PhD
Center for Molecular and
Cellular Bioengineering
Dresden University of Technology
Dresden, Germany

Docent Teemu Ihalainen, PhD
Faculty of Medicine and
Health Technology
Tampere University
Tampere, Finland

Opponent

Professor Adam J. Engler, PhD
Department of Bioengineering
University of California
San Diego, La Jolla, CA, USA

The originality of this publication has been checked in accordance with the University of Turku quality assurance system using the Turnitin OriginalityCheck service.

ISBN 978-951-29-9672-8 (PRINT)
ISBN 978-951-29-9673-5 (PDF)
ISSN 2736-9390 (Print)
ISSN 2736-9684 (Online)
Painosalama, Turku, Finland 2024

To my family and friends

UNIVERSITY OF TURKU
Faculty of Technology
Department of Life Technologies
Biochemistry
ALEKSI ISOMURSU: Biomechanics of Cancer Cell Motility
Doctoral Dissertation, 243 pp.
Doctoral Programme in Technology
April 2024

ABSTRACT

Metastatic cancer is a devastating disease and an unmet clinical need. The local invasion and colonization of distant organs by cancer cells are both dependent on cell migration, a conserved cellular process that allows eukaryotic cells to traverse complex tissue microenvironments. This is achieved by dynamic regulation of the intracellular cytoskeleton and varying degrees of adhesion between cells and the extracellular milieu. Integrins are dimeric transmembrane receptors and the main cell adhesion molecules responsible for mediating interactions between cells and the extracellular matrix (ECM). They transmit cytoskeletal forces to the ECM, facilitating cell migration and ECM remodeling, and simultaneously inform the cell of the molecular composition and biomechanical properties of the local microenvironment. Malignant tumors are characterized by aberrant ECM architecture and other physical traits that differ markedly from healthy tissues. Tissue biomechanics can influence most cellular processes, including migration, but many of the underlying mechanisms are still inadequately understood.

This thesis provides new insights into the direct and indirect mechanisms that contribute to the biomechanical regulation of cancer cell motility. New tools for preparing cell culture substrates with stiffness gradients or dynamic micropatterns were established and used to investigate mechanically directed cell migration, cell polarization in response to local ECM geometry, and mechanosensitivity of ECM-remodeling adhesions. We found that the growth of fibrillar adhesions (FB), integrin adhesion complexes (IAC) responsible for fibronectin fibrillogenesis, is directly responsive to substrate stiffness. Further, we observed for the first time that human glioblastoma cells can migrate preferentially toward more compliant environments. This behavior, and the conventional positive durotaxis in other adherent cells, was explained by the molecular clutch model of cell adhesion. Finally, we found that cell front-rear polarization on anisotropic micropatterns is dependent on the biochemical composition of the substrate, impacting migration when the cells are released on fibronectin. Taken together, the results presented here improve our understanding of the different biomechanical cues that regulate and guide the movement of human cells. They also provide technological advancements for studying various aspects of cancer mechanobiology.

KEYWORDS: cancer, cell migration, cell polarity, mechanobiology, integrin, extracellular matrix, cytoskeleton, durotaxis, micropatterning

TURUN YLIOPISTO
Teknillinen tiedekunta
Bioteknologian laitos
Biokemia
ALEKSI ISOMURSU: Syöpäsolujen liikkeen biomekaniikka
Väitöskirja, 243 s.
Teknologian tohtoriohjelma
Huhtikuu 2024

TIIVISTELMÄ

Metastaattinen syöpä on tappava tauti, ja siihen käytettävissä olevat hoitokeinot ovat edelleen rajalliset. Syöpäsolujen paikallinen leviäminen ja etäpesäkkeiden lähettäminen terveisiin kudoksiin ovat molemmat riippuvaisia solumigraatiosta, solujen kyvystä liikkua erilaisissa monimutkaisissa mikroympäristöissä. Solujen liikettä edistävät sekä solunsisäisen tukirangan dynaaminen säätely että solujen tarttuminen toisiin soluihin ja ympäröivään soluväliaineeseen. Integriinit ovat dimeerisiä solukalvoreseptoreja, ja ne ovat päävastuussa solujen ja soluväliaineen välisistä suorista vuorovaikutuksista. Reseptorit välittävät solun tukirangan tuottamia voimia soluväliaineeseen, mikä edistää solujen liikkumista ja soluväliaineen muokkausta. Samalla solut saavat tietoa paikallisen mikroympäristön biokemiallisista ja mekaanisista ominaisuuksista. Pahanlaatuisten kasvaimien sekä terveiden kudosten fysikaaliset ominaisuudet, esimerkiksi soluväliaineen rakenne, poikkeavat usein huomattavasti toisistaan. Kudosten biomekaniikka puolestaan säätelee useimpia biologisia prosesseja, muun muassa solumigraatiota, mutta monet tähän liittyvistä molekyylitason mekanismeista tunnetaan vielä verrattain huonosti.

Tämä väitöskirja tarjoaa lisätietoa syöpäsolujen liikkeen biomekaaniseen säätelyyn liittyvistä suorista ja epäsuorista mekanismeista. Tutkimuksessa kehitettiin uusia tekniikoita erilaisten jäykkyysgradientteja tai dynaamisia mikrokuvioita sisältävien soluviljelyalustojen tuottamiseksi. Näitä menetelmiä käytettiin mekaanisesti ohjatun solumigraation, solujen polarisaation ja soluväliainetta muokkaavien adheesioiden tutkimiseen. Havaitsimme, että soluväliaineen muokkaamiseen osallistuvien fibrillaaristen adheesioiden kasvu on riippuvainen solun kasvuympäristön jäykkyydestä. Tulokset osoittavat myös, että tietyt ihmisen glioblastoomasolut voivat liikkua jäykistä ympäristöistä pehmeämpiä kohden. Tämä ilmiö sekä tavanomaisempi positiivinen durotaksis, solujen liike pehmeistä jäykkiin ympäristöihin, selittyvät molemmat niin sanotulla molekyylikytkinmallilla. Lopuksi havaitsimme, että solujen etu-takasuuntainen polarisaatio epäsymmetrisillä mikrokuvioilla on riippuvainen mikrokuvioiden biokemiallisesta koostumuksesta, mikä vaikuttaa myös solujen myöhempään migraatioon. Tulokset tarjoavat tärkeää lisätietoa solumigraation biomekaanikasta. Lisäksi uudet menetelmät soveltuvat hyvin myös muiden syövän mekanobiologiaan liittyvien mekanismien tutkimiseen.

ASIASANAT: syöpä, solumigraatio, solun polarisaatio, mekanobiologia, integriini, soluväliaine, solun tukiranka, durotaksis, mikrokuviointi

Table of Contents

Abbreviations

ABS	actin-binding site
AFM	atomic force microscopy
Arp2/3	actin-related protein 2/3
BCR	B cell antigen receptor
BM	basement membrane
BSA	bovine serum albumin
CAF	cancer-associated fibroblast
Cdc42	cell division control protein 42 homolog
CIL	contact inhibition of locomotion
CLASP	CLIP-associated protein
CMS	cell migration simulator
cryo-ET	cryo-electron tomography
DABCO	1,4-diazabicyclo[2.2.2]octane
DCIS	ductal carcinoma in situ
DMEM	Dulbecco's Modified Eagle's Medium
DOK1	docking protein 1
ECM	extracellular matrix
EdU	5-ethynyl-2′-deoxyuridine
EM	electron microscopy
EMT	epithelial-to-mesenchymal transition
ERK	extracellular signal-regulated kinase
EVL	Ena/VASP-like
FA	focal adhesion
F-actin	filamentous actin
FAK	focal adhesion kinase
FB	fibrillar adhesion
FBS	fetal bovine serum
FDA	Food and Drug Administration
FITC	fluorescein isothiocyanate
FMNL3	formin-like 3
FRET	Förster resonance energy transfer

GAP	GTPase-activating protein
GEF	guanine nucleotide exchange factor
GPCR	G protein-coupled receptor
HIC-5	hydrogen peroxide-inducible clone 5
HIF-1	hypoxia-inducible factor 1
IAC	integrin adhesion complex
IF	intermediate filament
ILK	integrin-linked kinase
KANK	KN motif and ankyrin repeat domains
LINC	linker of nucleoskeleton and cytoskeleton
LN-521	laminin-521
MDCK	Madin-Darby canine kidney
mDia	mammalian Diaphanous-related formin
MEF	mouse embryonic fibroblast
MFS	metastasis-free survival
MLC2	myosin light chain 2
MLCK	myosin light chain kinase
MMP	matrix metalloproteinase
MRTF	myocardin-related transcription factor
MSC	mesenchymal stem cell
MT	microtubule
MTOC	microtubule-organizing center
NA	nascent adhesion
NEAA	non-essential amino acid
Par6	partitioning-defective protein 6
PBS	phosphate-buffered saline
PDMS	polydimethylsiloxane
PEG	polyethylene glycol
PI3K	phosphoinositide 3-kinase
PIP_3	phosphatidylinositol-3,4,5-trisphosphate
PKCζ	protein kinase C zeta
PLL-g-PEG	polyethylene glycol-grafted poly-L-lysine
PTEN	phosphatase and tensin homolog
PyMT	polyoma middle T
Rac1	Ras-related C3 botulinum toxin substrate 1
RhoA	transforming protein RhoA
ROCK	Rho-associated protein kinase
RPE	retinal pigment epithelial
RPMI	Roswell Park Memorial Institute
RTK	receptor tyrosine kinase

SA-FN	streptavidin-fibronectin
SHARPIN	SHANK-associated RH domain-interacting protein
Src	proto-oncogene tyrosine-protein kinase Src
SRF	serum response factor
TAZ	transcriptional co-activator with PDZ-binding motif
TFM	traction force microscopy
TIF	telomerase-immortalized fibroblast
TIRF	total internal reflection fluorescence
UVO	ultraviolet-ozone
VASP	vasodilator-stimulated phosphoprotein
VEGF	vascular endothelial growth factor
YAP	yes-associated protein 1

List of Original Publications

This dissertation is based on the following original publications, which are referred to in the text by their Roman numerals:

I Barber-Pérez N.*, Georgiadou M.*, Guzmán C., Isomursu A., Hamidi H., and Ivaska J. Mechano-responsiveness of fibrillar adhesions on stiffness-gradient gels. *Journal of Cell Science*, 2020; 133(12): jcs242909.

II Isomursu A.*, Park K.-Y.*, Hou J.*, Cheng B.*, Mathieu M., Shamsan G.A., Fuller B., Kasim J., Mahmoodi M.M., Lu T.J. Genin G.M., Xu F., Lin M., Distefano M.D., Ivaska J., and Odde D.J. Directed cell migration towards softer environments. *Nature Materials*, 2022; 21(9): 1081-1090.

III Isomursu A., Alanko J., Hernández-Pérez S., Saukkonen K., Saari M., Mattila P.K., and Ivaska J. Dynamic micropatterning reveals substrate-dependent differences in the geometric control of cell polarization and migration. *Small Methods*, 2024; 8(1): e2300719.

*These authors contributed equally to this work.

1 Introduction

Cells are the fundamental units of life. Together with the surrounding extracellular matrix (ECM)—fibrous proteins and proteoglycans that act as a physical scaffold and serve other, more specialized functions—different cell types make up the various tissues and organs in the human body. It comes as no surprise that the embryonic development and homeostasis of any complex multicellular organism depends strictly on effective signaling and crosstalk between cells and the ECM. Different cells have to be in the right place, at the right time, and engaged in the right tasks. Disruption of this intricate spatiotemporal organization will typically result in severe pathological conditions, including cancer.

In order to fulfil their biological roles, such as immune surveillance or wound healing, cells are often required to move unassisted from one location to another. Cell migration is a conserved trait in eukaryotic cells, and cells can employ distinct phenotypic strategies to move around in heterogeneous tissue microenvironments. When these mechanisms are co-opted by malignant tumors, cancer cells can disseminate into adjacent tissues and colonize distant organs. The resulting metastatic cancer is a deadly systemic disease that is often difficult or even impossible to treat. Because of this, there is increasing clinical interest in preventing cancers from spreading in the first place. However, before we can hope to target cell migration for therapeutic purposes, we must first understand its molecular mechanisms.

Cell migration is driven primarily by the intracellular cytoskeleton. Actin microfilaments act as dynamic cellular “muscles” that can be assembled, disassembled, and contracted using myosin family motor proteins. This allows cells to exert pulling and pushing forces on the neighboring cells and the ECM, facilitating net forward movement. In addition, cells are often physically connected to their environment using different cell adhesion molecules. Integrins are the principal adhesion receptors mediating interactions between cells and the ECM, and they can play a pivotal role in cell migration. By clustering together and recruiting additional scaffold proteins and enzymes to the plasma membrane, integrins serve as a bidirectional signaling hub—in addition to transmitting cytoskeletal forces to the ECM, they inform the cell of the biochemical and physical properties of the

surrounding tissue. This information is conveyed to different intracellular signaling networks and ultimately to the nucleus, where it can elicit changes in gene expression to regulate survival, proliferation, cell identity, and more.

We have begun to appreciate that the altered cell mechanics and aberrant ECM deposition and remodeling in different solid tumors give rise to biophysical traits that are vastly different from the corresponding healthy tissues. Mechanical gradients and local tissue architecture can guide cell migration, but many of the mechanistic details behind these processes—and whether they can contribute to cancer invasion—remain poorly understood. The purpose of this thesis is to present new insights into the molecular mechanisms and players that regulate cancer cell motility in response to external biomechanical cues. To this end, I have established new reductionist tools for investigating cell behavior on stiffness gradients and under reversible spatial confinement. Further, I have combined these new techniques with stochastic modeling and optical imaging to study 1) the composition and mechanosensitivity of ECM-remodeling fibrillar adhesions (FB), 2) the molecular underpinnings of positive and negative durotaxis, and 3) the combined effect of ECM geometry and composition on cancer cell front-rear polarity and migration.

2 Review of the Literature

2.1 Invasion and metastasis—hallmarks of cancer

Cancer remains a major clinical, societal, and economic challenge. Globally, the five most common cancer types—breast, lung, colorectal, prostate, and stomach cancer—account for approximately 9 million new cases every year, and cause around 4.5 million deaths (Ferlay et al., 2021). A common denominator for all of these diseases is that they are solid tumors where the primary lesion is often curable with the current therapeutic options. In other words, localized cancer rarely kills the patient (Dillekås et al., 2019). It is after the cancer spreads that the prognosis can become grim.

Malignant tumors are defined by their uncontrolled growth and capacity to invade nearby tissues. Left unchecked, this process often results in the colonization of distant sites and organs. Metastatic cancer is a systemic disease that is notoriously deadly and difficult to treat due to a combination of continuous clonal selection, metabolic adaptations, progressive immune evasion and therapy resistance, and extraordinary phenotypic plasticity resulting from the co-option of different developmental and regenerative programs (Gerstberger et al., 2023). Thus, targeting the cellular processes that enable cancer cell motility and/or survival outside the original tumor microenvironment, to prevent the disease from spreading in the first place, would appear a promising therapeutic opportunity.

2.1.1 When cell migration kills

Activation of local invasion and metastasis is considered a core hallmark of cancer (Hanahan & Weinberg, 2011). The full metastatic cascade is a complex, multi-step process that typically involves tumor cell migration inside and out of the tumor microenvironment, hematogenous or lymphatic intravasation and entry into the circulation, transit to the site of metastasis, extravasation, and gradual formation of micro- and macrometastasis (Lambert et al., 2017) (Figure 1). Alternatively, cancer cells may spread considerable distances by migrating along established tissue tracks, such as the abluminal surfaces of blood vessels (known as extravascular migratory metastasis) or nerves (Liebig et al., 2009; Lugassy et al., 2020).

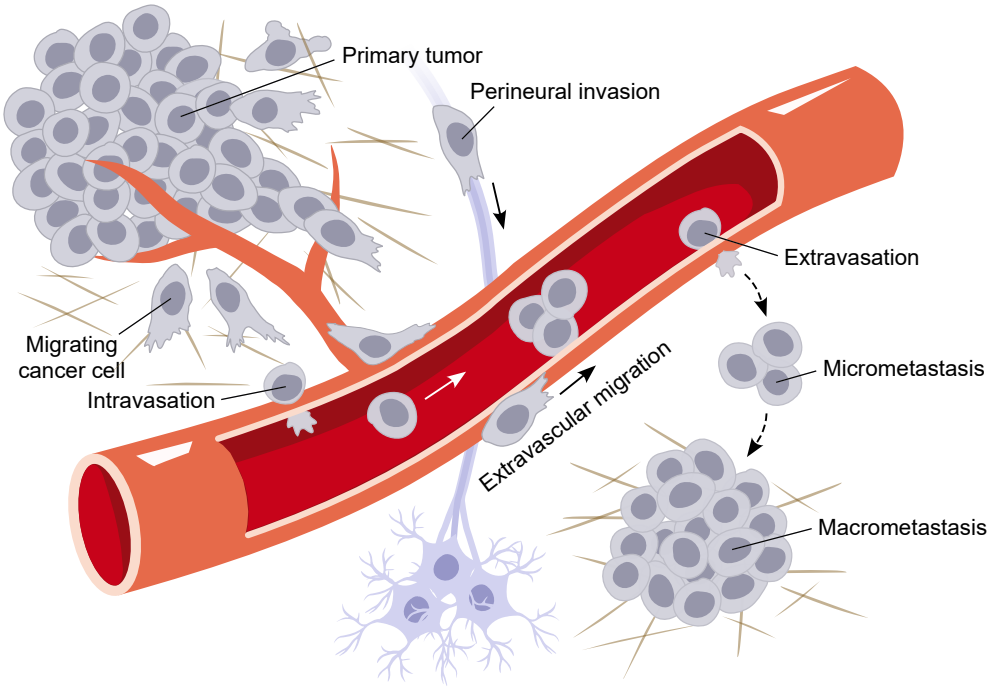

Figure 1. Simplified schematic presentation of the metastatic cascade and associated cancer cell migration. Examples of metastatic pathways that do not necessitate cancer cell entry into the circulation are also depicted. Solid arrows denote cell movement and dashed arrows denote transitions between biological states. Such transitions may involve additional steps that are not shown, e.g., cancer cell dormancy. Based on (Liebig et al., 2009; Lambert et al., 2017; Lugassy et al., 2020).

No matter which route the cancer cells take, distant metastasis is almost invariably preceded by active cell migration in complex tissue microenvironments. Individual tumor cells, cell clusters, and long strands comprising hundreds of carcinoma cells can invade the surrounding stroma with remarkable efficiency, employing a variety of molecular mechanisms (Friedl & Alexander, 2011). This phenotypic plasticity of migrating cells will be explored in detail in the next chapter. Given its importance in cancer progression, local invasion plays a major role in the histopathological evaluation and staging of different malignant tumors. For example, one of the main goals of bladder cancer staging is to determine the presence or absence of muscle invasion, which drastically worsens the prognosis and warrants more aggressive treatment and follow-up (Wong et al., 2021). In cutaneous melanoma, the depth of invasion in the primary lesion directly predicts the likelihood of regional and distant metastasis. Together with other tumor attributes like ulceration, this “Breslow’s depth” is used as a basis for melanoma staging (Davis et al., 2019). Moreover, perineural and/or lymphovascular invasion have been linked to poor prognosis in

many cancer types, including head and neck squamous cell carcinoma, cervical cancer, prostate cancer, and pancreatic tumors (Liang et al., 2016; Chang et al., 2019; Tang et al., 2019; Ström et al., 2020).

Malignant cell migration and invasion (strictly defined as degradative or restructuring movement of cells across 3D matrices and barriers) can have devastating consequences even when they don't lead to distant metastasis and colonization of additional organs. For example, tumors of the central nervous system rarely form extraneural metastases, but glioblastoma—the most common and aggressive type of brain cancer—is characterized by diffuse growth patterns and extensive cancer cell invasion into the healthy brain parenchyma. This makes a complete surgical resection of the tumor impossible and contributes to an abysmal prognosis (Seker-Polat et al., 2022). In some cases, cell migration may even constitute a form of therapy resistance. Anti-angiogenic treatments targeting the vascular endothelial growth factor (VEGF) pathway inhibit neovascularization but may promote cancer cell invasion into the surrounding tissue, as suggested by the increased metastasis in preclinical models of glioblastoma and pancreatic neuroendocrine carcinoma (Pàez-Ribes et al., 2009).

2.1.2 Therapeutic targeting of cancer cell migration

Despite the biological rationale pointing to a central role of cancer cell migration and invasion in disease progression and unfavorable clinical outcomes, the specific category of anti-invasive and anti-metastatic therapeutics—so-called migrastatics—has been extremely limited (Gandalovičová et al., 2017). Some of this discrepancy stems from the commonly approved clinical endpoints, which traditionally have equated therapeutic efficacy with cytotoxicity and tumor shrinkage. Thus, funding and interest toward anti-metastatic research have been low.

In principle, malignant cell migration can be targeted at multiple levels. These include the actual physical (receptor-mediated) interactions between the cells and their microenvironment, different signaling pathways and second messengers that regulate the intracellular migratory machinery, as well as the cytoskeletal components that are ultimately responsible for cell locomotion (Gandalovičová et al., 2017). For example, integrins are a widely expressed class of cell adhesion molecules that are integral for cell migration and other biological functions, and they have been studied extensively in most, if not all, cancer types (Hamidi & Ivaska, 2018). However, given the complex and sometimes antagonistic functions of different integrin subtypes in tumorigenesis and cancer progression, therapeutic targeting of these molecules has been challenging. A prime example of this is cilengitide, a selective inhibitor of αvβ3 and αvβ5 integrins which—in combination with temozolomide—failed to show efficacy against newly diagnosed glioblastoma

in the phase 3 CENTRIC trial (Stupp et al., 2014). Indeed, similar plasticity and redundancy characterize most signaling pathways upstream of cell migration (much like those regulating survival and proliferation), and targeting only one pathway is likely to result in therapy resistance (Gillis & McLeod, 2016).

Another approach to pharmacologically restricting cancer cell invasion is to directly target the cytoskeletal elements that are responsible for cell shape changes and movement. In particular, numerous inhibitors of the actomyosin cytoskeleton and its direct upstream regulators, including Rho-associated protein kinases (ROCK) 1/2 and myosin light chain kinase (MLCK), have been studied extensively as anti-invasive agents. For example, ROCK inhibitor Y-27632 has been shown to limit the invasiveness of various human cancer cell lines, including MDA-MB-231 breast cancer cells and LS174T colon carcinoma cells (Sahai & Marshall, 2003; Yoshioka et al., 2003). In mice, Y-27632 inhibits liver colonization by HT-29 colorectal cancer cells (Voorneveld et al., 2014). AT13148, another ROCK inhibitor that also targets AKT kinases, has been shown to elicit anti-invasive and anti-metastatic effects in preclinical models and was later investigated in a phase 1 trial for the treatment of solid tumors (McLeod et al., 2020). However, further AT13148 development was not recommended due to the compound's narrow therapeutic index and unfavorable pharmacokinetics.

One of the reasons behind the limited clinical use of actomyosin-targeting compounds has been the abundance and importance of actin-related biological processes, and the potential adverse effects that can result from interfering with them. However, the successful implementation of different microtubule (MT)-targeting agents as anti-cancer drugs, including key pharmaceuticals like vinblastine and docetaxel, could weaken this argument (Gandalovičová et al., 2017). In addition, therapeutics that are deemed too potent or toxic for clinical use could be conjugated to specific delivery systems, limiting their effects to malignant tissues. TR100 is a small molecule that has been used to selectively disrupt actin filaments in cancer cells, impeding the motility and viability of human neuroblastoma and melanoma cells (Stehn et al., 2013). TR100 exerts its functions by targeting cancer-associated tropomyosin Tpm3.1 (Tm5NM1). Interestingly, the compound can also disrupt actin-mediated spindle repair, resulting in synergistic anti-cancer activity when used in conjunction with low concentrations of anti-MT vinca alkaloids (Wang et al., 2020).

Another potential issue related to the use of migrastatics in the clinic stems from cancer biology. There is compelling evidence indicating that cryptic metastasis can take place very early during tumorigenesis. By the time the primary tumor is detected, the lesion may have already seeded distant organs (Rhim et al., 2012; Hosseini et al., 2016). Consequently, preventing metastasis completely by targeting cancer cell migration and local invasion may not be possible in a significant number

of cases. Nevertheless, anti-invasive and anti-metastatic treatments may still benefit these patients by restricting tumor self-seeding. Circulating tumor cells from metastases are particularly efficient at infiltrating other tumors at distant sites, including the primary lesion, which can increase tumor growth and promote other malignant adaptations (Kim et al., 2009b). Existing metastases may also continue seeding new, previously unaffected tissues and organs (Gundem et al., 2015). In addition, computational modeling suggests that even short-range migration and dispersal of cancer cells can significantly increase the growth rate of a newly established metastatic tumor (Waclaw et al., 2015).

It is worth noting that the goal of migrastatics is not necessarily to replace anti-proliferative or cytotoxic therapy, but rather to complement it. In fact, different compounds targeting cell adhesion molecules, the actin cytoskeleton and/or intracellular contractility may have intrinsic anti-proliferative characteristics (Paszek et al., 2005; Lomonaco et al., 2011; Kümper et al., 2016). Even if direct therapeutic targeting of cell motility is not feasible, understanding the molecular mechanisms and routes of cancer invasion can be beneficial, e.g., to inform the maximal safe resection of neurological tumors (Seker-Polat et al., 2022).

The 2018 U.S. Food and Drug Administration (FDA) approval of metastasis-free survival (MFS)—defined as the time from randomization to either imaging-detectable distant disease or death—as a valid endpoint in clinical trials marks a major milestone in the clinical development of anti-invasive and anti-metastatic therapies. The decision was primarily motivated by the results of different clinical trials that sought to prevent systemic progression in non-metastatic castration-resistant prostate cancer (Beaver et al., 2018). Now, MFS is also being used as a primary clinical endpoint in CHIC, a phase 3 study evaluating the impact of peri-operative chemotherapy on the progression of high-risk localized soft tissue sarcoma (Filleron et al., 2020). These and other recent studies, as well as the ongoing efforts to repurpose existing therapeutic agents as migrastatics, highlight a new-found clinical interest in malignant cell migration and invasion (Maiques et al., 2021; Solomon et al., 2021; Raudenská et al., 2023).

In summary, invasion and metastatic progression are key features of malignant tumors and contribute disproportionately to cancer-related mortality. Both processes are also critically dependent on cancer cell migration, the unassisted movement of cancer cells from one location to another. Despite extensive research into the basic mechanisms of cell migration over the past decades, our understanding of cancer cell motility in structurally and compositionally complex microenvironments is still lacking. For example, contrary to the examples above, ROCK inhibition has also been reported to *increase* the local invasion of scirrhous gastric carcinoma and astrocytoma cells (Matsuoka et al., 2011; Salhia et al., 2005). Such results are likely to reflect a contractility-dependent shift in the migration mode employed by the cell

as discussed below. However, the findings may also be linked to the ability of cancer cells to detect and respond to alterations in local tissue biomechanics. Mechanosensitive cell migration and some of its molecular underpinnings are investigated and the results reported in this thesis. With the current advent of clinically relevant migrastatics, studying the fundamentals of cancer cell migration to inform preclinical and clinical cancer research is more important than ever.

2.2 Eukaryotic cell migration

The fundamental characteristics of crawling metazoan cells were formulated in 1970's by Michael Abercrombie and his peers, who observed that migrating stromal fibroblasts adhered stably to planar 2D substrates and moved by adding material to their front (Abercrombie et al., 1970; Abercrombie, 1980). Actin microfilaments were also quickly deemed indispensable for this type of cell motility (Spooner et al., 1971). Later, the prototypical model of cell migration was refined and became recognized as a carefully coordinated multi-step process: initial symmetry breaking is followed by plasma membrane protrusion in the direction of migration, formation of attachments with the extracellular environment, generation of contractile forces and traction that facilitate translocation, and eventual retraction of the cell's trailing edge (Lauffenburger & Horwitz, 1996). We now understand that these constituent processes of cell locomotion do not reflect separate, temporally segregated events. Instead, they tend to occur simultaneously and exhibit significant overlap over the course of cell migration.

2.2.1 Phenotypic plasticity of migrating cells

Today, the classic model of cell migration has become known as mesenchymal (lamellipodial) migration and additional migration modes have been characterized (Figure 2). Mesenchymal cell migration is the prevalent mode of migration in 2D environments, which includes most cell culture substrates. In addition, various cell types employ similar mechanisms to migrate in complex 3D environments. Notable examples of cells undergoing mesenchymal migration include stromal fibroblasts (Caballero et al., 2017; Doyle et al., 2021), neural crest cells during embryonic development (Barriga et al., 2018), and many cancer cells originating from, e.g., breast adenocarcinoma, fibrosarcoma, squamous cell carcinoma, and glioblastoma (Wang et al., 2019; Doyle et al., 2021; Anderson et al., 2023).

Mesenchymal migration is characterized by elongated cell morphology and polarization that results in the formation of a defined leading edge. Cells use this leading edge to extend actin-rich protrusions into the surrounding microenvironment, including thin, sheet-like lamellipodia that are characterized by

a branched actin network, and long, finger-like filopodia that are supported from the inside by bundles of parallel actin filaments. Filopodia, in particular, probe the local microenvironment and provide the cell with new sites of attachment (Jacquemet et al., 2015). Indeed, extensive receptor-mediated adhesion between a cell and the surrounding ECM is another defining feature of mesenchymal cell migration, and the cells use it to generate traction for protrusion and locomotion. Some cell types can also present with more specialized actin-based projections, such as proteolytic invadopodia that promote invasion in many malignant cells (Artym et al., 2015).

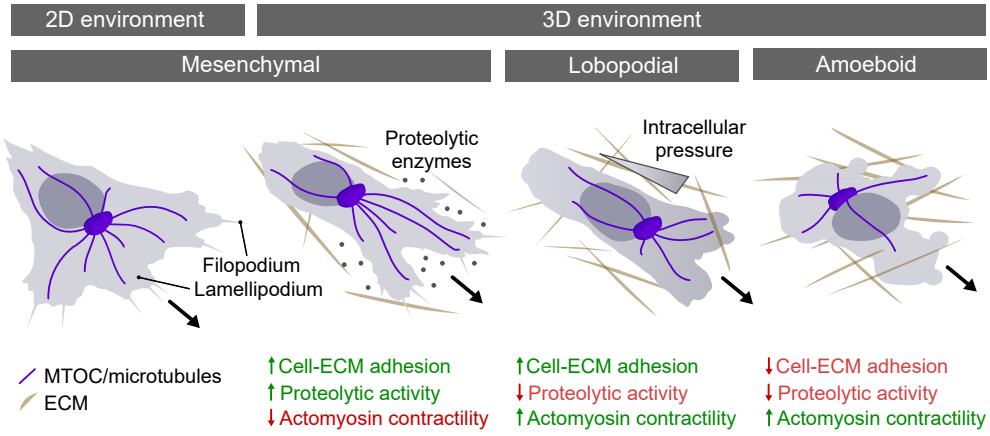

Figure 2. Different modes of single-cell migration. Large arrows denote the direction of movement. Adapted from (Yamada & Sixt, 2019; Seetharaman & Etienne-Manneville, 2020).

The best-studied alternative to mesenchymal cell migration is amoeboid migration, so called because it resembles the movement of different protist amoebas. Amoeboid migration is characterized by a rounded or irregular cell morphology and projection of large, actin-rich pseudopodia and actin-free blebs. Amoeboid cells typically present with fewer adhesive interactions with the extracellular milieu. Instead, cycles of contraction and expansion allow the cells to rapidly squeeze through gaps in the ECM, and traction is generated by lateral protrusions and actin flow against surrounding topographic features (Tozluoğlu et al., 2013; Reversat et al., 2020). In humans, amoeboid cell migration is exhibited first and foremost by cells of the immune system. Leukocytes conducting immune surveillance benefit from fast migration that is mostly independent of dedicated adhesion receptors, and thus compatible with different biochemically distinct tissue microenvironments (Kameritsch & Renkawitz, 2020). However, many tumor cells can also undergo amoeboid migration (Wolf et al., 2003).

In reality, mesenchymal and amoeboid migration do not represent strictly defined and segregated migration strategies adopted by different cell types. Instead, these migration modes reflect the practical outcome of various cell-intrinsic and -extrinsic factors (Yamada & Sixt, 2019). In particular, the relative balance between actin-mediated protrusion, cell-ECM adhesion and intracellular contractility greatly impacts cell migration: efficient protrusion and adhesion favors mesenchymal migration, while high cortical contractility promotes amoeboid migration. Such differences can arise from qualitative or quantitative changes in the cell's molecular machinery. For example, expression of hydrogen peroxide-inducible clone 5 (HIC-5), a homolog of another adhesion component, paxillin, promotes a shift from amoeboid to mesenchymal migration in a variety of cancer cell lines (Gulvady et al., 2018). On the other hand, increased ROCK-mediated contractility is enough to induce a shift toward more amoeboid-type motility in BE colon carcinoma cells (Sahai & Marshall, 2003).

Besides cell-intrinsic factors, the extracellular microenvironment plays a critical role in cell migration, and simple spatial confinement of mesenchymal cells can be enough to elicit a switch to amoeboid migration (Tozluoğlu et al., 2013; Liu et al., 2015b). This observation has profound implications for cell migration in physiological environments: the ECM in many tissues presents a significant steric hindrance to migration, and as a result, effective mesenchymal migration requires proteolytic activity. Inhibiting matrix metalloproteinases (MMP) can induce a shift from mesenchymal to amoeboid cancer cell migration in dense collagen matrices and in vivo (Wolf et al., 2003; Friedl & Wolf, 2009).

In addition to mesenchymal and amoeboid migration, a third distinct mode of single-cell migration is often recognized. In lobopodial migration, tightly adherent cells lacking proteolytic activity use actomyosin contractility and hydrostatic pressure to employ their nucleus as a "piston", generating blunt bleb-like protrusions called lobopodia (Petrie et al., 2014, 2017). The rigid nucleus can also become a rate-limiting structure when cells are migrating in confined environments. Nuclear mechanics are impacted by chromatin structure and the composition of nuclear lamina, a protein meshwork lining the nucleoplasmic surface of the inner nuclear membrane. This results in a tradeoff between the cell's capacity to migrate in confined spaces and its ability to protect the nuclear envelope and DNA from damage (Harada et al., 2014).

The phenotypic plasticity of cell migration—as well as its responsiveness to a myriad of extracellular cues—highlights the importance of cell motility for normal human physiology and homeostasis. These features make cell migration remarkably robust, a trait that is a boon in healthy tissue microenvironments but can have devastating consequences when it's co-opted by cancer. Despite the differences outlined above, there are several key features that appear to characterize all cell

migration. For any movement to occur, the cell has to exert physical force on its surroundings. These forces almost invariably originate from the actin cytoskeleton that acts in conjunction with other cytoskeletal elements (i.e., MTs and intermediate filaments [IF]) to pull, push, contract, and ultimately propel the cell forward (Yamada & Sixt, 2019; Seetharaman & Etienne-Manneville, 2020). Migration is an energy-intensive process, and cytoskeletal and other associated proteins are estimated to consume a significant portion of the available cellular energy. As a result, cell migration is intrinsically linked to metabolism (Zanotelli et al., 2021). This observation has given rise to the notion of "grow or go", a dichotomy where cell migration and proliferation are mutually exclusive (Giese et al., 1996).

2.2.2 Collective cell migration

Most human tissues are characterized by extensive cell-cell contacts that are needed for maintaining epithelial integrity and physiological compartmentalization. Tight junctions—consisting of proteins like occludin and claudins—are intercellular adhesions that help prevent the passage of molecules and ions between adjacent cells and contribute to the apico-basal organization of epithelial plasma membranes. Desmosomes tether IFs to the plasma membrane and contribute to the mechanical integrity of tissues. Finally, adherens junctions are well-known mechanosensors whose cadherin-catenin complexes are connected to actomyosin, transmitting mechanical forces between cells. Adherens junctions respond to cytoskeletal prestress and external tension by catenin- and vinculin-mediated reinforcement of the cell-cell adhesion, supporting epithelial adaptation to different biomechanical conditions (Angulo-Urarte et al., 2020).

Owing to this collective organization, many cell types are capable of migrating together in sheets or other multicellular arrangements, e.g., during gastrulation, wound healing, or intestinal epithelial turnover. Collective cell migration is also commonly observed in different solid tumors, perhaps reflecting the fact that up to 90% of cancers are of epithelial origin (Friedl & Alexander, 2011; Clark & Vignjevic, 2015). The mechanisms regulating cells' propensity for collective or single-cell migration are still incompletely understood, but they can include extracellular cues like spatial confinement due to slow ECM degradation, which promotes endothelial cell migration in collective strands (Trappmann et al., 2017), or hypoxia, which can promote hypoxia-inducible factor 1 (HIF-1) activation and single-cell migration in carcinomas (Lehmann et al., 2017).

Collectively migrating cells exhibit varying degrees of intercellular organization and cohesion. For example, some cells can essentially migrate as individuals, and collective behavior results from transient cell-cell interactions and contact stimulation of migration: any cells that race ahead and lose contact with the others

will cease migrating until the remaining cells have caught up (Thomas & Yamada, 1992). Alternatively, an opposite process—contact inhibition of locomotion (CIL)—can polarize cells in the front by preventing them from moving backward. CIL may also keep streaming cells from deviating from a common path (Abercrombie, 1970; Mayor & Etienne-Manneville, 2016). In many cases, however, collective migration involves extensive cell-cell adhesion and supracellular organization, where specific leader cells create migration tracks and sense environmental cues to guide the followers. The appearance of leader cells has been linked to reciprocal mechanical signaling between the cells in the collective, suggesting that the acquisition of leader traits is not a cell-intrinsic process (Vishwakarma et al., 2018). Once "elected", leader cells expend a significant amount of energy to create tracks for the followers. After a leader has depleted its ATP reserves, one of the follower cells may take its position and continue pathfinding as the new leader (Zhang et al., 2019). The importance of intercellular force transmission in collective cell migration is further highlighted by the fact that disrupting adherens junctions—or their capacity to respond to tensile forces—generally impairs coordinated collective migration (Sunyer et al., 2016; Seddiki et al., 2018).

Despite their obvious differences, both collective and single-cell migration are thought to share many of the same underlying mechanisms (Mayor & Etienne-Manneville, 2016). This thesis focuses primarily on the investigation of mesenchymal single-cell migration using cells of e.g., brain and breast cancer origin. Glioblastoma cells, in particular, are known for migrating in their native ECM environment using long adhesive projections, and they present a relevant model for studying migratory responses to tissue composition and biomechanics (Caspani et al., 2006; Seker-Polat et al., 2022; Anderson et al., 2023).

2.2.3 Directed cell migration

For cell migration to benefit an organism, the process has to be carefully controlled. Consequently, cells have the ability to detect and respond to a wide variety of extracellular cues that directly influence their migration. Changes in local microenvironment can induce or halt migration, regulate cell speed, or—importantly—direct cell migration toward or away from an extracellular signal. Such signals can include gradients of diffusible or extracellular vesicle-bound molecules, such as growth factors, chemokines, and products of the complement system (Ehrengruber et al., 1994; Haugh et al., 2000; Roussos et al., 2011); gradients of immobilized ligands, such as ECM components (Oudin et al., 2016); electric fields (Huang et al., 2016); or even the hydraulic resistance of the medium (Prentice-Mott et al., 2013). Notably, cell migration can also be guided by ECM mechanics and architecture. Durotaxis, the ability of cells to detect and migrate along gradients of

substrate stiffness, and different forms of directed migration in response to substrate topography are discussed in detail in the following chapters.

All forms of directed cell migration are thought to share four common principles (SenGupta et al., 2021). These include 1) the generation of the signal or gradient, a non-trivial process in many physiological environments; 2) sensing the signal, typically via suitable transmembrane receptors; 3) transmitting the signal to the intracellular machinery responsible for migration, a process that often involves signal amplification; and 4) application of asymmetric force to move the cell as outlined above. Before we discuss the biomechanical characteristics of tumor microenvironments, and how cells can sense and interpret these features to regulate their own motility, we will review a concept that is integral to many types of directed cell migration: front-rear polarity.

2.2.3.1 Front-rear polarity and persistent migration

Most cells in the human body are polarized, i.e., they exhibit morphological and functional asymmetry that is necessary for normal tissue homeostasis. Epithelia—with their carefully controlled apico-basal organization and trafficking—are a prototypical example of polarized cells, but polarity is equally important for processes like asymmetric cell division. Interestingly, many of the same molecular programs that regulate apico-basal polarity are reused time and again to establish polarity in different cell types and biological contexts (Campanale et al., 2017).

Unlike epithelia, migrating mesenchymal cells are polarized parallel to their axis of movement. This so-called front-rear polarity is initiated by symmetry breaking that can happen spontaneously or as a response to external cues, typically via transmembrane receptor activation. For example, the activation of different receptor tyrosine kinases (RTK) or G protein-coupled receptors (GPCR) can initiate polarization, leading to localized recruitment and activation of additional signaling molecules and polarity factors (Roussos et al., 2011). Importantly, the engagement of integrins with ECM components can also mediate front-rear polarization in migrating cells (Etienne-Manneville & Hall, 2001; Maninová et al., 2013). This indicates that the same receptors that link the cells to their extracellular environment to mediate force transmission and locomotion can also be used by the cells to probe their surroundings directly, guiding migration. We will revisit integrins and the broader implications of their dual role in the following chapters.

The signal from initial receptor activation is amplified by the generation of second messengers and activation of downstream signaling pathways. This includes the recruitment of various GTPase-activating proteins (GAP) and guanine nucleotide exchange factors (GEF) that modulate the activity and interactions of Rho family GTPases, key regulators of the actin cytoskeleton during cell polarization and

migration (Lawson & Ridley, 2018). Out of the different Rho family members, classic Rho GTPases like cell division control protein 42 homolog (Cdc42), Ras-related C3 botulinum toxin substrate 1 (Rac1), and transforming protein RhoA (RhoA) are particularly well-studied. All three proteins are present in the anterior of a migrating cell, where they exhibit carefully controlled, spatially and temporally segregated cycles of activation and inactivation to drive the net protrusion of the leading edge (Machacek et al., 2009; Martin et al., 2016; Bolado-Carrancio et al., 2020). In addition, RhoA is important for the contraction and retraction of the cell rear (Pertz et al., 2006; Iwanicki et al., 2008; Bolado-Carrancio et al., 2020).

Phosphatidylinositol-3,4,5-trisphosphate (PIP_3) is another important signaling molecule that is spatially restricted to the leading edge in various cell types. Its role in directed cell migration and regulation of actin dynamics is particularly well-studied in neutrophils and the social amoeba *Dictyostelium discoideum*, but PIP_3-dependent polarization is also implicated in the migration of fibroblasts and breast adenocarcinoma cells (Haugh et al., 2000; Funamoto et al., 2002; Srinivasan et al., 2003; Petrie et al., 2012; Saito et al., 2021). Localized PIP_3 accumulation is supported by crosstalk between the lipid and its negative regulator phosphatase and tensin homolog (PTEN): mutual inhibition between PIP_3 and PTEN at the plasma membrane results in steep, bistable, and opposite gradients across the cell, promoting polarization and migration (Matsuoka & Ueda, 2018).

The characteristic anterior activity of different polarity regulators, including Cdc42, Rac1, and PIP_3, has been observed in both 2D and 3D environments (Petrie et al., 2012). Moreover, these signaling networks exhibit significant crosstalk and multiple feedback loops. For example, Cdc42-based positive feedback involving localized actin polymerization and further Cdc42 accumulation has been suggested to contribute to spontaneous symmetry breaking in the absence of extracellular signaling gradients (Wedlich-Soldner et al., 2003), while active Rac1 and PIP_3 promote each other's accumulation at the leading edge in polarized neutrophils (Srinivasan et al., 2003).

There are also indications that the polarization of migrating cells can happen "back to front". In fibroblasts, bundled actin is critical for preventing isotropic protrusion and promotes the establishment of cell rear in the absence of external polarity cues. The process is dependent on myosin IIB, and the protein is also required for downstream organelle reorientation along the axis of cell movement (Vicente-Manzanares et al., 2007, 2008). Recently, a similar graded intracellular distribution of myosins IIA and IIB was observed in front-rear polarized breast cancer cells in 3D collagen/fibronectin matrices (Newman et al., 2023). These findings are further supported by a study suggesting that dense filamentous actin (F-actin) in the membrane-proximal layer of the actin cortex can suppress membrane protrusion, stabilizing front-rear polarization (Bisaria et al., 2020).

Besides the actin cytoskeleton and its regulators, other cytoskeletal elements are also polarized and functionally important in migrating cells. IFs like vimentin are constantly deployed in new protrusions at the leading edge, while the whole network exhibits a continuous retrograde flow toward the perinuclear region (Leduc & Etienne-Manneville, 2017). This asymmetric organization and movement of IFs is dependent on Cdc42 activity, F-actin dynamics, and active retrograde and anterograde transport by MT-associated motor proteins (Jiu et al., 2015; Leduc & Etienne-Manneville, 2017). Vimentin, in turn, templates and stabilizes the MT network, regulates nuclear positioning and cell-substrate adhesion dynamics, and promotes directionally persistent cell migration (Gregor et al., 2014; Jiu et al., 2015; Gan et al., 2016).

2.2.3.2 Golgi, microtubules, and front-rear polarity

Arguably the most characteristic feature of front-rear polarized cells is the orientation of the nucleus-centrosome-Golgi axis along the direction of movement. In mesenchymal-migrating cells, this typically means that the centrosome and closely associated Golgi apparatus are both positioned in front of the nucleus, toward the leading edge. This results in a concomitant polarization of the MT network in the same direction (Meiring et al., 2020) (Figure 2). Some examples of cells where forward-facing centrosomes and Golgi have been observed include fibroblasts, endothelial cells, astrocytes, *Dictyostelium*, and different cancer cells (Gotlieb et al., 1981; Kupfer et al., 1982; Ueda et al., 1997; Etienne-Manneville & Hall, 2001; Maninová et al., 2013; Dubois et al., 2017). In fact, centrosome repositioning away from the apical pole and toward the ECM is a key step in epithelial-to-mesenchymal transition (EMT), and it precedes cell scattering in mammary and kidney epithelia (Burute et al., 2017).

Several partially independent mechanisms are thought to regulate centrosome and Golgi orientation. In astrocytes, Cdc42 and its effectors partitioning-defective protein 6 (Par6) and protein kinase C zeta (PKCζ) promote MT anchoring to the plasma membrane. In conjunction with dynein-dynactin activity, this leads to active positioning of the centrosome near the cell centroid (Etienne-Manneville et al., 2005; Gomes et al., 2005). The final location is further constrained by the geometry of the intracellular actomyosin network (Jimenez et al., 2021). In addition, Cdc42 regulates organelle reorientation by promoting myosin II activation and retrograde flow of actin that positions the nucleus behind the centrosome (Gomes et al., 2005). This nuclear repositioning requires an intact linker of nucleoskeleton and cytoskeleton (LINC) complex, indicating that the process is dependent on a direct mechanical connection between actin and the nucleus (Maninová et al., 2013). Actin retrograde flow has also been suggested to promote persistent front-rear polarization by

redistributing polarity factors inside the cell (Maiuri et al., 2015). Finally, several additional molecular players that are important for the reorientation of the centrosome and Golgi in migrating cells have been indentified. These include key regulators of cell-ECM interactions, such as focal adhesion kinase (FAK), proto-oncogene tyrosine-protein kinase Src (Src), and paxillin (Maninová et al., 2013; Dubois et al., 2017).

Once established, the polarized nucleus-centrosome-Golgi axis and MT array are thought to promote persistent cell migration in multiple ways. MTs associate with focal adhesions (FA)—sites of integrin-mediated cell-ECM adhesion—at the leading edge, regulating their turnover via GEF-H1-RhoA signaling axis and local ECM degradation (Stehbens et al., 2014; Rafiq et al., 2019; Seetharaman et al., 2022). The loss of centrosome and associated MTs in retinal pigment epithelial (RPE) cells leads to excessive activation of Rac1 at FAs, disrupting polarity (Cheng et al., 2019). Importantly, the orientation of the Golgi and MTs toward the leading edge is also necessary for polarized anterograde trafficking and exocytosis, key requirements for sustained front-rear polarity and persistent migration (Stehbens et al., 2014; Xing et al., 2016; Vaidžiulytė et al., 2022). Moreover, rearward nuclear positioning has been postulated to ensure that the nucleus is in proper orientation to be pulled forward as the cell extends (Gomes et al., 2005). This is in stark contrast to amoeboid cells that often position their nucleus in front of the centrosome to facilitate pathfinding in complex extracellular environments (Renkawitz et al., 2019). However, such cells still need dynamic MTs to retract any lingering cytoplasmic projections from the smaller pores.

The specific role of the Golgi in persistent cell migration is further supported by the observation that decoupling the organelle from the centrosome perturbs polarization and directed migration (Hurtado et al., 2011). Indeed, the Golgi acts as an independent microtubule-organizing center (MTOC) that nucleates and stabilizes compositionally and functionally distinct non-centrosomal MTs (Chabin-Brion et al., 2001; Wu et al., 2016). In many cell types, including endothelial and renal epithelial cells, centrosomal MTs are dispensable but a polarized array of CLIP-associated protein (CLASP)-coated Golgi MTs is required for polarized trafficking and persistent/directional migration (Miller et al., 2009; Martin et al., 2018; Hao et al., 2020).

Some aspects of the MTOC polarization in mesenchymal cell migration remain controversial. Zhang and Wang reported that randomly migrating NIH 3T3 fibroblasts preferentially position their centrosome at the cell rear, behind the nucleus, which may facilitate an asymmetric distribution of protrusion-suppressing factors in the cell (Zhang & Wang, 2017). Such “polarity reversion” may be further accentuated by the spatial confinement of cells on narrow, linear substrates (Pouthas et al., 2008). Moreover, previous observations have suggested that while centrosome

orientation toward a nascent pseudopod in *Dictyostelium* promotes the stabilization of the protrusion (Ueda et al., 1997), Golgi orientation in fibroblasts and RPE cells correlates poorly with the future direction of migration (Chen et al., 2013; Vaidžiulytė et al., 2022). In Rat2 rat fibroblasts, the Golgi aligned toward the direction of migration in wounded monolayers but not in freely migrating individual cells (Uetrecht & Bear, 2009). Taken together, the extent to which the nucleus-MTOC axis really directs single-cell migration remains elusive—particularly in the context of transformed cells.

2.3 Biomechanics of the tumor microenvironment

Historically, cancer has often been considered a disease of the cell—one that results from mutations in the genes controlling cell identity, survival, and proliferation. While biology has provided many valuable insights into cancer behavior, it is now widely acknowledged that the physical properties of the tumor play an equally important role during carcinogenesis and cancer progression (Nia et al., 2020; Papavassiliou et al., 2023). Cancer cells, like their benign counterparts, are highly responsive to a wide variety of external mechanical cues. Cells can convert this information into intracellular biochemical signals that regulate phenotype, up to and including gene expression, in a process called mechanotransduction (Iskratsch et al., 2014).

The mechanical properties of biological materials and living tissues are often complex. Various synthetic materials like polyacrylamide or polydimethylsiloxane (PDMS) are used for studying cellular responses to substrate stiffness (i.e., the ability of an object to resist deformation in response to an applied force) in vitro. Such polymers are typically linearly elastic, meaning that they deform reversibly and there is a linear relationship between strain and stress. The ratio of stress to strain is known as the material's elastic modulus, and it encompasses several independent but related metrics such as Young's modulus (E), for tensile stress (often simply called elastic modulus); shear modulus (G), for shear stress; and bulk modulus (K), for volumetric stress (Caliari & Burdick, 2016). While elastic cell culture substrates have proved very useful for investigating the mechanobiology of normal and malignant cells, most tissues and ECMs also exhibit varying degrees of non-linear elasticity, viscoelasticity (time-dependent elastic responses to loading and deformation), and plasticity (irreversible deformations) (Chaudhuri et al., 2020). The term stiffness is often used in scientific literature colloquially to refer to the elasticity of tissues and cell culture substrates—stiff materials have a high elastic modulus. This thesis follows the same nomenclature. Moreover, unless otherwise indicated, all the elastic moduli discussed herein refer to the material's Young's modulus.

In tumors, different compressive, tensile, and shear forces transmitted by the solid and (visco)elastic components of the microenvironment tend to constitute a significant solid stress. Increased tumor volume resulting from cell proliferation, cell infiltration, and ECM deposition can push and displace existing structures and the surrounding tissue, resulting in stresses that can reach over 5 kPa in an orthotopic mouse model of pancreatic ductal adenocarcinoma (Nia et al., 2016). Furthermore, actomyosin-mediated contraction of cells—in particular, activated cancer-associated fibroblasts (CAF)—contracts ECM components and can generate significant tensile forces. Solid stress compresses blood and lymphatic vessels, contributing to hypoxia and limiting the delivery of therapeutic agents into the tumor (Chauhan et al., 2013). The forces can also have direct biological effects on the cancer cells, e.g., by inducing oncogenic β-catenin signaling (Fernández-Sánchez et al., 2015).

Tumor vasculature is usually fragile and leaky. Together with the compromised drainage resulting from solid stress and compression of blood and lymphatic vessels, this can lead to increased interstitial fluid pressure in the tumor microenvironment (Swartz & Lund, 2012). Elevated fluid pressure drives interstitial flow, exposing cancer and stromal cells to shear stress. This can significantly impact the biology of the tumor, including endothelial sprouting and MMP secretion (Qazi et al., 2011; Song & Munn, 2011). High interstitial fluid pressure may also negatively impact the convection and spreading of therapeutic agents into the tumor (Jain & Baxter, 1988).

Arguably the most obvious and significant biophysical alterations in cancer result from changes to the ECM. Desmoplasia, generation of a dense stroma by aberrant ECM deposition and remodeling, is a well-known trait of many solid tumors. Cancer-specific alterations to the ECM include its composition, concentration, post-translational modifications, crosslinking, and microarchitecture (Cox & Erler, 2011). Some of the most common and abundant ECM components deposited in tumors include fibrillar collagens and fibronectin, although many other proteins are also implicated and the exact ECM composition varies based on tumor location (Provenzano et al., 2008; Mayorca-Guiliani et al., 2017). Desmoplastic stroma presents a steric barrier that may impede immune infiltration (Xiao et al., 2023). Importantly, desmoplasia can also have a drastic effect on the mechanical properties of the tumor. Increased tissue stiffness is a common and tangible mechanical abnormality in many solid cancers and its use as a diagnostic marker (e.g., during palpation) predates modern cancer medicine. Mammographic density in healthy individuals varies considerably and high density is a well-known risk factor for breast cancer (Boyd et al., 2007), but stiffening of the tumor microenvironment has been linked directly to increased malignancy and/or poor prognosis in many different cancer types. Notable examples include breast cancer (Paszek et al., 2005; Lee et al., 2019), pancreatic cancer (Rice et al., 2017), glioma (Miroshnikova et al., 2016), and colorectal cancer (Baker et al., 2013).

CAFs are the main cells responsible for laying down and remodeling the ECM in tumors. These stromal cells are also sensitive to matrix stiffness, which activates yes-associated protein 1 (YAP), a mechanosensitive transcriptional co-regulator, and the myocardin-related transcription factor/serum response factor (MRTF/SRF) pathway. YAP and MRTF/SRF signaling jointly promote and sustain fibroblast activation and the contractile CAF phenotype, leading to positive mechanobiological feedback that promotes tumor desmoplasia (Calvo et al., 2013; Foster et al., 2017). The importance of this stromal component in cancer progression is evident from studies showing a phenotypic reversal or growth suppression of cancer cells in normal ECM (Bissell & Hines, 2011; Kaukonen et al., 2016).

2.3.1 Physical traits of the tumor regulate migration

The different physical traits of the tumor stroma are also intrinsically linked to cancer cell migration and invasion. For example, in vitro experiments suggest that compressive stress can directly promote the motility of breast carcinoma cells by stimulating leader cell behavior and enhancing cell-substrate adhesion (Tse et al., 2012). Other studies have indicated that solid stress promotes migration in neuroglioma cells, via extracellular signal-regulated kinase (ERK) pathway activation (Kalli et al., 2019), and in pancreatic cancer cells, by triggering Rho GTPase-mediated cytoskeletal remodeling and contraction (Kalli et al., 2022).

Similarly, the shear forces resulting from interstitial flow can have a drastic effect on cell migration. Depending on cancer type and cell line, physiological shear forces can either inhibit (Qazi et al., 2011) or promote (Qazi et al., 2013) 3D migration in collagen matrices in an MMP-dependent manner. Interstitial flow may also contribute to invasion via so-called autologous chemotaxis: autocrine secretion of chemokines combined with fluid flow results in a pericellular signaling gradient that drives chemotaxis and migration in the direction of the flow (Polacheck et al., 2011; Swartz & Lund, 2012). However, in MDA-MB-231 breast cancer cells this effect is counteracted by another competing mechanism, possibly via flow-induced mechanical activation of integrins. Flow strength, as well as cell density, dictate the final directional bias—with or against the flow (Polacheck et al., 2011).

ECM organization and mechanical properties are key regulators of cancer cell invasion and migration. Perhaps the most obvious example of this is the basement membrane (BM). This dense, collagen IV- and laminin-rich ECM sheet lines the basal surfaces in healthy epithelia, stratifying the tissues and supporting their normal apico-basal polarity. During tumorigenesis, normal tissue organization is impaired and carcinoma cells have to cross the BM before they can invade the surrounding stroma (Lee & Vasioukhin, 2008; Peglion & Etienne-Manneville, 2023). For example, mouse mammary ductal carcinoma in situ (DCIS) lesions lacking myosin

X-positive filopodia present with disrupted BMs, leading to an EMT-like phenotype and rapid progression to an invasive disease (Peuhu et al., 2022). Importantly, the nanoporous BM can act as a physical barrier to invasion and cancer cells typically cross it using proteolytic or—in the case of sufficiently plastic/malleable viscoelastic BM—purely physical mechanisms (Wisdom et al., 2018). Netrin-4 is a laminin binding partner that has recently been indicated as a key regulator of BM mechanics and permissivity to cancer cell invasion. Surprisingly, high netrin-4 expression correlates with improved survival in breast cancer and impedes local invasion and metastasis in mice, despite making the BMs softer and more porous (Reuten et al., 2021).

Cancer cell invasion can also be influenced by mechanical interactions with CAFs. First, CAFs can facilitate the breaching of the BM by physically pulling and stretching the structure, creating gaps through which the cancer cells can migrate (Glentis et al., 2017). Second, local invasion can be driven by heterotypic E-cadherin/N-cadherin interactions between the cancer cells and CAFs. Nectin and afadin promote CAF repolarization away from the cancer cells, while cadherins and α-catenin/vinculin mechanically couple the two cell types together. The CAFs then exert pulling forces on the cancer cells, leading them away from the bulk of the tumor (Labernadie et al., 2017). Third, CAFs may also restrict cancer cell migration by physically confining the tumor. Active compression of the cancer cells by CAFs is supported by a supracellular fibronectin network. Besides limiting cancer cell motility directly, CAF-mediated solid stress can also influence cancer cell mechanotransduction, e.g., by triggering YAP inactivation and nuclear exit (Barbazan et al., 2023).

Stromal ECM remodeling is also regulated by CAFs, and interstitial ECM organization plays a critical role in both normal and malignant cell migration. Proteolytic migration can create gaps and channels in the ECM, and such preformed structures may serve as conduits for T lymphocyte movement in normal tissues (Friedl & Bröker, 2000). Similarly, invading tumor cells often progress along pre-existing paths of least resistance (Gaggioli et al., 2007; Gritsenko et al., 2012). In addition, specific cancer-associated changes to the stromal ECM architecture are common in solid tumors and can directly contribute to cancer cell migration (Clark & Vignjevic, 2015). Radial collagen organization at the tumor-stroma interface facilitates invasion in preclinical models of breast cancer (Provenzano et al., 2006; Goetz et al., 2011), and the same tumor-associated collagen signature correlates with poor prognosis in human breast carcinoma (Conklin et al., 2011). CAF-derived ECM is also typically stiffer than normal interstitial ECM, and this pathological stiffness promotes further anisotropy in both stromal cells and newly synthesized ECM (Goetz et al., 2011; Malik et al., 2019). Thus, despite the overall increase in ECM density, desmoplastic stroma with its tracks and pro-migratory cues can often

facilitate cancer cell invasion instead of acting as a physical barrier. Interestingly, fibronectin appears to be a key ECM component promoting cancer cell migration along stromal tracks (Erdogan et al., 2017; Gopal et al., 2017). Inhibiting fibronectin assembly by CAFs impedes the invasion of CT26 mouse colon cancer cells—but without influencing the aligned topography of the surrounding collagen matrix (Attieh et al., 2017).

Physical guidance cues are not necessarily limited to tissue-scale tracks and barriers. Instead, many normal and cancer cells can detect and respond to different micro- and nanoscale substrate topographies. In particular, many cells preferentially elongate, align, and migrate parallel to linear nanoridges or nanogrooves—comparable in size to collagen fibrils—in a process called contact guidance (Kim et al., 2012). Contact guidance is generally thought to result from polarized alignment and organization of FAs and actomyosin that biases cell motility (Kim et al., 2009a; Robitaille et al., 2024). However, recent studies have suggested that the process is also heavily dependent on the cells' ability to penetrate into the spaces between the topographic features, which in turn is influenced by competing actin-related protein 2/3 (Arp2/3)- and formin-dependent actin architectures, microtubules, and the overall migratory phenotype (amoeboid versus mesenchymal) (Tabdanov et al., 2018, 2021). It is not surprising, then, that the exact dimensions of the topographic features are also important for contact guidance, and nanoridges that are too close to each other or too far apart can both inhibit polarized migration (Kim et al., 2009a).

In complex tissue microenvironments, the spacing between different micro- and nanotopographic features is unlikely to be even. "Topotaxis" refers to cell migration that is guided by a gradient of nanoscale topographic features, such as the density of ECM-coated nanopillars (Park et al., 2018). Topotactic responses are dictated by cortical contractility and the resulting deformability of the cell: if the cell is very compliant (i.e., it can fully envelop the topographic features) or fully non-compliant (i.e., it is localized on top of the features and unable to penetrate into the spaces between them), the directional cue is considered to be similar to haptotaxis and cells migrate up the gradient of ECM density (i.e., toward higher density of topographic features). However, in the case of intermediate cellular compliance, the cell may exhibit higher penetration between topographic features in the sparser substrate regions, biasing cell migration in the same direction (Park et al., 2018). This mechanism regulates in vitro topotaxis in different melanoma cell lines downstream of the phosphoinositide 3-kinase (PI3K) and ROCK pathways (Park et al., 2016), but the significance of topotaxis in cancer cell migration and invasion in vivo is currently unknown.

While the majority of studies have focused on the physical characteristics of the tumor stroma, the cancer cells themselves can also have distinct biomechanical properties. Somewhat paradoxically, the rigid tumors often house cancer cells that

are softer than the corresponding non-transformed cells (Alibert et al., 2017). Reduced cell stiffness also seems to correlate with more advanced disease and metastatic potential, and it is tempting to speculate that deformability supports cancer cell movement in complex microenvironments—either directly, by allowing migration through narrow constrictions, or through alternative mechanisms like topotaxis. However, it is still unclear whether any single biomechanical state can support cell motility and survival during every step of the metastatic cascade (e.g., within the bulk of the tumor and in the circulation), or if the successfully metastasizing cells have the ability to dynamically alter their intracellular machinery and mechanics to deal with different physical challenges (Gensbittel et al., 2021). For example, expression of oncogenic H-Ras^{G12V} makes breast epithelial cells softer during interphase, but the same cells exhibit increased mitotic stiffening. This helps limit DNA segregation errors during confined cell division (Matthews et al., 2020).

2.3.2 Cell migration and substrate stiffness

Cell migration is not only responsive to physical tracks and barriers. Instead, the bulk mechanical properties of the substrate can have a tremendous impact on cell motility. Tissue stiffness can induce EMT and collective migration in *Xenopus laevis* neural crest in vivo (Barriga et al., 2018), regulate traction force generation and migration speed in glioblastoma cells (Bangasser et al., 2017), and even promote persistent migration in fibroblasts and neutrophils (Oakes et al., 2009; Missirlis & Spatz, 2014). Adherent cells in soft environments tend to be round or isotropically spread, while stiffer substrates usually result in an elongated cell shape, polarized cytoskeleton, more stable and structurally distinct cell-ECM attachments, and higher traction forces exerted on the substrate—with some notable exceptions that will be addressed below and in the findings reported in this thesis (Ladoux et al., 2016; Kechagia et al., 2019).

2.3.2.1 Durotaxis in vitro and in vivo

Semantically, all of the above examples of mechanosensitive cell migration can be considered durokinesis, i.e., non-directional migratory responses induced by a strictly positional mechanical signal. However, substrate stiffness is also a well-known directional cue. Durotaxis (from Latin *durus*, hard, and Greek *taxis*, arrangement or order) was first described in 2000 by Lo and colleagues, who reported that NIH 3T3 fibroblasts grown on elastic polyacrylamide substrates coated with type I collagen could easily transition from soft to stiff hydrogel, but cells migrating from the stiff side turned around as soon as they reached the mechanical boundary (Lo et al., 2000). Since then, durotaxis has been reported to occur in

numerous different cell types, including mouse embryonic fibroblasts (MEF) (Plotnikov et al., 2012), mesenchymal stem cells (MSC) (Tse & Engler, 2011), and vascular smooth muscle cells (Isenberg et al., 2009; Hartman et al., 2016). Importantly, durotaxis is also commonly observed in different human cancer cells (DuChez et al., 2019; Zhang et al., 2020). The range and slope of the gradient both influence durotaxis, such that directed migration is usually stronger on steeper gradients (Isenberg et al., 2009; Vincent et al., 2013; Hadden et al., 2017) and on low-to-intermediate (~physiological or pathological/cancerous) stiffnesses. For example, MDA-MB-231 breast cancer cells and different glioblastoma cell lines display maximal durotaxis on gradients with elastic moduli (E) of 2–7 kPa, while their responsiveness is significantly decreased on 13–18 kPa gradients (DuChez et al., 2019). Durotaxis is also dependent on the ECM composition, and the vast majority of studies have been conducted using fibronectin as the bioactive ligand. In contrast, laminin-111 does not support durotaxis—at least in vascular smooth muscle cells (Hartman et al., 2016). Despite these variations in durotactic behavior, one thing has been observed relatively consistently: cells tend to migrate from soft to stiff environments, but not vice versa (Figure 3a).

Durotaxis is particularly well-studied on planar 2D substrates, but less is known about durotaxis in 3D and physiological settings (Shellard & Mayor, 2021a). Knockdown of Ena/VASP-like (EVL) inhibited MCF-7 breast cancer cell durotaxis in 2D and also impeded 3D migration from a 0.2 kPa collagen plug into surrounding 0.4 kPa matrix, whereas migration from 0.2 kPa to 0.2 kPa collagen matrix was not disrupted. However, the authors did not demonstrate bona fide directed migration between soft and stiff 3D matrix, and possible confounding factors like pore size were not investigated (Puleo et al., 2019). MSCs can migrate vertically into a compliant collagen overlay from soft but not stiff polyacrylamide hydrogels, suggesting that these cells might be capable of 3D durotaxis (Raab et al., 2012).

Durotaxis is also implicated in different developmental processes. *Xenopus* neural crest cells generate a stiffness gradient in the adjacent placodal tissue, then migrate up the gradient toward increasing stiffness via collective, polarized Rho GTPase activity and actomyosin contraction. Durotaxis and Sdf1-mediated chemotaxis cooperatively regulate neural crest cell migration in the developing embryo (Shellard & Mayor, 2021b). Durotaxis was also suggested to play a role in mouse development, where a stiffness gradient is established in the early limb bud in a Wnt5a-dependent manner. This gradient appears to direct mesodermal cell migration, however, these results could also be explained by haptotaxis along the overlapping fibronectin gradient (Zhu et al., 2020). In addition to embryonic development, durotaxis has been postulated to contribute to wound healing and/or pathological conditions like fibrosis, although there is a lack of conclusive experimental evidence for either claim (Yang & Plotnikov, 2021; Guo et al., 2023).

Durotaxis in the context of malignant tumors is a particularly interesting open question that will be discussed in detail below.

2.3.2.2 Molecular mechanisms of durotaxis

Numerous studies have addressed the molecular determinants of durotaxis, mainly by investigating individual cells in a 2D setting. In particular, there is an overwhelming amount of evidence linking the principal cellular mechanosensors, actomyosin and FAs, to directed migration toward stiffer substrates. High-resolution traction force microscopy (TFM) was used to show that the FAs in MEFs repetitively and autonomously "tug" on the underlying substrate, i.e, the location and magnitude of the traction force peak within the FA fluctuates. Tugging is more common on soft substrates and correlates with slower random migration. On stiffness gradients, preventing tugging behavior by targeting paxillin phosphorylation abolished MEF durotaxis (Plotnikov et al., 2012). Other tension-sensitive FA components, including vinculin (Plotnikov et al., 2012), zyxin (Yip et al., 2021), and FAK (Wang et al., 2001; Lachowski et al., 2018; Puleo et al., 2019) are also important for durotaxis. Additional proteins that localize at FAs, such as LIMD1, CdGAP (a Cdc42/Rac1 GAP), and EVL, help modulate FA maturation and dynamics. Knocking down these molecules impedes directed migration from soft to stiff environments (Wormer et al., 2014; Puleo et al., 2019; Wang et al., 2021).

As discussed above, actomyosin is fundamental to cell migration. Consequently, intracellular contractility and different actin regulators are also implicated in durotaxis. Inhibition of the actin-nucleating Arp2/3 complex impedes durotaxis in U-87MG glioblastoma cells (DuChez et al., 2019). However, Arp2/3 is not necessary for durotaxis in human RPE cells (Rong et al., 2021). This controversy may be at least partially explained by Hakeem and colleagues, who reported that either Arp2/3-dependent lamellipodia or fascin- and formin-like 3 (FMNL3)-dependent filopodia are sufficient to drive fibroblast durotaxis. However, both modes of mechanically directed migration require actomyosin contraction (Hakeem et al., 2023). MSCs on stiffness gradients exhibit rearward polarization of myosin IIB, and this myosin isoform was deemed particularly important for durotaxis (Raab et al., 2012). Finally, a linkage to cortical actomyosin also contributes to plasma membrane tension. Durotaxing cells present with asymmetric membrane tension, where the tension is higher at the leading edge (Hetmanski et al., 2019; Yang et al., 2020b). Low membrane tension at the cell rear promotes caveolae formation, RhoA activation, and rear retraction. Retraction also lowers local membrane tension, leading to biomechanical feedback that supports persistent migration and durotaxis (Hetmanski et al., 2019).

The key mechanotransducer YAP is required for durotaxis in hepatic stellate cells (Lachowski et al., 2018). YAP and its homolog transcriptional co-activator with PDZ-binding motif (TAZ) are both activated by cell spreading and stress fiber/FA formation on stiff substrates. The two proteins, in turn, regulate FA dynamics by promoting FA formation (Nardone et al., 2017) and/or by limiting overt FA maturation and cytoskeletal prestress, which was shown to enhance migration in endothelial colony-forming cells (Mason et al., 2019). Thus, the actin cytoskeleton, integrin-mediated adhesions, and YAP/TAZ activity are all interconnected and linked to cell migration and durotaxis.

Different organelles and additional cytoskeletal elements have also been linked to durotaxis. For example, durotaxis is inhibited by the disruption of MTs with nocodazole (Vincent et al., 2013; Rong et al., 2021). In RPE cells undergoing durotaxis, the Golgi is positioned in front of the nucleus—toward the stiffer substrate—to maintain front-rear polarity. Golgi-associated MTs, but not centrosomal MTs, were found necessary for normal FA dynamics and durotaxis (Rong et al., 2021). Polarized, anterior localization and fission of mitochondria provides ATP for cell migration, a process that is necessary for durotaxis in primary human lung fibroblasts (Guo et al., 2023).

2.3.2.3 Modeling durotaxis

Since the discovery of the phenomenon more than 20 years ago, researchers have attempted to create coherent theoretical models of durotaxis based on existing molecular-scale data and known cellular mechanoresponses. A so-called persistence-driven model posits that durotaxis could arise simply from increased migratory persistence on stiffer substrates (Novikova et al., 2017; Yu et al., 2017). While the notion of stiffness-dependent persistence is indeed supported by some experimental observations (Oakes et al., 2009; Missirlis & Spatz, 2014) and the mechanism could feasibly contribute to durotaxis, the model does not explain biased spreading and migration on steep stiffness gradients, where the cells have to break symmetry and polarize without first moving around (Breckenridge et al., 2014). The non-directional persistence-driven model can also be considered a type of durokinesis (Novikova et al., 2017).

Cell-ECM adhesion and application of traction forces on the substrate are ubiquitous to directed mesenchymal migration (Fortunato & Sunyer, 2022). Substrate stiffness-dependent and polarized traction forces have been observed in cells undergoing durotaxis (Lo et al., 2000; Trichet et al., 2012; Breckenridge et al., 2014) and, more recently, traction force asymmetry in MEFs was associated directly with preferential migration from soft to stiff environments (Jun et al., 2023). Accordingly, several computational models have reproduced single-cell durotaxis

by focusing on the mechanical features of actomyosin and FAs. Such models have assumed—a priori, but based on experimental evidence—that the formation and lifetimes of actin stress fibers and/or FAs are dependent on substrate stiffness and cytoskeletal tension (Bischofs & Schwarz, 2003; Dokukina & Gracheva, 2010; Feng et al., 2019; Rens & Merks, 2020). Harland and colleagues proposed a model where the generation of stress fibers is a stochastic, substrate stiffness-dependent process. The fibers are under tension and connected to FAs that provide drag, resulting from transient connections between adhesion receptors and the ECM. The model recapitulates some key aspects of durotaxis, including its responsiveness to the slope and range of the gradient (Harland et al., 2011). Moreover, some models focus on the mechanical qualities of fibrous ECM environments and how those impact the propagation of tension to elicit durotactic responses in the cells (Kim et al., 2018; Feng et al., 2019).

All of the above examples treat durotaxis as something that is intrinsic to individual cells. However, mechanically directed migration can also appear as an emergent property in larger cell collectives. Even when individual epithelial cells exhibit minimal durotaxis, cell-cell junctions can allow the contractile forces to be propagated across the whole monolayer. This leads to larger substrate displacements on the more compliant side, resulting in a net expansion and movement of the monolayer toward the stiffer substrate (Sunyer et al., 2016). Emergent collective durotaxis was explained quantitatively using a variant of the so-called “molecular clutch” model. This model and its broader significance for cell migration and durotaxis will be discussed at the end of this literature review. It should also be noted that durotaxis is not necessarily restricted to cell-ECM interactions. Instead, collective durotaxis of carcinoma cell clusters was observed also on E-cadherin-coated hydrogels. Similar to cell migration on ECM, a balance of cell-substrate adhesiveness, intracellular contractility, and out-of-plane surface tension (driven by cell-cell interactions) regulates spreading and directed motility on these mechanically graded substrates (Pallarès et al., 2023).

2.3.2.4 Is durotaxis always unidirectional?

Most cancers are characterized by extensive intra- and intertumor heterogeneity. Such variations are both genetic and phenotypic, and they include the biomechanical properties (e.g., elastic modulus) of the tumor (Plodinec et al., 2012; Acerbi et al., 2015; Miroshnikova et al., 2016). In breast cancer, the overall tissue stiffness and mechanical heterogeneity tend to increase from tumor core to periphery (Plodinec et al., 2012; Acerbi et al., 2015). Could durotaxis, then, drive cancer cell migration and dissemination in vivo? This line of thinking quickly leads to an apparent paradox, since most tumors are ultimately stiffer than the adjacent healthy tissue. In order to

leave the bulk of the tumor and metastasize, the cancer cell would have to migrate down a stiffness gradient. This contradiction has been recognized and dubbed a "migration paradox" (Shatkin et al., 2020).

Directed migration of cancer cells out of the tumor is likely driven by multiple mechanisms, including the previously discussed autologous chemotaxis. However, invasion could also be facilitated by an ability of cancer cells to either disregard local stiffness cues (adurotaxis) or migrate preferentially toward more compliant environments (negative durotaxis). So far, few reports have supported the existence of negative durotaxis. HT-1080 fibrosarcoma cells embedded in CRGDS peptide-functionalized polyethylene glycol (PEG) hydrogel can migrate from stiff (360 Pa) to soft (100 Pa) gel unimpeded, but their movement from soft to stiff regions is much more inefficient (Singh et al., 2014). This could be indicative of negative durotaxis, or it may reflect a steric hindrance resulting from different matrix architectures. When FA maturation was inhibited in MCF-7 cells by depleting EVL, the cells started turning away from locally strained substrate (Puleo et al., 2019). However, the most unequivocal evidence for directed cell movement toward softer tissue comes from neurons. In the embryonic *Xenopus* brain, axons of the retinal ganglion cells elongate to reach the optic tectum. Their pathfinding is facilitated by a gradient of decreasing stiffness—both in vitro and in vivo—and disrupting the gradient by pharmacological or mechanical interventions impairs normal neural development (Koser et al., 2016; Thompson et al., 2019). While mechanosensitive elongation alone is not considered bona fide durotaxis, neural growth cones contain dynamic actomyosin and cell-ECM adhesions, known as point contacts, and the structures share many similarities with migrating mesenchymal cells (Franze, 2020).

2.3.3 Geometric control of front-rear polarity and migration

Directed cell migration typically results from long-range gradients of soluble or immobilized cues that either attract or repel the moving cells. Such stable gradients can be difficult to establish and maintain in complex tissue microenvironments, particularly in the highly heterogeneous solid tumors (SenGupta et al., 2021). However, robust directed migration can also be achieved without any long-distance chemo-, hapto-, or durotactic signals. The trajectories of migrating cells are often described as persistent random walks. A local guidance cue can introduce a temporary bias to this process, directing cell motility. When such local cues are introduced to the cell repeatedly and consistently, the end result is long-range directed cell migration (Caballero et al., 2015).

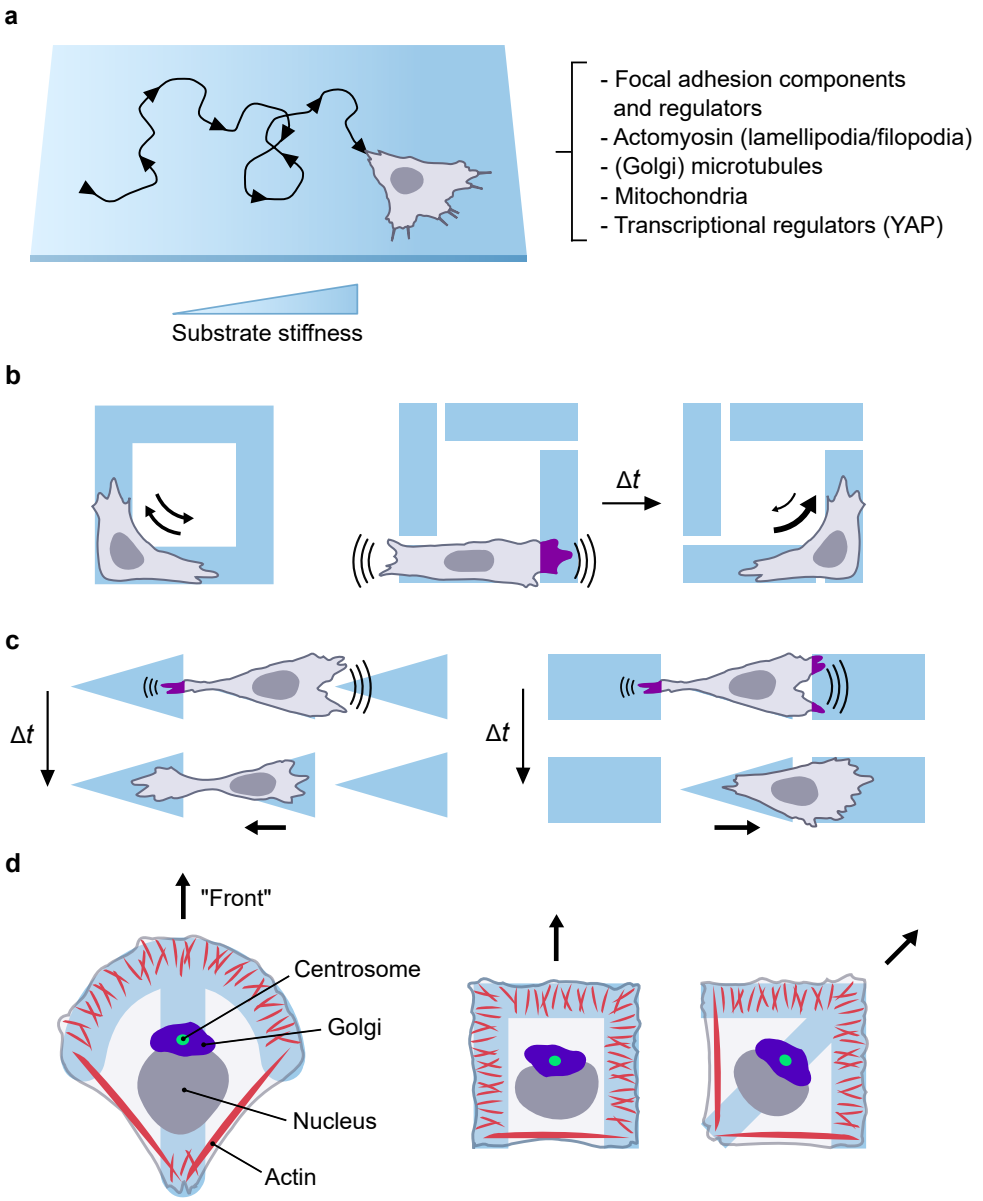

Figure 3. Cell migration and polarization are responsive to physical cues. **a**) Most cells migrate preferentially from soft to stiff environments (left). Examples of intracellular elements and organelles that have been linked to durotaxis (right). **b–c**) Geometry of the nearby ECM environment controls cell migration. Intermittent confinement of cells constrains their protrusive activity, leading to counterclockwise motion (b). Directed migration results from protrusion and the probability of the new projections to adhere and stabilize (c). Adapted from (Caballero et al., 2015). **d**) Anisotropy of the local ECM microenvironment induces front-rear polarization. Contractile stress fibers span the non-adhesive edges. MTs and FAs have been omitted for clarity. Adapted from (Théry et al., 2006).

Early work by Jiang and colleagues indicated that local substrate geometry can drastically bias cell migration. When NIH 3T3 fibroblasts were confined on adhesive micropatterns—shaped like teardrops or triangles to mimic the common polarized morphology of migrating mesenchymal cells—and later released to migrate, most cells started moving in the direction of the wide end of the pattern (Jiang et al., 2005). This behavior was recapitulated when multiple micropatterns were prepared end-to-end, allowing the fibroblasts to reach and migrate from one pattern to the next (Kumar et al., 2011). However, subsequent studies have demonstrated that context matters, and cell motility on repeating micropattern "ratchets" is dependent on the shapes of the individual patterns as well as their positions relative to one another. For example, elongated cells probe their environment by generating protrusions mainly from their two ends. Consequently, cells on cyclic paths consisting of four connected rectangles display no directional bias, but confining the cells intermittently by introducing narrow non-adhesive gaps in the path results in robust clockwise or counterclockwise migration (Ko et al., 2013) (Figure 3b). Cell migration on triangular ratchets is responsive to similar positional cues: if the triangles are wider or further apart, cells struggle to form stable adhesions on the narrow end of the adjacent pattern, favoring migration toward the larger neighboring region instead—in the direction of the narrow end of the original pattern. This bias is inverted when both adjacent micropatterns present the cells with similar target areas, and the cells simply migrate toward the direction they are more likely to probe (Caballero et al., 2014) (Figure 3c). Because the migratory responses to substrate geometry rely on a balance between cell protrusion and the likelihood of the new projections to bind ECM and stabilize, cell types with different morphologies—e.g., those with broad lamellae and those with longer, more narrow protrusions—can have different directional responses to the same environment. Indeed, some micropatterned ratchets have been used for sorting melanoma and breast cancer cells from normal fibroblasts (Mahmud et al., 2009).

What regulates cell protrusion on anisotropic substrates? New projections could be formed preferentially near the existing sites of cell-ECM attachment: for example, cells on square or rectangular micropatterns form FAs and exert traction forces on the underlying substrate mainly in their corner regions. The same sites also generate the majority of new lamellipodia (Parker et al., 2002; Chen et al., 2013). However, this does not explain the tendency of cells confined on teardrop-shaped micropatterns to generate protrusions (and eventually migrate) preferentially toward their blunt ends. Instead, work by Théry and colleagues demonstrated how the anisotropy of the local ECM microenvironment contributes to front-rear polarization and intracellular organization in human RPE cells (Théry et al., 2006) (Figure 3d). The side or region that contains more ECM—physiological integrin ligand—becomes the "leading edge", and cells position their centrosome, Golgi and MT array to face that side. This

process appears independent of actual cell shape, since even square cells can be forced to polarize simply by altering the underlying ECM distribution (Théry et al., 2006).

The importance of ECM-mediated signaling in the geometric control of cell polarity and motility was underscored by the finding that MEF migration on teardrop-shaped ratchets can be reversed by altering the ligand distribution on each individual micropattern. When the narrow end of the micropattern contains more fibronectin than the blunt end, polarity is inverted and the cells start migrating toward the narrow end (Lee et al., 2021). Moreover, migration on ratchets imparts the cells with a mechanical memory, and prior movement between two anisotropic micropatterns—forward or backward—further biases the next transition (Caballero et al., 2014). Clearly front-rear polarization influences migration and migration reinforces polarity as discussed above.

Additional biomechanical cues may influence the capacity of cells to detect and respond to local ECM anisotropy. Stiff ECM promotes frontward distribution of MTs in MSCs, and cells that are confined on crossbow-shaped micropatterns on soft (6 kPa) polyacrylamide gels lack the usual front-rear polarized distribution of myosin IIB (Raab & Discher, 2017). In mouse mammary epithelial cells, substrate stiffness directly promotes front-rear polarization and MTOC orientation toward ECM (Burute et al., 2017). The impact of ECM composition on front-rear polarity is less well understood. Most studies on the geometric control of cell polarity have been conducted using fibronectin-coated substrates, and very high surface concentrations of the protein have been suggested to inhibit morphological polarization in freely migrating CHO cells via dysregulated Rho GTPase signaling (Cox et al., 2001). In addition, the Cdc42/Rac1 GEF β-PIX is recruited from FAs to the leading edge to activate Cdc42 and suppress RhoA in fibrillar collagen but not fibronectin matrices. Consequently, depleting β-PIX leads to a severe collagen-specific migration defect in fibroblasts (Kutys & Yamada, 2014). Despite the significant influence of ECM composition on cell migration, including directional persistence (Missirlis et al., 2016), no systematic studies have been conducted on different matrix components in front-rear polarization and geometric control of cell migration.

Front-rear polarization in response to local ECM anisotropy has been observed in many cell types, including human cancer cells (Dubois et al., 2017). As mentioned, EMT leads to Par3-dependent repositioning of the centrosome from the apical pole to the center of the cell, which primes mesenchymal cells for migration and scattering (Burute et al., 2017). Cells in intermediate states of EMT, however, are characterized by destabilized MTs and decreased actomyosin contractility, which impedes normal front-rear polarization and MTOC reorientation in response to local ECM cues. Interestingly, such hybrid E/M states were suggested to be particularly common in triple-negative breast cancer cells (Margaron et al., 2019). It is currently

unknown whether local guidance cues, such as the anisotropy of the immediate ECM microenvironment, can meaningfully impact cancer cell migration in vivo. Nevertheless, the remarkable complexity of the typical tumor stroma should provide plenty of opportunities for this. In the absence of obvious interstitial tracks, local ECM geometry and composition may still bias cell movements and cooperate—or compete—with different long-range directional cues to regulate cancer cell invasion (Caballero et al., 2015).

2.4 Integrins

Integrins are the principal cell adhesion molecules mediating interactions between cells and the ECM. They are expressed in almost all human cells—with the exception of mature erythrocytes—and play key roles in practically all aspects of cell biology, from cell survival, growth, and division to more specialized processes like the regulation of cell identity. Integrins accomplish this by informing the cell about the biochemical and physical makeup of the extracellular milieu and by relaying these cues to different intracellular signaling networks (Humphries et al., 2019).

Integrins are obligate heterodimers. In humans, 18 different α subunits and 8 β subunits are needed to generate the 24 known integrin subtypes (Hynes, 2002). These 24 integrins are commonly stratified into four subfamilies based on their ligand recognition and expression profile (Figure 4a). Two of the groups bind the tripeptide sequence RGD and BM laminins, respectively, and their ancient orthologs are also found in other metazoans like flies and nematodes. In addition, vertebrates have a set of collagen-binding integrins and two related receptors (α4β1, α9β1) that recognize both ECM proteins and Ig-superfamily cell surface receptors. The fourth and final integrin subfamily consists of leukocyte-specific integrins. In reality, there is significant overlap between the binding specificities of the receptors in different integrin subfamilies. However, most integrins still appear to serve critical, non-redundant functions (Hynes, 2002).

Each integrin subunit consists of a large multi-domain extracellular part, a single-pass transmembrane domain, and a cytoplasmic tail. With the exception of integrin β4, the cytoplasmic domains are short (approximately 70 amino acids or less) but integral to the receptor's function. Integrins are often further classified into two groups based on their head domain: half of the α subunits (α1, α2, α10, α11, αL, αM, αX, αD, αE) contain an additional αI domain that serves as the ligand-binding site, but subunits lacking this domain still contribute to ligand binding specificity. In such cases, both α and β subunits are complexed to form the ligand binding head of the integrin (e.g., fibronectin engages βI domain via its RGD sequence but also binds the α5 subunit propeller domain via its synergy sequence) (Campbell & Humphries, 2011; Zhang & Chen, 2012). Integrin subunits dimerize in the endoplasmic

reticulum, and the receptors undergo post-translational modification in Golgi before transportation to the plasma membrane in a calcium-bound inactive state. At the cell surface, displacement of Ca^{2+} by Mg^{2+} (the main physiological cation) or Mn^{2+} enables integrin activation and ligand binding (Tiwari et al., 2011). In addition, some heterodimers may undergo rapid anterograde trafficking that bypasses the Golgi entirely (Lerche et al., 2022).

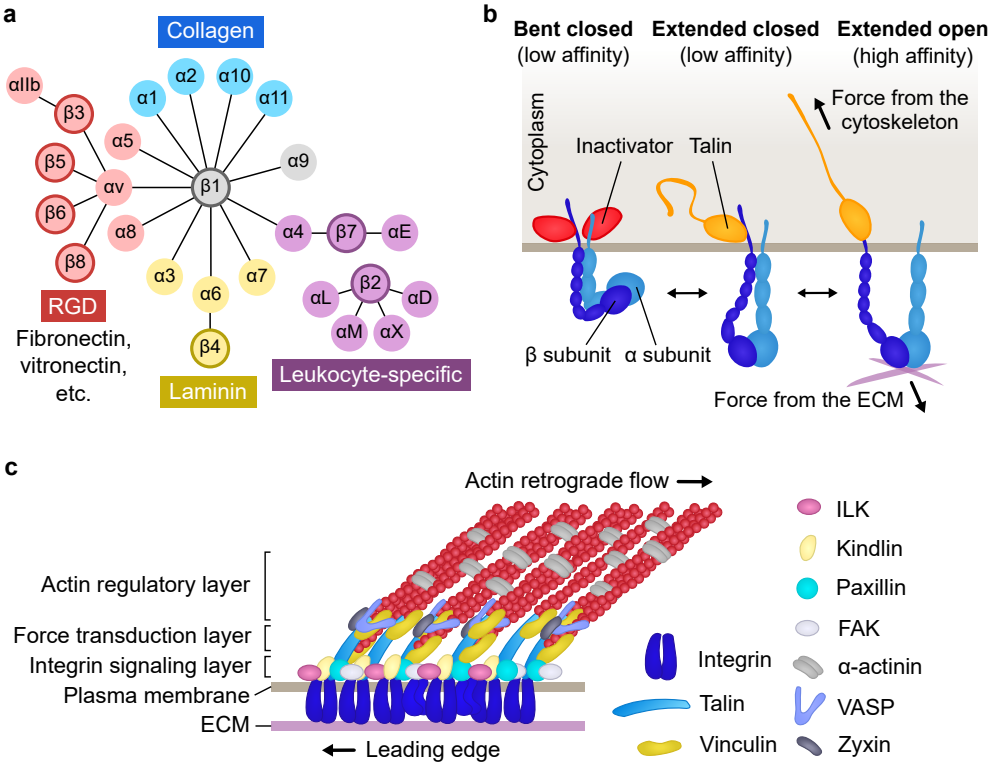

Figure 4. Integrins are key mediators of cell-ECM interactions. **a**) Mammalian integrin subunits and their classic stratification based on ligand recognition. Adapted from (Hynes, 2002). **b**) The switchblade model of integrin activation. Adapted from (Chastney et al., 2021; Kanchanawong & Calderwood, 2023). **c**) Simplified schematic representation of the FA (vertical) nanoscale organization. Adapted from (Kanchanawong et al., 2010; Isomursu et al., 2019; Kanchanawong & Calderwood, 2023).

After the integrins have reached the plasma membrane, their activation (and inactivation) remains tightly regulated. The ligand-binding receptor headpiece is connected to the transmembrane domains via α and β subunit "legs". Numerous X-ray crystallography, (cryo-)electron microscopy (EM) and cryo-electron tomography

(cryo-ET) studies have revealed that integrin heterodimers can undergo remarkable conformational changes (Xiong et al., 2001; Takagi et al., 2002; Nishida et al., 2006; Cormier et al., 2018; Sorrentino et al., 2021). In particular, integrins can adopt a bent conformation where the headpiece folds back against the legs, while the legs, transmembrane domains and cytoplasmic tails of the two subunits are kept close to one another. Although the extent of bending may vary between different integrin subtypes (Miyazaki et al., 2018; Schumacher et al., 2021), this conformation is now widely accepted to represent an inactive form of integrins that exhibits low affinity to extracellular ligands. Upon receptor activation, the headpiece swings out, and the subsequent separation of the integrin legs and cytoplasmic tails leads to allosteric changes in the headpiece that promote ligand binding (Campbell & Humphries, 2011; Chastney et al., 2021) (Figure 4b). The extended open conformation is colloquially known as the active integrin conformation.

How are the different conformational states of integrins regulated? The bent conformation can be stabilized by different integrin inactivators that engage the tail of the α (e.g., SHANK-associated RH domain-interacting protein [SHARPIN]) or β (e.g., filamin, docking protein 1 [DOK1]) subunit (Bouvard et al., 2013). In contrast, binding of talin to the β subunit cytoplasmic domain decouples the integrin tails, favoring the high-affinity extended open conformation. Kindlin cooperates with talin in integrin activation by stabilizing the talin-integrin bond and by facilitating integrin clustering and binding to multivalent ECM ligands (Theodosiou et al., 2016; Li et al., 2017; Lu et al., 2022; Bodescu et al., 2023). Talin- and kindlin-mediated conformational changes and subsequent ligand engagement in the high affinity state are often referred to as inside-out integrin signaling. Conversely, it is thought that integrin activation can also be initiated by the binding of extracellular ligands in the low-affinity state, which then supports a shift to the extended open conformation. This notion of outside-in signaling was recently supported by the discovery that the low-affinity integrin conformations have faster ligand binding kinetics (as well as significantly higher off-rates) than the high-affinity extended open state. Thus, integrin binding to the ECM could initially happen in the low-affinity state, which would then be followed by a rapid conversion to the high-affinity state that supports coupling to cytoplasmic adaptors and the actin cytoskeleton (Li et al., 2021).

In addition to being important for normal homeostasis, integrins are implicated in different pathological conditions like cancer. Altered integrin expression profiles have been reported in many types of solid tumors, and the receptors can drive cell survival and proliferation, regulate dormancy, or contribute to drug resistance (Hamidi & Ivaska, 2018). Integrins are also central components of the multimolecular assemblies that link the intracellular cytoskeleton to the ECM to drive cancer invasion. Next, we will review how these remarkably complex structures are assembled, organized, and used by the cell to probe the extracellular

environment and transmit tensile forces necessary for ECM remodeling and cell migration.

2.4.1 Structural and functional heterogeneity of integrin adhesion complexes

Cell-ECM interactions take place at various specialized, multimolecular structures called integrin adhesion complexes (IAC). IACs are used by the cell to sense and exert physical forces, and they also serve as sophisticated intracellular signaling hubs. To this end, the dynamics and composition of the IACs have to be carefully regulated (Chastney et al., 2021; Kanchanawong & Calderwood, 2023).

Nascent adhesions (NA) are the first IACs that appear at the leading edge when a cell generates new lamellipodia and moves forward. They are small and contain <100 integrin heterodimers (Changede et al., 2015). Integrin clustering to NAs is supported by receptor activation, talin, kindlin—the first component complexed with integrins in these structures—and actin polymerization, but myosin II activity or rigid substrate are not necessary for NA formation (Choi et al., 2008; Bachir et al., 2014; Changede et al., 2015). Paxillin, FAK, and vinculin are also quickly recruited to these early IACs (Zaidel-Bar et al., 2003; Choi et al., 2011; Bachir et al., 2014). In addition, transient α-actinin-integrin complexes were suggested to help nucleate NAs in CHO-K1 cells (Bachir et al., 2014).

Most NAs are short-lived, and they turn over and disappear within ~2 min (i.e., when they reach the back of the lamellipodium). However, some NAs can grow in size and undergo a series of tension-dependent compositional and structural changes, known as adhesion maturation, to become focal complexes and later FAs (the distinction is somewhat arbitrary due to a lack of strict criteria for each IAC) (Kanchanawong & Calderwood, 2023). FAs are elongated, ordered, and often comparatively stable structures that are typically ~1–5 μm in size. They are the most extensively studied IACs and play a key role in cell-ECM adhesion and migration—as eluded to in the previous chapters.

Systematic mapping of the 3D organization of IACs has been facilitated by advances in optical imaging. In 2010, the vertical nanoscale organization of FAs was resolved in MEFs and U-2OS osteosarcoma cells and revealed multiple partially overlapping layers (Kanchanawong et al., 2010) (Figure 4c). The ~20-nm region around integrin cytoplasmic tails is called the integrin signaling layer and contains most of the kindlin, FAK, paxillin, and integrin-linked kinase (ILK) molecules. The talin N-terminal head domain that binds the integrins is also located in this layer. The adjacent layer is known as the force transduction layer, so called because it contains two key mechanosensory molecules, talin and vinculin. The third and final layer—the actin regulatory layer—is located ~40–80 nm above the plasma membrane, and

it is characterized by actin-associated proteins like zyxin, vasodilator-stimulated phosphoprotein (VASP), and α-actinin that mediate a connection between the FA and actomyosin. This multilayer hierarchy appears highly consistent in FAs of different shapes and sizes (Kanchanawong et al., 2010). Importantly, subsequent studies have reproduced many of these findings in other cells, albeit highlighting some cell type-specific differences (Liu et al., 2015a; Stubb et al., 2019).

Mature IACs are also organized laterally. For example, the distal end of the FA (i.e., toward the cell periphery) is often enriched in paxillin and phosphotyrosine, while different actin-associated proteins—such as vinculin, zyxin, and tensin—are concentrated at the proximal end (Zamir et al., 1999; Legerstee et al., 2021). In addition, superresolution microscopy has revealed the presence of distinct nanoclusters within FAs. These are punctate regions of high local IAC protein density, with diameters in the order of 100 nm or less (Rossier et al., 2012; Spiess et al., 2018). Interestingly, active and inactive β1 integrins segregate into separate nanoclusters, which are further aligned into linear substructures within the FA (Hu et al., 2015; Spiess et al., 2018). This suggests that integrin activity in each nanocluster can be coordinated locally. Inactive integrins can also diffuse laterally in the plasma membrane until they engage an extracellular ligand. Unsurprisingly, receptor immobilization is more prevalent inside than outside FAs (Rossier et al., 2012).

The molecular mechanisms governing FA nanoarchitecture have not been fully elucidated. However, talin is thought to play a significant role in IAC organization. The protein is long—50–60 nm even when fully folded and typically longer in cellulo (Gough & Goult, 2018)—and adopts a highly polarized orientation in mature IACs, spanning the whole vertical nanoscale structure from the integrin signaling layer to the actin regulatory layer (the protein is reportedly aligned ~15° relative to the plasma membrane). Truncated talin mutants alter the axial positions of other FA components like VASP, indicating that talin serves as a molecular "backbone" that governs FA organization (Liu et al., 2015a). Moreover, full-length talin contains a C-terminal dimerization domain that is important for talin-mediated integrin clustering and ligand binding, suggesting that talin may also contribute directly to lateral IAC nanoarchitecture (Lu et al., 2022). Finally, talin also interacts with the KN motif and ankyrin repeat domains (KANK) family of adaptor proteins, mediating MT targeting to FAs (Bouchet et al., 2016).

Mature FAs are compositionally diverse, consisting of a large number of different scaffolding proteins and enzymes. In fact, nearly 20% of the human kinome has been associated with IACs (Schoenherr et al., 2018). Mass spectrometry-based analyses of IACs purified from different cell types have revealed a so-called "meta-adhesome" consisting of >2,400 proteins. This list of IAC-associated proteins was further refined and narrowed down to yield a near-ubiquitous "consensus adhesome"

of 60 proteins (Horton et al., 2015). Integration of these results with the literature-curated adhesome (Horton et al., 2016) and additional studies analyzing proximity-labeled IAC components (Dong et al., 2016; Chastney et al., 2020) illustrate the staggering molecular and topological complexity of IACs in human cells. Nevertheless, the core adhesome components have been broadly divided into four canonical signaling modules, centered around ILK, PINCH, parvin, and kindlin; FAK and paxillin; talin and vinculin; and α-actinin, zyxin, and VASP. These modules can be further stratified into two main signaling axes, responsible for cytoskeletal mechanotransduction and protein phosphorylation/GTPase signaling (Horton et al., 2016; Humphries et al., 2019). Regulation of the Rho GTPases by the IACs, for example, helps explain the connection between integrin activation, cell protrusion, and front-rear polarity (Etienne-Manneville & Hall, 2001; Theodosiou et al., 2016). Other prominent signaling networks activated by integrins—often in conjunction with other receptors like the GPCRs—include the FAK/Src, ERK, and AKT pathways (Lee & Juliano, 2000; Short et al., 2000; Sulzmaier et al., 2014).

Integrin-mediated signaling can be induced via integrin activation, i.e., by increasing the affinity of individual integrin heterodimers to their extracellular ligands. However, increasing integrin avidity via receptor clustering can also promote downstream signaling responses. The distinction is surprisingly important, as several studies have indicated that integrin ligation and clustering can have overlapping but dissimilar biological outcomes. In leukocytes, activation of integrin αLβ2 using Mn^{2+} is not sufficient to elicit receptor clustering without a separate multimeric ligand (Kim et al., 2004). Clustering of αMβ2 integrin, another leukocyte-specific integrin subtype, is enough to stimulate AKT and ERK signaling even when the receptors are locked in the low-affinity state. αMβ2 activation, on the other hand, promotes AKT but not ERK signaling. Functionally, clustering of inactive αMβ2 in the presence of concomitant pro-apoptotic cues protects the cells from apoptosis, but receptor ligation leads to cell death (Whitlock et al., 2000). The major platelet integrin αIIbβ3 also appears to rely on clustering to exert its functions: platelet activation promotes αIIbβ3 avidity via increased clustering to multivalent ligands, but without influencing αIIbβ3 affinity to monovalent targets (Bunch, 2010). This effect is probably mediated by kindlins (Ye et al., 2013).

Similar observations have been made regarding β1 integrins. In a study by Miyamoto et al., soluble monovalent ligands like GRGDS did not induce tyrosine phosphorylation in fibroblasts (Miyamoto et al., 1995). However, beads coated with mAb13—a bivalent monoclonal antibody that binds the headpiece of integrin β1 and stabilizes the closed, low-affinity receptor conformations (Su et al., 2016)—were sufficient to elicit integrin clustering and signaling responses. The authors suggested that both β1 ligation and clustering are needed to recruit all the core IAC components to the receptors (Miyamoto et al., 1995). Taken together, it appears clear that integrin

cytoplasmic domains can remain biologically active even in the absence of heterodimer opening, so long as the receptors are brought to close proximity. In other words, integrin clustering is a key functional aspect of IAC-mediated signaling.

It is worth noting that most of our knowledge about the IACs comes from studies conducted on planar 2D substrates. Migrating cells have also been shown to present with punctate or elongated IACs in vivo, on artifical cell-derived matrices, and while fully embedded in reconstituted 3D ECM (Cukierman et al., 2001; Harunaga & Yamada, 2011). However, while these structures contain many of the same consensus adhesome components as the 2D IACs, 3D and 2D adhesions are often morphologically and compositionally distinct. Much of this variation is likely to be explained by the different biophysical properties (e.g., topography, viscoelasticity) of each microenvironment (Doyle & Yamada, 2016). Recently, a proximity labeling- and proteomics-based study compared paxillin- and talin-associated MDA-MB-231 breast cancer cell adhesomes in 2D versus 3D microenvironments. While the IACs in both conditions contained many of the same proteins, the results also revealed several differences and highlighted the enrichment of β-PIX and the unconventional myosin 18A at 3D adhesion sites (Newman et al., 2023).

In addition to FAs and their precursors, there are other specialized IACs that serve different biological functions. Filopodia tip adhesions are recently characterized, small, and compositionally distinct IACs that are enriched in myosin X. When the cell moves over stabilized filopodia, the tip adhesions can give rise to NAs that later mature into FAs (Jacquemet et al., 2019). Reticular adhesions are another recently reported type of IAC. These integrin αvβ5-containing structures lack many of the common IAC components and features, including talin and F-actin. However, reticular adhesions have already been implicated in e.g., cell migration and coordination of mitosis (Lock et al., 2018; Hakanpää et al., 2023). Invadopodia, and the closely related podosomes in non-malignant cells like macrophages, are specialized proteolytic structures. They are small, cylindrical, and contain typical IAC components like talin and paxillin organized around a protrusive actin core. Unlike FAs, the invadopodia are often associated with low actomyosin contractility (Linder et al., 2023).

In some cell types, such as fibroblasts, FAs may undergo further maturation into thin, elongated IACs known as FBs (Zamir et al., 1999). FBs are more centrally located, enriched in integrin α5β1 and tensins, and they play a key role in fibronectin fibrillogenesis and ECM remodeling as discussed below.

2.4.2 IACs and the extracellular matrix

The ECM refers to the non-cellular component present in all human tissues and organs. Composed mainly of water, proteoglycans (e.g., hyaluronic acid, heparan

sulfate), and different fibrous proteins (e.g., collagens, fibronectin, laminin), the various tissue-specific ECMs are unique in their architecture and molecular makeup (Frantz et al., 2010). Moreover, tumorigenesis and cancer progression elicit drastic changes in the stromal ECM, leading to altered mechanoresponses and cell migration (Cox & Erler, 2011; Nia et al., 2020).

ECM composition influences the mechanical properties of the tissue. However, it also determines the subset of cell adhesion molecules—typically integrins—the cells can use to interact with the matrix. Different integrin subtypes have overlapping but distinct ligand specificities and, importantly, they can also exhibit different ligand binding kinetics and downstream signaling responses (Seetharaman & Etienne-Manneville, 2018). For example, integrin α4β1 has a significantly lower tension threshold for initiating cell spreading on fibronectin than two other fibronectin-binding β1 integrins, α5β1 and αvβ1 (Jo et al., 2022). The RGD-binding integrins α5β1 and αvβ3 have particularly well-studied and complementary biomechanical and signaling properties, where α5β1 promotes strong attachment to the substrate, myosin II-mediated contractility, and coordinated force transmission, while αvβ3 is more responsive to external mechanical cues and promotes actin polymerization through mammalian Diaphanous-related formin (mDia) activation (Roca-Cusachs et al., 2009; Schiller et al., 2013; Balcioglu et al., 2015). Both heterodimers cooperate to drive persistent cell migration on fibronectin matrices (Missirlis et al., 2016). Thus, cellular responses to tissue biomechanics are in fact a collective outcome of the mechanical and biochemical properties of the ECM as well as the integrin repertoire and cytoskeletal machinery of the mechanosensing cell (Seetharaman & Etienne-Manneville, 2018; Isomursu et al., 2019). The functional implications of this are obvious, and ECM composition can significantly influence nuclear mechanotransduction (Kechagia et al., 2023), cancer cell invasion in biomimetic hydrogels (Taubenberger et al., 2016), or durotaxis (Hartman et al., 2016).

In addition to cell migration and other, cell-intrinsic functions, integrins are also needed for ECM deposition and remodeling. Fibronectin is a large ECM protein that consists of two nearly identical 230–270 kDa subunits, both composed of multiple type I, type II, and type III repeats. The 10th type III repeat contains an RGD motif, and the 9th type III repeat contains the synergy sequence that is needed for efficient integrin α5β1 binding. The two fibronectin subunits are held together by C-terminal disulfide bonds (Singh et al., 2010). Fibronectin is a major component of fibrotic and malignant interstitial matrices and plays a key role in cancer cell invasion (Attieh et al., 2017; Gopal et al., 2017). In addition, there is ample evidence that fibronectin can template and promote the assembly of other matrix components, including collagens, fibrillin, and tenascin-C, making the protein important for the overall

ECM organization (McDonald et al., 1982; Chung & Erickson, 1997; Velling et al., 2002; Sabatier et al., 2009; Saunders & Schwarzbauer, 2019; Musiime et al., 2021).

Integrin α5β1 is a key mediator of fibronectin fibrillogenesis. In specific cell types, such as fibroblasts and endothelial cells, fibronectin-bound α5β1 translocates centripetally out of peripheral IACs. The receptors move, pulled by the actomyosin cytoskeleton, and exert tensile forces on the bound fibronectin. This leads to conformational changes in the fibronectin molecules, promoting their assembly into fibrils (Zhong et al., 1998; Pankov et al., 2000; Zamir et al., 2000; Smith et al., 2007; Singh et al., 2010). The centrally located and α5β1-rich FBs are characterized by the replacement of talin by tensin, mediated possibly by phosphorylation of the β1 cytoplasmic tail membrane-proximal NPxY motif (Zamir et al., 1999; McCleverty et al., 2007). Out of the three full-length tensin isoforms in humans, tensin-1 and tensin-3 have been shown to localize at FBs (Clark et al., 2010). This talin-to-tensin switch is considered functionally important, as dominant-negative tensin prevents FB formation and fibrillogenesis without disrupting the peripheral FAs (Pankov et al., 2000). However, others have reported unimpeded fibronectin assembly despite a combined knockdown of all three tensin isoforms (Clark et al., 2010). Despite the loss of talin in FBs, the majority of α5β1 heterodimers remain active and are recognized by the conformation-specific SNAKA51 antibody. This is due to tensins retaining the integrins in their extended open conformation and connected to the actin cytoskeleton (Georgiadou et al., 2017). Moreover, priming the α5β1 integrins with SNAKA51 promotes fibrillogenesis (Clark et al., 2005).

Despite the integral role of the α5β1 heterodimer in fibronectin assembly, other integrins are also implicated in the process. Ligation of integrin αvβ3 is necessary for fibronectin fibrillogenesis in primary human fibroblasts (Pankov et al., 2000), and the receptor is also needed for CAF-mediated fibronectin assembly and subsequent invasion of colon cancer cells in 3D collagen matrices (Attieh et al., 2017). In the latter model, αvβ3 activation and clustering preceded integrin α5β1-mediated fibrillogenesis. However, even in the absence of active α5β1, αvβ3 integrins may assemble fibronectin matrix that is biochemically indistinguishable from α5β1-associated fibronectin (Wu et al., 1996).

Complex microenvironments may further alter the composition of fibronectin-assembling IACs. For example, adhesion to BM components promotes fast and robust fibrillogenesis, where the entire α5β1-based FA slides along the matrix through myosin IIA-dependent actomyosin contraction. Unlike the classic FBs, these atypical IACs are phosphotyrosine-rich and contain paxillin and FAK (Lu et al., 2020). Similar integrin α5β1-, paxillin-, FAK-, and phosphotyrosine-rich—but αvβ3-poor—IACs were observed parallel to fibronectin fibers in cell- and tissue-derived 3D matrices. Preventing fibronectin remodeling through matrix fixation and

crosslinking abolished the formation of these elongated adhesions (Cukierman et al., 2001).

In addition to integrins, tensin, and actomyosin, fibronectin fibrillogenesis is regulated by e.g., AMPK (Georgiadou et al., 2017), Rho GTPases (Sundararaman et al., 2020), and HIC-5 (Goreczny et al., 2018). Because fibronectin assembly relies on mechanical tension to elicit conformational changes in the fibronectin molecules, soft substrates can inhibit fibrillogenesis (Carraher & Schwarzbauer, 2013). This suggests yet another pathological feedback loop that is relevant to fibrosis and cancer-associated stromal remodeling. Moreover, substrate rigidity has been reported to stabilize tensin-1 in FAs (Stutchbury et al., 2017), and very soft (1 kPa) substrates can limit the formation of tensin-1-positive FBs in polyoma middle T (PyMT) CAFs (Goreczny et al., 2018). However, a systematic survey of FB sensitivity to substrate mechanics has not been conducted.

2.4.3 IACs sense and transmit forces

As the principal receptors connecting the intracellular cytoskeleton to the ECM, integrins are uniquely poised to sense and transmit physical forces across the plasma membrane. Conversely, the physicochemical properties of the extracellular microenvironment regulate integrin activation and IAC function on multiple levels, leading to intricate biomechanical crosstalk that influences most aspects of cell biology—including migration (Sun et al., 2016; van Helvert et al., 2018; Kechagia et al., 2019).

Previously, we discussed how conformation influences integrin affinity to extracellular ligands. In addition to the cytoplasmic adaptor proteins, integrin activation can be facilitated directly by forces exerted through bound ligands. Molecular dynamics simulations have predicted (Zhu et al., 2008; Puklin-Faucher & Vogel, 2009; Chen et al., 2011) and single-molecule measurements confirmed (Chen et al., 2012, 2017) that physiologically relevant piconewton-scale forces can promote receptor extension and/or headpiece opening in different integrin heterodimers. This observation is interesting for two reasons. First, it further supports the concept of outside-in signaling, where rapid ligand engagement in the low-affinity (but high on-rate) state would allow the application of forces on the heterodimer, promoting a switch to the high-affinity conformation (Li et al., 2021). Second, even when the integrin engages its ligand in the active state, mechanical tension may help retain the receptor in the extended open configuration, stabilizing the interaction with the ligand.

Chemical bonds that are strengthened by the application of force are called catch bonds, in contrast to the more intuitive slip bonds, where force decreases bond lifetime. In practice, even catch bonds will enter a slip regime when a specific force

threshold is reached, and increasing the force even further will weaken the bond (Rakshit & Sivasankar, 2014). Such catch-slip bonds have been observed in many integrin subtypes, including α5β1, αvβ3, and α4β1 (Friedland et al., 2009; Kong et al., 2009; Choi et al., 2014; Chen et al., 2017). Interestingly, integrin catch-slip behavior can be influenced drastically by different ionic conditions (Kong et al., 2009) or crosstalk with other signaling pathways (Choi et al., 2014). In addition to integrins and their ligands, catch bonds have also been observed in other IAC components. For example, vinculin forms a directionally asymmetric catch-slip bond with F-actin, which may help establish long-range order in the actin cytoskeleton (Huang et al., 2017). The mechanosensitive nature of individual integrin heterodimers may be fundamental to their activation. Thermodynamic evaluation of the different integrin conformations has indicated that only the combination of adaptor proteins—like talin—and cytoskeletal forces in the low piconewton range can activate integrins in a sensitive, switch-like manner, i.e., over a reasonably narrow range of signal input (Li & Springer, 2017).

Integrin clustering and IAC organization are also regulated by physical forces. For example, the mechanical properties of the underlying substrate can restrict the lateral movement of ligand-bound integrins. If the ligand density is sufficiently low, this may prevent integrin clustering altogether (Chaudhuri et al., 2014). On the other hand, the glycocalyx—a glycoprotein and glycolipid coat surrounding the cells—can facilitate integrin clustering. Because the glycocalyx extends further from the plasma membrane than the ~20-nm length of integrins, it creates a steric barrier to integrin-ECM interactions. In order to bind the substrate, the integrins must locally bend the plasma membrane and compress the glycocalyx. This exerts a tensile force on the ligand-bound integrins, influencing their conformation and downstream signaling. Further, laterally diffusing integrins in the vicinity of the ligated heterodimers are in close proximity of the ECM, and therefore more likely to interact with it (Paszek et al., 2009, 2014).

The gradual maturation of NAs into FAs is a tension-dependent process (Pelham & Wang, 1997; Galbraith et al., 2002; Kanchanawong & Calderwood, 2023). In fact, physical forces are so integral to the composition and function of these IACs that it is possible to predict the forces exerted by the cell on its substrate using only images of a single FA protein like zyxin as input (Schmitt et al., 2024). Different adhesome proteins are recruited to and retained in the IACs in a tension-dependent manner, and force influences the post-translational modification and downstream signaling of various IAC components (Kuo et al., 2011; Stutchbury et al., 2017; Tao et al., 2023). In addition, cytoskeletal tension (or lack thereof) is thought to play a role in the disassembly and turnover of FAs behind the leading edge and at the cell rear—a key requirement for efficient cell migration (Crowley & Horwitz, 1995; Kuo et al., 2011;

Yu et al., 2015). But what makes IACs and their components so sensitive to physical forces?

Many core IAC components can undergo conformational changes in response to mechanical force, which may influence their binding and unbinding kinetics as discussed above. More importantly, large changes in tertiary structure and partial unfolding may reveal additional cryptic binding sites that are recognized by other proteins. The mechanosensitive recruitment of vinculin to talin following the unfolding of talin rod domain, in particular, is a critical step that precedes FA maturation and associated downstream signaling responses (del Rio et al., 2009; Carisey et al., 2013; Atherton et al., 2015; Austen et al., 2015; Rahikainen et al., 2017; Goult et al., 2018). The two talin isoforms in humans both consist of an N-terminal FERM domain, a disordered linker region, and a C-terminal rod with 13 multihelix bundles (R1–R13). Most of the rod subdomains are known to contain cryptic binding sites for vinculin. In addition, talin contains three distinct actin-binding sites (ABS) (Goult et al., 2018). The current model for talin-mediated FA maturation is based on a series of progressive mechanosensing events: after talin has engaged the β1 integrin cytoplasmic tail via its FERM domain, actin binding to talin C-terminal ABS3 results in tension that opens the rod R3 subdomain. This allows actin binding to ABS2 and vinculin recruitment to the adjacent binding site, preventing talin refolding and reinforcing the connection between talin and the actin cytoskeleton, which enables FA formation and increased transmission of cytoskeletal forces to the substrate (Atherton et al., 2015). In addition to talin and vinculin, other adhesome proteins like p130Cas can undergo major force-mediated conformational changes that have been linked to IAC maturation and/or signaling (Sawada et al., 2006; Zhao et al., 2016; Jacquemet et al., 2019). α-actinin- and myosin II-mediated actin bundling is also important for IAC maturation, and aligned actin filaments may serve as templates for the hierarchical addition of other IAC components (Choi et al., 2008).

IACs exhibit reciprocal crosstalk with other mechanosensory pathways and organelles. For example, mechanosensitive ion channels Piezo1 and Piezo2 associate with IACs at the leading edge, regulating their maturation and turnover. However, this interaction appears less pronounced in cancer cells (Pardo-Pastor et al., 2018; Yao et al., 2022). Piezo channels can regulate cellular responses to substrate stiffness (Pardo-Pastor et al., 2018) and deformation, even at the nanoscale (Peussa et al., 2023), suggesting that these proteins play a key role in maintaining cellular mechanostasis. Integrin clustering and IAC maturation can also promote actin polymerization and stress fiber formation, which often directly influences the subcellular localization and activity of other proteins, including MRTF and YAP (Vartiainen et al., 2007; Das et al., 2016). In addition, mechanical forces can be propagated through IACs and actomyosin to the nucleus and nucleoskeleton, where

they may influence transcription and/or other phenotypic adaptations by facilitating the (de)phosphorylation of nuclear proteins, by increasing the permeability of the nuclear pores (which further facilitates the nuclear transport of proteins like YAP), and by physically deforming chromatin (Kirby & Lammerding, 2018).

Integrins and IACs play a key role in transmitting cytoskeletal forces to the extracellular microenvironment to drive ECM remodeling and cell motility. Based on the above examples, it is also clear that physical forces fundamentally influence IAC composition, nanoarchitecture, and function, leading to phenotypic adaptations at the cellular level. But how can cells detect and respond to passive biomechanical properties of the ECM, such as elasticity, in the absence of external forces? To probe substrate stiffness, cells have to use their own actomyosin cytoskeleton and IACs to deform the substrate. The resulting forces will vary based on ECM rigidity, and cells can use this information to indirectly detect differences in substrate mechanics (Kechagia et al., 2019). Such active probing can occur even in small integrin nanoclusters, where contractile actomyosin units have been shown to respond to substrate stiffness by initating the recruitment of α-actinin and presumably other IAC components (Ghassemi et al., 2012; Wolfenson et al., 2016; Yang et al., 2020a).

2.4.3.1 The molecular clutch

The molecular clutch model (also known as the motor-clutch model) refers to a general biomechanical model that is now commonly used to explain actin movements, dynamics of cell adhesion molecules, membrane protrusion, and generation of traction forces in adherent cells (Figure 5a). In addition, the model recapitulates well different cellular responses to substrate biomechanics, including ECM stiffness and ligand density (Case & Waterman, 2015; Elosegui-Artola et al., 2018).

Following a number of experimental findings, including the observation that actin undergoes constant treadmilling at the leading edge in migrating fibroblasts (Wang, 1985), Tim Mitchison and Marc Kirschner proposed the molecular clutch model in the late 1980's to explain the movement of neural growth cones during axon outgrowth (Mitchison & Kirschner, 1988). The model posits that actin polymerization against the plasma membrane at the leading edge, together with myosin II-mediated contraction, creates a net rearward flow of F-actin. In order to protrude forward and move, the cell must link these actin filaments physically to the underlying ECM using transmembrane "clutches" (most commonly IACs). At the same time, this mechanical connection transmits cytoskeletal traction forces to the substrate. Since the retrograde flow of actin is constant but forward movement tends to be variable, the coupling between actin and the ECM must incorporate slippage—the clutches have to be transient (Mitchison & Kirschner, 1988).

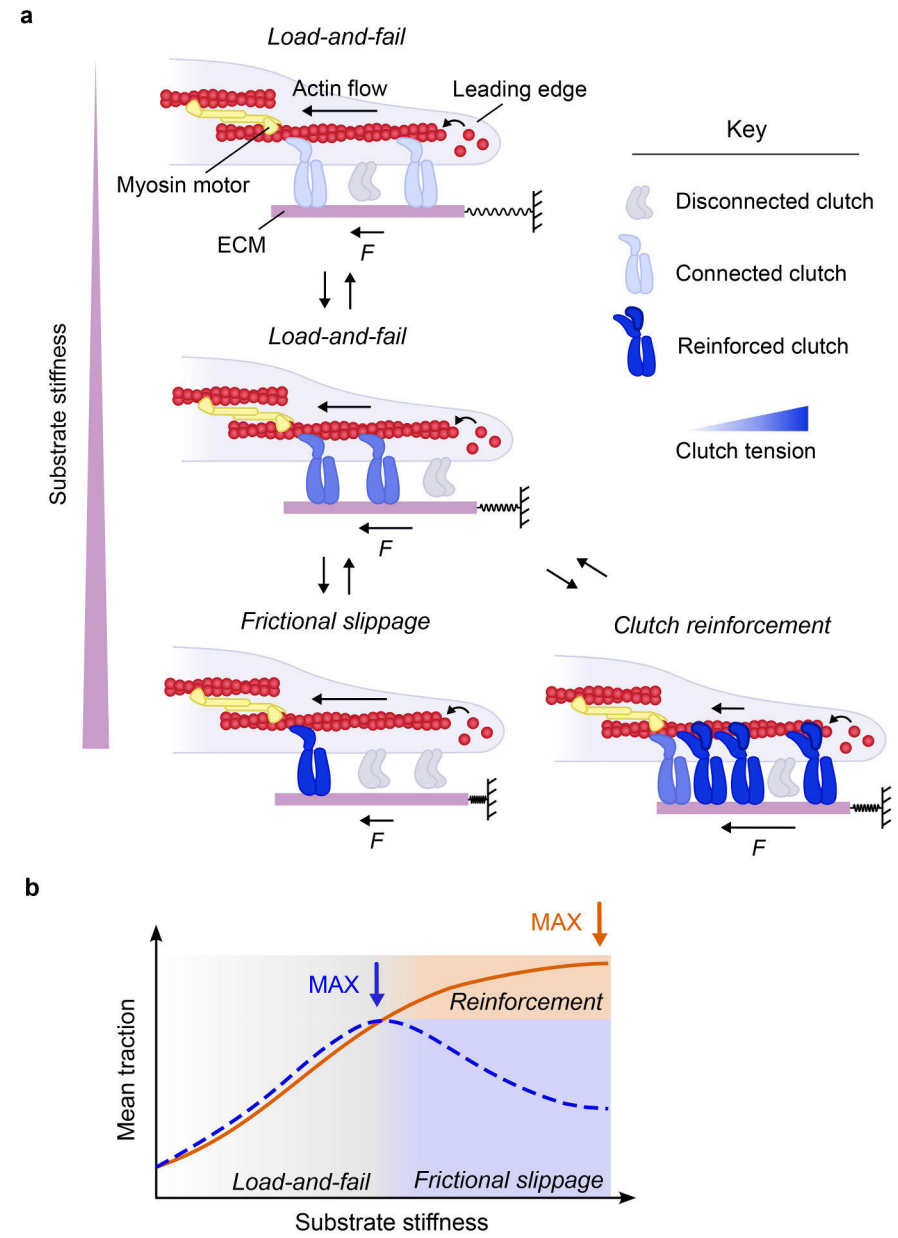

Figure 5. The molecular clutch model of protrusion and traction force generation. **a**) Substrate stiffness influences the force loading rate of the clutches. Soft-to-intermediate stiffness regimes are characterized by cyclically oscillating traction forces, as clutches are engaged progressively before the whole ensemble undergoes a catastrophic failure. On stiffer substrates, individual clutches are overloaded and disengage quickly. This “frictional slippage” can be prevented by talin- and vinculin-mediated clutch reinforcement and FA formation. **b**) Mean traction force as a function of substrate stiffness. Clutch models with (orange line) and without (blue dashed line) reinforcement are depicted.

After these early studies, several experimental observations have indicated that the molecular clutch model is a useful representation of actin and adhesion dynamics in mesenchymal cell migration. Different IAC components exhibit a retrograde flux that coincides with the rearward flow of actin, suggesting partial clutch slippage (Guo & Wang, 2007; Yamashiro et al., 2023). The movements of actin-associated proteins in the uppermost actin regulatory layer are particularly well correlated with F-actin motion (Hu et al., 2007). On the other hand, actin flow rate is inversely correlated with cell protrusion and migration speed (Lin & Forscher, 1995; Hons et al., 2018). The relationship between actin flow and traction forces appears a bit more complex. Despite a general inverse correlation between the two—consistent with the molecular clutch model—actin flow rates immediately adjacent to large FAs tend to be lower and correlate positively with traction. This interesting observation suggests that the connection between actomyosin and the ECM in mature IACs is very robust, and the conversion of F-actin motion into traction stress is mainly impeded by dissipative binding and dissociation between actin and the IAC components (Gardel et al., 2008). In addition to the various studies conducted using planar cell culture substrates, retrograde slippage of IAC components has also been reported in 3D microenvironments, albeit with some quantitative differences (Owen et al., 2017).

The molecular clutch model can also explain how cells probe substrate stiffness, and how the resulting changes in clutch dynamics regulate traction forces and cellular level processes like migration. As discussed above, the lifetimes of the chemical bonds in the IACs are subject to the physical forces exerted on these molecules. When the forces are high enough, any slip or catch-slip bonds will be drastically weakened (Rakshit & Sivasankar, 2014). Substrate stiffness, on the other hand, influences the force loading rates of the clutch molecules. On rigid substrates, individual clutches are overloaded and fail quickly, which leads to "frictional slippage"—fast actin retrograde flow and low traction forces. When the substrate is more compliant, there is enough time for additional clutches to bind the ECM and strengthen the adhesion. This gives rise to oscillatory "load-and-fail" cycles, where new clutches engage progressively until the forces grow too large and the whole ensemble undergoes a catastrophic failure (Elosegui-Artola et al., 2018). Experimentally, cytoskeletal tension has been shown to influence the dissociation constants of various IAC components, indicating that the assumption of the clutch molecules responding to force loading is valid (Wolfenson et al., 2011).

A striking prediction of the molecular clutch model is the existence of a specific stiffness optimum at some intermediate substrate stiffness, where the cells can, on average, exert maximal traction and actin retrograde flow is minimized. The exact location of the optimum depends on multiple parameters, including the number of clutches and molecular motors (Bangasser et al., 2013; Bangasser & Odde, 2013). Distinct stiffness optima have indeed been observed in some cell types, such as

embryonic chick forebrain neurons (Chan & Odde, 2008), U-251MG glioblastoma cells (Bangasser et al., 2017), and primary mouse mammary gland stromal fibroblasts (Lerche et al., 2020). Combining multiple clutch modules with a central cell body has been used in stochastic computational simulations to investigate cellular level responses—including cell migration speed—to substrate stiffness and clutch expression levels, and the results have revealed similar biphasic behavior (Bangasser et al., 2017; Klank et al., 2017).

Contrary to the results obtained in neurons and glioblastoma cells, most adherent cell types do not exhibit obvious biphasic responses to substrate rigidity. Instead, traction forces tend to increase monotonically as a function of substrate stiffness, until they plateau at some point (Ghibaudo et al., 2008; Elosegui-Artola et al., 2016; Kuipers et al., 2018). This is thought to result mainly from talin- and vinculin-mediated clutch reinforcement and IAC maturation. Under sufficiently high force (~5 pN), unfolding of the talin R3 subdomain is faster than the average clutch lifetime. Talin unfolding, actin binding to the ABS2, and subsequent vinculin recruitment strengthens the connection between the integrin heterodimer and actin. In addition, clutch reinforcement supports further integrin recruitment and FA formation, and depleting both talin isoforms in MEFs abolishes IAC maturation and forces the cells into the biphasic traction force regime predicted by the standard molecular clutch model (Elosegui-Artola et al., 2016) (Figure 5a–b). In addition to the talin- and vinculin-mediated reinforcement mechanism, cells can adapt to different substrate mechanics by expressing multiple integrin heterodimers with different ligand binding and unbinding kinetics (Elosegui-Artola et al., 2014). Moreover, integrins may also be linked to the actin cytoskeleton through other adaptor proteins like kindlins (Bledzka et al., 2016).

While the majority of the work on the molecular clutch model has focused on IACs, the same principles should apply to any transmembrane receptors that connect the actin cytoskeleton to the extracellular microenvironment. In particular, the hyaluronic acid receptor CD44 has been shown to act as a clutch in different glioblastoma models, and the receptor is thought to be important for glioblastoma cell migration in vivo (Klank et al., 2017; Wolf et al., 2020; Anderson et al., 2023). In addition to substrate elasticity, the molecular clutch model has been used to recapitulate and explain cellular responses to other biophysical cues, including ligand nanospacing and ECM viscosity (Oria et al., 2017; Bennett et al., 2018).

It is worth noting that the molecular clutch model has been used previously to investigate the molecular underpinnings of collective durotaxis. In the model, forces were balanced directly between the two sides of a continuous cell monolayer. This resulted in similar traction forces being exerted on the soft and rigid sides of the stiffness gradient. Nevertheless, the more compliant region of the substrate deformed more, leading to net cell movement toward the stiffer substrate (Sunyer et al., 2016).

The fact that asymmetric traction forces have been observed in individual cells undergoing durotaxis (Breckenridge et al., 2014; Jun et al., 2023) and both traction force generation and actin dynamics are subject to regulation by the molecular clutch raises an interesting possibility: differences in clutch parameters, including IACs and intracellular contractility, may explain some of the qualitative and quantitative differences in single-cell durotaxis.

2.5 Tools for studying mechanobiology

As the interest in mechanobiology and cancer biomechanics has increased, so has the need for new experimental tools and techniques to study them. The current state-of-the-art for measuring and manipulating cellular forces and mechanical properties includes quencher- or Förster resonance energy transfer (FRET)-based molecular tension sensors, optogenetic tools, laser ablation, microneedles and -pipettes, optical and magnetic tweezers, and different microfluidic systems (Sugimura et al., 2016; Roca-Cusachs et al., 2017). Even in vivo estimation of tensile or compressive forces is possible by inserting deformable materials with known mechanical properties in the tissue of interest (Campàs et al., 2014). However, contractile forces are more commonly studied at the cellular level using TFM. In conventional (2D) TFM, elastic substrates—arrays of micropillars or hydrogels supplemented with fluorescent fiducial markers—are functionalized and used for culturing adherent cells. Traction forces exerted by the cells deform the underlying substrate, and the resulting displacements can be quantified by measuring pillar deflections or by relaxing or removing the cells before reimaging the same hydrogel regions. Equations and assumptions related to resolving cellular traction forces based on the displacements provided by TFM are described in detail in an excellent recent review (Zancla et al., 2022). In addition, force transmission between cells and the ECM can be studied in 3D settings using specialized TFM pipelines (Cóndor et al., 2017; Barrasa-Fano et al., 2021).

Atomic force microscopy (AFM) is another research technique that is commonly used in bioengineering and mechanobiology. AFM systems employ a flexible cantilever that has a molecularly sharp or spherical probe at one end. When the probe contacts a sample, the cantilever bends and a laser beam that is being reflected into a quadrant photodiode is shifted. The spring constant of the cantilever is known, which allows relating centilever deflection to the applied force. AFM has been used for applying and measuring forces in the pico- to micronewton range and investigating mechanical properties at the single-molecule, cellular, and tissue level (Krieg et al., 2019).

In order to investigate cellular responses to ECM and tissue mechanics, cells are often grown on elastic or viscoelastic substrates with specified mechanical

properties. Polyacrylamide-based hydrogels are some of the most common elastic cell culture substrates, and they have been used for studying stem cell lineage specification (Engler et al., 2006), epigenetic regulation of cancer cells (Kaukonen et al., 2016), and cell migration (Bangasser et al., 2017). Polyacrylamide is inexpensive and non-toxic once polymerized, and its elastic modulus can be easily adjusted to mimic a wide range of physiological and pathological tissues. The material is also readily compatible with most light microscopy systems. Most polyacrylamide substrates are isotropic (i.e., they have uniform stiffness), and while these can be very useful in their own right, they do not reflect the highly heterogeneous and complex tumor microenvironment very well. In particular, mechanically graded substrates are needed for investigating some of the more dynamic cellular processes, including durotaxis.

Several methods have been developed for generating stiffness gradient hydrogels, each with their own advantages and disadvantages (Isenberg et al., 2009; Vincent et al., 2013; Hartman et al., 2016; Zhang et al., 2020). The main limitations often include complex, time-consuming methodologies that may prevent the adoption of the techniques by non-specialists. Photoinitiated polymerization or crosslinking is sometimes used for generating the gradient, which can be fairly straightforward but requires appropriate equipment (Tse & Engler, 2010; Sunyer et al., 2016). One technique for preparing linear stiffness gradients involves sequential polymerization of two-layered hydrogels on initially slanted coverslips (Hadden et al., 2017). The method is simple, inexpensive, and compatible with a range of different gradients. However, the resulting gels are relatively thick (~1 mm), which limits their use for high-resolution light microscopy. One of the more commonly used techniques for stiffness gradient preparation is to partially mix together two different acrylamide solutions while they are polymerizing (Lo et al., 2000; Koser et al., 2016; Hetmanski et al., 2019). This method can be very simple and efficient, and supplementing one of the two solutions with fluorescent marker allows visualizing the final gradient. However, relying on just fluorescence intensity for gradient detection is prone to variations resulting from e.g., the microscope used, and additional methods like AFM are often needed to confirm hydrogel stiffness along the gradient.

Micropatterning refers to a group of microfabrication techniques that are used to confine cells on substrates of predefined size, shape, and molecular composition. The method can be used for regulating intracellular organization or recapitulating specific niche architectures and cell-cell or cell-ECM interactions in a controlled setting (Théry, 2010; Albert & Schwarz, 2016). As discussed above, micropatterning has also been used extensively to study the influence of local ECM geometry on cell polarization and migration. Most conventional micropatterns are prepared using microcontact printing or photopatterning (Théry, 2010). They are also static,

meaning that the adhesion-permissive regions are surrounded by permanently non-adhesive substrate. In contrast, dynamic micropatterns allow reverting specific substrate regions adhesive (or non-adhesive) at will, making the patterns a useful tool for investigating more dynamic cellular processes. Non-adhesive surface coatings can be removed or ligand molecules uncaged using electric voltage (Jiang et al., 2005; Raghavan et al., 2010), light (Rolli et al., 2012; Salierno et al., 2013), or changes in temperature (Tsuda et al., 2005). While these physical stimuli are generally well tolerated by the cells, they may still influence more sensitive biological systems and potentially confound the results (Nakajima et al., 2015; Alghamdi et al., 2021). More importantly, many such methods rely on non-specific adsorption of ligands from the growth medium, which can result in comparatively slow binding kinetics and/or limit the amount of control the user has over specific cell-ECM interactions. Despite these shortcomings, some maskless photopatterning systems allow extremely versatile regulation of substrate geometry (Vignaud et al., 2012; Strale et al., 2016).

Cell adhesion and spreading on previously non-adhesive substrates can also be driven by selective addition of specific secondary ligands. Examples include sequential microcontact printing of ECM and neutravidin, which allows a controlled release of micropatterned cells on biotinylated ECM molecules (Rodriguez et al., 2014). The method benefits from high spatial resolution and efficient capture chemistry. However, it is subject to the usual limitations of microcontact printing, e.g., pattern geometry and spacing may be restricted by the stamp aspect ratio (Perl et al., 2009). So-called click chemistries—high-yielding molecular conjugations—are also used in dynamic micropatterning. While fast and efficient, they typically necessitate extensive synthesis and use of specific custom peptides, limiting the selection of available secondary ligands (van Dongen et al., 2013; Costa et al., 2014). In summary, there is a need for new dynamic micropatterning approaches that are both easy to adopt and compatible with a wide range of specific ECM compositions.

3 Aims of the Study

Orderly and controlled migration of cells is a feature shared by many uni- and multicellular organisms, and the phenomenon is a critical part of normal human development and homeostasis. When co-opted by malignant tumors, cell migration can lead to invasion, metastasis, and a life-threatening systemic disease. Despite an increasing interest in targeting cells' migratory machinery to combat cancer progression, most clinical studies thus far have yielded underwhelming results (Gandalovičová et al., 2017; Hamidi & Ivaska, 2018). The poor trade-offs between therapeutic efficacy and toxicity highlight a need for more nuanced understanding of cancer cell motility, and how it is regulated by the complex extracellular milieu characteristic of many solid tumors.

Altered tissue biomechanics are a key feature of human cancer (Nia et al., 2020). The concomitant regulation of eukaryotic cells by different biochemical and physical cues is well appreciated, yet many of the mechanisms that transduce such signals into changes in cell behavior remain poorly understood. In particular, the regulation of cell motility by local matrix architecture and viscoelatic properties, as well as how reciprocal mechanosignaling between cells and the EMC shapes tissue mechanics in situ remain important outstanding questions. One practical reason for the current shortcomings is the lack of specialized tools and sufficient know-how to conduct mechanobiological research. Despite the significant number of methods already available, many of them require specialized and costly laboratory equipment or necessitate extensive synthesis of new reagents. This raises the barrier to entry for most researchers in the fields of cell and cancer biology.

Here, I have characterized biomechanically regulated cell migration using two complementary approaches. First, I have studied the impact of substrate stiffness on the formation and growth of FBs, integrin-based structures used by e.g., stromal fibroblasts to generate and remodel fibronectin matrices. Understanding the feedback between ECM mechanics and further ECM deposition and remodeling is important for deciphering the mechanisms that drive tumor desmoplasia and the generation of physically heterogeneous environments in vivo. Second, I have studied directly the migratory responses of human cancer cells to both stiffness gradients and substrate geometry. Special attention has been given to the investigation of the

theoretical framework and molecular mechanisms governing positive and negative durotaxis, directed cell migration along gradients of substrate stiffness. All the abovementioned studies have been carried out using various reductionist tools that allow careful segregation of different physical and biochemical extracellular cues—a task that is currently impossible to recapitulate fully in vivo. To this end, several new experimental techniques were established and made available for the wider cell biology community.

The specific aims of this thesis were:

1. To design effective and accessible tools for studying the impact of substrate mechanics and microarchitecture on cell biology, including cell migration.
2. To investigate the molecular composition and mechanosensitivity of ECM-remodeling FBs.
3. To study the mechanisms regulating positive and negative durotaxis in human cancer cells.
4. To investigate the role of ECM composition and integrin signaling in the geometric control of cell front-rear polarization and migration.

4 Materials and Methods

The experimental procedures used to generate the data in this thesis are listed in Table 1. In addition, key reagents and methodology are summarized below in separate subsections. More detailed information is available in the original publications (I, II, III).

Table 1. Experimental procedures used in the thesis.

Method	Original publication
Atomic force microscopy (AFM)	I
Cell culture	I, II, III
Computational modeling of cell migration	II
DNA and siRNA transfections	I, II, III
Dynamic micropatterns	III
EdU incorporation (proliferation) assay	II
Elastic cell culture substrates (polyacrylamide hydrogels)	I, II
Finite element analysis	II
Light microscopy (fluorescence, brightfield) and image analysis	I, II, III
Immunofluorescence microscopy	I, II, III
Videomicroscopy (e.g., cell tracking, actin flow measurements)	II, III
Liquid chromatography	III
Measuring hydrogel stiffness by bead indentation	II
Organic synthesis	II
Pharmacological inhibition of actomyosin and adhesion components	II, III
Preparation of streptavidin-conjugated ligand molecules	III
Quantitative real-time PCR	I
Regulating integrin activity with monoclonal antibodies	II, III
Statistical analysis	I, II, III
Synchronized B lymphocyte activation	III
Traction force microscopy (TFM)	II
UV photopatterning	II, III
Western blotting	II, III

4.1 Cell culture (I, II, III)

The cell lines and culture media used in the experiments are listed in Table 2. The cells were acquired from the following sources: American Type Culture Collection, HeLa, MDA-MB-231; Leibniz Institute DSMZ—German Collection of Microorganisms and Cell Cultures, U-2OS; Dr. Jim Norman (Beatson Institute, Glasgow, UK), TIF; Dr. Facundo Batista (The Ragon Institute of MGH, MIT and Harvard), A20 [D1.3]; and Dr. G. Yancey Gillespie (The University of Alabama at Birmingham), U-251MG. Both MDA-MB-231 and U-251MG were authenticated using a short tandem repeat assay (DSMZ). All cell lines were routinely tested for mycoplasma contamination and cultured at +37 °C/5% CO_2 in a humidified incubator.

Table 2. Cell lines and culture media used in the experiments. RPMI, Roswell Park Memorial Institute; FBS, fetal bovine serum; DMEM, Dulbecco's Modified Eagle's Medium; NEAA, non-essential amino acid; TIF, telomerase-immortalized fibroblast.

Cell line	Culture medium	Original publication
A20 [D1.3]	RPMI 1640, 10% FBS, 2.05 mM L-glutamine, 50 µM β-mercaptoethanol, 10 mM HEPES, 100 U/ml penicillin-streptomycin	III
HeLa	DMEM (high-glucose), 10% FBS, 2 mM L-glutamine, 1% NEAAs, 100 U/ml penicillin-streptomycin	I
MDA-MB-231	DMEM (high-glucose), 10% FBS, 2 mM L-glutamine, 1% NEAAs	II, III
TIF	DMEM (high-glucose), 20% FBS, 2 mM L-glutamine, 20 mM HEPES	I
U-251MG	DMEM/F-12, 8% FBS, 2.5 mM L-glutamine (base)	II, III
U-2OS	DMEM (high-glucose), 10% FBS, 2 mM L-glutamine, 1% NEAAs	II, III

4.2 Transfections, plasmids, and siRNAs (I, II, III)

Transient downregulation of target proteins was performed by transfecting the cells with 20–50 nM siRNA oligonucleotides (Table 3) using Opti-MEM reduced serum medium (Thermo Fisher Scientific) and Lipofectamine RNAiMAX (Thermo Fisher Scientific) according to the manufacturer's instructions. The transfected cells were cultured for 24 (beginning of some longer live-cell experiments) to 72 h before they were used for experiments.

In order to generate a stably EGFP-centrin-2-expressing U-251MG cell line, parental U-251MG cells were transfected with pEGFP-centrin-2 (a gift from Dr.

Erich Nigg, Addgene plasmid #41147) using Lipofectamine 2000 (Thermo Fisher Scientific). The cells were passaged onto a clean 6-well plate at ~40% confluency and supplemented with 500 ng of the DNA and 1.25 µl of the reagent in 200 µl of Opti-MEM. The transfected U-251MGs were selected by supplementing the growth medium with 400 µg ml^{-1} G418 (Sigma-Aldrich) for two weeks and later sorted using SH800 (Sony).

Table 3. siRNA oligonucleotides used in the experiments.

Target	Source	Cat. number	Original publication
N/A (control)	Dharmacon (Horizon Discovery)	D-001810-10	I
N/A (control)	QIAGEN	1027281	II
Talin-1	QIAGEN	SI00086975	II
Talin-1	QIAGEN	SI00086968	II
Talin-2	QIAGEN	SI00109277	II
Talin-2	Dharmacon (Horizon Discovery)	J-012909-05	II
Tensin-1	Dharmacon (Horizon Discovery)	L-009976-00	I

4.3 Antibodies and reagents (I, II, III)

Different primary antibodies were used for immunoblotting and immunofluorescence microscopy, for blocking integrin β1 function, and as substrates for cell attachment (Table 4). In addition, different Alexa Fluor-conjugated anti-mouse, anti-rabbit, anti-rat and anti-goat secondary antibodies (Invitrogen) were used for immunofluorescence. IRDye 800CW donkey anti-mouse IgG (LI-COR Biosciences), IRDye 800CW donkey anti-rabbit IgG (LI-COR Biosciences), IRDye 680LT donkey anti-mouse IgG (LI-COR Biosciences), Azure Spectra 650 Ab goat anti-mouse (Azure Biosystems), and Azure Spectra 800 Ab goat anti-rabbit (Azure Biosystems) were used for immunoblotting.

The following proteins, peptides and small molecules were used in the experiments: fibronectin (Sigma-Aldrich, PromoCell); FN-FITC (Sigma-Aldrich); fibronectin fragment FNIII 7–10 (in-house production); type I collagen (Sigma-Aldrich); recombinant human laminin 521 (BioLamina); collagen mimetic peptide H-GPC$(GPP)_5$GFOGER$(GPP)_5$GPC-NH_2 (made to order by Auspep, Melbourne, Australia); 1–5 µM H-1152 (Calbiochem) was used for inhibiting ROCK1/2; 5–25 µM (–)-blebbistatin (STEMCELL Technologies) was used for inhibiting myosin II; 5 µM PF-573228 (MedChem) was used for 90 min to inhibit FAK. In addition, Alexa Fluor 555 and 647 conjugates of fibrinogen (Thermo Fisher Scientific) and bovine

serum albumin (BSA) (Thermo Fisher Scientific) were used for visualizing micropatterns. The following fluorescent counterstains were used for visualizing DNA and filamentous actin: DAPI (4',6-diamidino-2-phenylindole), SiR-DNA (Spirochrome), SPY555-DNA (Spirochrome), SPY650-DNA (Spirochrome), Alexa Fluor 488 phalloidin (Invitrogen), phalloidin Atto 647N (Invitrogen), Acti-Stain 670 phalloidin (Cytoskeleton), SiR-actin (Spirochrome), and SPY650-Fastact (Spirochrome).

Table 4. Primary antibodies used in the experiments. See the original publications (I, II, III) for additional details and concentrations.

Antigen	Host	Source	Cat. number	Application	Original publication
AKT	Mouse	Cell Signaling Technology	2920	WB	III
AKT (phospho-S473)	Rabbit	Cell Signaling Technology	9271	WB	III
Centrin-2	Rat	BioLegend	698602	IF	III
ERK1/2	Rabbit	Cell Signaling Technology	9102	WB	II
ERK1/2	Mouse	Cell Signaling Technology	4696	WB	III
ERK1/2 (phospho-T202/Y204)	Rabbit	Cell Signaling Technology	4370	WB	II, III
FAK	Mouse	BD Biosciences	610088	WB	II, III
FAK (phospho-Y397)	Rabbit	Cell Signaling Technology	8556	IF, WB	I, II, III
Fibronectin	Rabbit	Sigma-Aldrich	F3648	IF, WB	I, II, III
GAPDH	Mouse	HyTest	MAb 6C5	WB	II
Integrin α5 (active, clone SNAKA51)	Mouse	M. Humphries, University of Manchester, UK	N/A	IF	I
Integrin β1 (active, clone 12G10)	Mouse	In-house production	N/A	IF, cell attachment	II, III
Integrin β1 (inactive, clone mAb13)	Rat	In-house production	N/A	Integrin β1 blocking, cell attachment	II, III
MLC2	Rabbit	Cell Signaling Technology	3672	WB	II
MLC2 (phospho-T18/S19)	Rabbit	Cell Signaling Technology	3674	IF, WB	II

Mouse IgM (Fab fragment)	Goat	Jackson ImmunoResearch	115-007-020	B lymphocyte activation	III
N/A (normal IgG2a kappa isotype)	Rat	eBioscience	14-4321-85	Integrin β1 blocking (ctrl)	II
Paxillin	Mouse	BD Biosciences	612405	IF	I, II, III
Paxillin	Rabbit	Santa Cruz Biotechnology	sc-5574	IF	II
Paxillin	Rabbit	Abcam	ab32084	IF	III
Paxillin (phospho-Y118)	Rabbit	Cell Signaling Technology	2541	IF	I
Talin-1	Mouse	Sigma-Aldrich	T3287	IF	I
Talin-1	Mouse	Novus	NBP2-50320	WB	II
Talin-2	Mouse	Novus	NBP2-50322	WB	II
Tensin-1	Rabbit	Sigma-Aldrich	SAB4200283	IF	I
Tensin-3	Rabbit	Merck Millipore	ABT29	IF	I
TGN46	Rabbit	Abcam	ab50595	IF	III
Vimentin	Rabbit	Cell Signaling Technology	5741	WB	II
Vinculin	Mouse	Sigma-Aldrich	V9131	IF, WB	I, II
YAP	Mouse	Santa Cruz Biotechnology	sc-101199	IF	I, II
γ-tubulin	Mouse	Abcam	ab11316	IF	III

4.4 Elastic polyacrylamide hydrogels (I, II)

ECM biomechanics have a profound impact on cell shape and function. Here, we made extensive use of polyacrylamide, readily available, non-toxic hydrogel whose elastic modulus can be adjusted freely across a physiologically relevant range to emulate different healthy and malignant tissues. Both isotropic and graded polyacrylamide hydrogels were used as substrates for cell culture. Specifically, we established a new method for generating 2D cell culture substrates with continuous stiffness gradients for mechanobiological studies (I) and used these gradients to investigate the mechanoresponsiveness of FBs (I) and directed cell migration (II).

4.4.1 Preparation of isotropic hydrogels

In order to prepare hydrogel substrates with uniform stiffness, a glass-bottom dish with no. 1.0 glass (Cellvis D35-14-1-N) was first treated with 100 µl of Bind-Silane

solution—a mix of 7.15% (v/v) 3-(trimethoxysilyl)propylmethacrylate (Sigma-Aldrich) and 7.15% acetic acid in absolute ethanol—for 20 min at r.t. Bind-Silane was aspirated, and the glass was washed 2× with ethanol and air-dried completely. Predefined ratios (Table 5) of 40% (w/v) acrylamide (Sigma-Aldrich) and 2% N,N-methyl-bis-acrylamide (Sigma-Aldrich) in water were mixed in phosphate-buffered saline (PBS) on ice and carefully vortexed. In hydrogels intended for TFM, the solution was also supplemented with fluorescent microbeads as described below.

Polymerization was initiated by supplementing the prepolymer mix with 0.1% ammonium persulfate (Bio-Rad) and 0.2% N,N,N′,N′-tetramethylethylenediamine (Sigma-Aldrich). Immediately following this, the solution was vortexed vigorously and a 13 µl droplet was pipetted onto the glass-bottom dish. A circular 13 mm coverslip was placed carefully on top of the droplet. After polymerization for ~1 h at r.t., the gel was immersed in PBS for 5 min, the coverslip was gently removed using a bent needle, and the gel was washed 2× with PBS to remove any unpolymerized acrylamide. The hydrogel was stored covered in PBS at +4 °C.

Table 5. Polyacrylamide hydrogel compositions and approximate Young's moduli measured by AFM. See 4.4.3 and the original publication (I) for details on AFM measurements.

PBS (µl)	Volume of 40% acrylamide (µl)	Volume of 2% bis-acrylamide (µl)	Final AA %	Final bis-AA %	Young's modulus (~kPa)
397	63	10	5.4	0.04	0.5
365	63	17.5	5.7	0.08	2
356	94	50	7.5	0.2	9.6
300	150	50	12	0.2	22
175	225	100	18	0.4	60

Prior to use, the hydrogels were functionalized with ECM components. 500 µl of 50 mM HEPES with 0.2 mg ml^{-1} Sulfo-SANPAH (Thermo Fisher Scientific) and 2 mg ml^{-1} N-(3-dimethylaminopropyl)-N′-ethylcarbodiimidehydrochloride (Sigma-Aldrich) was added on top of the hydrogel, and the gel was incubated for 30 min at r.t., protected from light and subjected to gentle agitation. Next, the hydrogel and Sulfo-SANPAH solution were exposed to UV (ultraviolet-ozone [UVO] cleaner 342-220 from Jelight Company; low-pressure mercury vapor lamp, λ = 185 nm and 254 nm, 30~33 mW cm^{-2} at 254 nm with distance of ¼") at 5 cm distance for 10 min and washed 3× with PBS. Finally, the hydrogel was incubated with the indicated ECM components (in most cases, 10 µg ml^{-1} fibronectin in PBS) overnight at +4 °C.

4.4.2 Preparation of stiffness gradient hydrogels

Graded hydrogel substrates were prepared by first treating a glass-bottom dish with Bind-Silane solution as described above. After the glass surface had been washed with ethanol and air-dried, a reference mark was drawn on the underside of the dish with a permanent marker to indicate the orientation of the gradient. Two acrylamide solutions, one soft (0.5 or 2 kPa) and one stiff (22 or 60 kPa, respectively), were prepared on ice as described above to yield a substrate with an approximate gradient of 0.5–22 kPa or 2–60 kPa. See Table 5 for the corresponding acrylamide and crosslinker concentrations. ~3.6×10^{10} 0.1 µm fluorescent (505/515 nm) FluoSpheres (Thermo Fisher Scientific, F8803) were sonicated for 3 min and added into the stiff prepolymer mix. Both prepolymer mixes were vortexed and used immediately in the next step.

Polymerization of the soft prepolymer mix was initiated by adding 0.1% ammonium persulfate and 0.2% N,N,N′,N′-tetramethylethylenediamine, the solution was vortexed and a 7.8 µl droplet was pipetted onto the glass-bottom dish ~3 mm to the side and ~1 mm up from the reference mark, located at the side of the glass. The same procedure was repeated with the stiff prepolymer mix, and the new droplet was placed ~2 mm below the first one. A circular 13 mm coverslip was placed on top of the droplets by gently dropping it from the edge with the reference mark toward the opposite side of the dish, leading to partial mixing of the acrylamide solutions before their polymerization. After incubation for ~1 h at r.t., the coverslip was removed and the hydrogel was washed, stored at +4 °C, and functionalized prior to use as described above.

4.4.3 Relating bead density to substrate stiffness

In order to correlate the fluorescent bead density of graded hydrogels to local substrate stiffness, hydrogels featuring narrow- (0.5–22 kPa) and wide-range (2–60 kPa) stiffness gradients were prepared on gridded glass-bottom dishes (Cellvis D35-14-1.5GO). The grid was later used for locating the same substrate regions under different imaging modalities.

Fluorescent microbeads embedded in the substrate were imaged using a Marianas spinning disk confocal microscope equipped with a 40× objective (see 4.11.2 for details on the microscope). For each hydrogel, a tile scan of 12(x)×12(y)×7(z) images corresponding to an area of 4 mm×4 mm was acquired, wherein the upper limit of z was set to ~1 µm below the hydrogel surface. This resulted in 144 stacks of 324.48 µm×324.48 µm×10 µm per stiffness gradient. A corresponding brightfield tile scan (12(x)×12(y)) of the gridded glass bottom was also acquired. For each of the 144 stacks, a maximum intensity projection was created, segmented, and split into four commensurate parts to yield 576 distinct bead

masks. These masks were used to calculate bead densities per area unit ($1/10^4$ μm^2) which were then compiled into a 2D matrix to display the spatial distribution of results.

Hydrogel stiffness was assessed using a JPK Nanowizard I AFM with CellHesion module (JPK Instruments), mounted on an LSM510 confocal microscope (Zeiss) and fitted with a 1 N m^{-1} silicon nitride cantilever with a spherical 10 μm diameter tip (Novascan). A CCD camera was used for visualizing the grid on the dish. Measurements were then carried out at different locations inside the same 4 mm×4 mm region as above. The individual locations were 0.5 mm apart in x and y, and nine indentations following a 3×3 point grid (30 μm×30 μm) were carried out at each location. For each force curve, a corresponding Young's modulus was calculated in JPK DP v4.2 assuming a Hertz model of impact. The measurements were compiled into a 2D matrix to display the spatial variation in stiffness throughout the analyzed region.

By overlaying the matrices depicting bead densities and Young's moduli, the two variables were plotted against each other. Igor Pro v6.37 (Wavemetrics) was used to fit curves to the data. In both cases—narrow- (0.5–22 kPa) and wide-range (2–60 kPa) stiffness gradients—data from three independent hydrogels were pooled to generate the final correlation curve. The best fit for the narrow-range gradients was a linear function

$$y = 0.0044 \times x + 0.903 \quad (1)$$

where y is the Young's modulus (in kilopascals) and x is the measured bead density ($1/10^4$ μm^2). The best fit for the wide-range gradients corresponded to a logit function

$$y = 29.221 - 18.884 \times \log\left(\left(\frac{4720}{(x+179.59)}\right) - 1\right) \quad (2)$$

where y is the Young's modulus and x is the bead density. Error estimates for the models are described in the original publication (I). The two equations were used in subsequent experiments and studies (I, II) to approximate the local stiffness of graded substrates.

4.5 Ratiometric analysis of IAC components (I)

TIF cells were seeded on glass-bottom dishes pre-coated with 10 μg ml^{-1} fibronectin in PBS, grown overnight at +37 °C/5% CO_2, fixed, and prepared for immunofluorescence microscopy as described below. The samples were imaged using a DeltaVision OMX v4 microscope with a ring total internal reflection fluorescence (TIRF) module (see below for details).

Ratiometric analysis was conducted using a modified version of a previously described protocol (Zamir et al., 1999). Two-channel images of TIFs depicting the two proteins of interest were first subjected to background removal (rolling ball) and thresholding to remove noise. Ratio images were then calculated by dividing, pixel by pixel, the values of the first channel by the second channel. The final pixel values were assigned based on the following criteria: (1) a value of zero was assigned whenever the value of the pixel in both original channels was zero; (2) a value of 0.1 was assigned whenever the ratio between the numerator (first channel) and denominator (second channel) was ≤0.1; (3) a value of 10 was assigned whenever the ratio between the numerator and denominator was ≥10, or the numerator was >0 and the denominator was zero; (4) in all the remaining cases the pixel was assigned the ratio between the numerator and denominator. The final images were displayed in log scale using a color lookup table (Jet2 for all pixels >0 and gray for pixels with a value of zero), allowing the visualization of ratios over two orders of magnitude (from 0.1 to 10).

4.6 Cell migration on stiffness gradients (II)

15,000 (MDA-MB-231)–20,000 (U-251MG) cells were seeded on a fibronectin-functionalized 0.5–22 kPa stiffness gradient hydrogel. All the reagents and cell suspension were carefully equilibrated to +37 °C before starting, and an even initial distribution of cells was confirmed visually (using brightfield microscopy) and by recording the positions of the nuclei along the gradient (using SiR-DNA and fluorescence microscopy). The sample was returned to the incubator for 48 h (U-251MG)–72 h (MDA-MB-231), fixed, and the nuclei were imaged again using DAPI.

For live-cell videomicroscopy of U-251MG cells on the graded substrates, 30,000 cells were seeded on a hydrogel and left to adhere for one hour. In the indicated experiments, the medium was then supplemented with 1–5 μM H-1152, 5–25 μM blebbistatin or vehicle (dimethyl sulfoxide). Imaging was started 2–3 h after seeding the cells and time-lapse videos were acquired overnight at 15 min intervals. The cells were tracked, and tracks corresponding to individual cells were analyzed for angular displacement and forward migration index (defined here as displacement along the gradient divided by the total accumulated distance, where positive values correspond to migration toward stiffer regions).

4.7 Traction force microscopy (II)

Fibronectin-functionalized polyacrylamide hydrogels of varying stiffnesses were supplemented with ~1.5×10^{10} ml^{-1} 0.2 μm yellow-green (505/515 nm) fluorescent

microbeads (Invitrogen) and cast on glass-bottom dishes as described above. MDA-MB-231 cells were seeded on the gels (5,000 cells per plate) approximately 24 h after transfection with control or talin-1/2-targeting siRNAs and cultured for another 48 h before the experiment was continued. Brightfield images of cells and corresponding Z stacks depicting beads embedded in the hydrogel were acquired using a Marianas spinning disk confocal microscope (see below for details) with a stage-top incubator unit (+37 °C/5% CO_2). The same positions were imaged twice, before and after the cells had been detached by the addition of 2% (w/v) SDS.

The data were analyzed using a previously described implementation of Fourier-transform traction cytometry (Han et al., 2015). High-resolution subsampling was used for calculating the displacement fields, assuming no outward deformation of the substrate. A common regularization parameter ($\lambda = 5\times10^{-6}$) was determined using optimal L2 regularization and a set of data acquired from soft and stiff hydrogels. The background (i.e., noise) of the measurements was estimated by analysing five empty (i.e., no cells) fields of view per substrate stiffness.

4.8 Computational modeling of cell migration (II)

Cell migration on isotropic substrates and substrates with stiffness gradients was modeled using the Odde lab cell migration simulator (CMS) (Bangasser et al., 2017). A previously described C++ implementation of the model (Hou et al., 2019) was further modified to account for spatial variations in substrate rigidity and compiled using GNU Compiler Collection.

The CMS represents an individual cell on a 2D substrate, comprising multiple motor-clutch models (hereafter called modules) that mimic cellular protrusions. Each module contains a set number of clutches (e.g., integrins and their adaptors) that restrict motor (myosin)-induced inward flow of actin by connecting the cytoskeleton to the underlying substrate. Cell migration is determined by a force balance between the individual modules and a central node (cell body). New modules are nucleated stochastically, they elongate over time due to actin polymerization that is simultaneously counteracted by the retrograde flow, and modules are eventually removed when they become too short. The total intracellular pools of actin, clutches, and motors are kept constant in accordance with the conservation of mass.

The clutches in each module bind the substrate, modeled as elastic springs, at a constant rate k_{on}. In our iteration of the model, the stiffness of the substrate springs (k_s) can be constant or vary as a function of their y-coordinate. When the clutches connect the actin cytoskeleton to the substrate, they are concurrently exposed to forces originating from the actomyosin. The unbinding rate of a connected clutch, $k_{off,i}$, varies with force F_i according to the Bell model (Bell, 1978)

$$k_{off,i} = k^*_{off} \exp\left(\frac{F_i}{F_b}\right) \tag{3}$$

where k^*_{off} is the unbinding rate of an unloaded clutch, F_b is the characteristic clutch rupture force, and F_i is the force acting on the i^{th} clutch. The clutches are modeled as Hookean springs, and consequently the force on any individual clutch can be derived from

$$F_i = k_c x_i \tag{4}$$

where k_c is the clutch spring constant and x_i is the elongation of the i^{th} clutch. Myosin motors in each module drive actin flow at an effective rate

$$v_{m,j} = v^*_m \left(1 - \frac{F_j}{n_{m,j} F_m}\right) \tag{5}$$

where v^*_m is the unloaded actin flow rate, F_j is the total traction force exerted on module j, $n_{m,j}$ is the total number of motors in module j, and F_m is the characteristic stall force of one myosin motor. F_j can also be written as

$$F_j = \sum_{i=1}^{n_{c,on}} F_i \tag{6}$$

where $n_{c,on}$ is the total number of connected clutches in the module and F_i is the force acting on the i^{th} clutch. The central node contains additional clutches to recapitulate drag caused by the cell body, and the forces associated with these are resolved similar to equation (6). In addition, the sum of all forces acting on the cell must be zero:

$$F_{cell} + \sum_{j=1}^{n_{mod}} F_j = 0 \tag{7}$$

New actin monomers are added to the plus ends of all actin filaments at a polymerization rate

$$v_p = v^*_p \left(\frac{A_{free}}{A_{tot}}\right) \tag{8}$$

where v^*_p is the maximum actin polymerization rate, A_{free} is the total amount of free G-actin, and A_{tot} is the total intracellular pool of actin. Module elongation and retraction result from the net effect of polymerization and actin retrograde flow (v_m). Filaments can also be capped at a rate k_{cap}, which leads to arrested polymerization. When actin passes the position of the myosin motors, it is depolymerized and added back to the G-actin pool. Finally, actin filaments and the corresponding modules are removed and depolymerized entirely when their length falls below l_{min}. New modules are created at a nucleation rate

$$k_{mod} = k^*_{mod}\left(\frac{A_{free}}{A_{tot}}\right)^4 \quad (9)$$

where k^*_{mod} is the maximum nucleation rate. Upon nucleation, each module is assigned motors and clutches according to

$$n_m = n^*_m\left(\frac{N_{m,free}}{N_m}\right) \quad (10)$$

$$n_c = n^*_c\left(\frac{N_{c,free}}{N_c}\right) \quad (11)$$

where n^*_m is the maximum number of motors per module, n^*_c is the maximum number of clutches per module, $N_{m,free}$ is the total amount of free motors, $N_{c,free}$ is the total amount of free clutches, N_m is the total intracellular pool of motors, and N_c is the total intracellular pool of clutches. The initial direction (angle) of the new module is assigned randomly.

The CMS was implemented using a direct Gillespie stochastic simulation algorithm (Gillespie, 1977). For each iteration of the simulation, two (pseudo)random numbers are generated. In conjunction with the various event rates—k_{on}, $k_{off,i}$, k_{mod}, and k_{cap}—these random numbers are used to determine the time increment to the next event, as well as the event itself. All the model parameters and their numerical values are presented in Table 6, see the original publication (II) for citations. In brief, the model algorithm is as follows:

1. Initialize a cell with three equally interspaced modules of length l_{in}. All the clutches are unbound.
2. Calculate the module nucleation rate and clutch unbinding rates.
3. Determine the time to next event.
4. Determine which event will take place.
5. Calculate the actin flow rates for each module.
6. Shorten each module by the product of event time and actin flow rate.
7. Advance uncapped modules (clutch, substrate and reference positions) by the product of event time and actin polymerization rate.
8. Execute the event.
9. Remove any modules shorter than l_{min}.
10. Resolve the force balance to determine a new position for the cell body.
11. Calculate the clutch, cell spring, and substrate spring extensions based on the forces exerted on each module.
12. Return to step 2.

Here, the cells were simulated for 60 min to drive the system to a dynamic steady state, after which each cell was displaced to a substrate with (1) a defined uniform spring constant or (2) one or more stiffness gradients. The gradients had different lengths and ranges, and they all followed a normal cumulative distribution function. The different graded substrates were designed based on experimental observations and are described in full in the original publication (II). Cell positions and traction forces were recorded every second and the results were used to calculate random motility coefficients and mean traction forces per module. A custom MATLAB (MathWorks) code was used for the analyses. All CMS simulations were conducted at the Minnesota Supercomputing Institute.

The model was further refined to account for filopodial dynamics and neural growth cone steering on stiffness gradients. The filopodia were represented by individual motor-clutch modules that were arranged around a semicircular growth cone. Each filopodia was allocated a set number of clutches—the corresponding substrate clutches were distributed randomly and their spring constants varied linearly with position along the gradient. For more details on the modified growth cone model, see the original publication (II).

Table 6. Parameters used in the cell migration simulations (II).

Symbol	Parameter	Value
N_m	Total number of myosin motors	10,000
N_c	Total number of clutches	7,500
A_{tot}	Total available actin length	100 μm
v^*_p	Maximum actin polymerization rate	200 nm s^{-1}
k^*_{mod}	Maximum module nucleation rate	1 s^{-1}
k_{cap}	Module capping rate	0.001 s^{-1}
l_{in}	Initial module length	5 μm
l_{min}	Minimum module length	0.1 μm
k_{cell}	Cell spring constant	10,000 pN nm^{-1}
$n_{c,cell}$	Number of central (cell body) clutches	10
k_s	Substrate spring constant	0.3–300 pN nm^{-1}
n^*_m	Maximum number of motors per module	0.1 × N_m
F_m	Myosin motor stall force	2 pN
v^*_m	Unloaded actin flow rate	120 nm s^{-1}
n^*_c	Maximum number of clutches per module	0.1 × N_c
k_{on}	Clutch on-rate	1 s^{-1}
k^*_{off}	Unloaded clutch off-rate	0.1 s^{-1}
k_c	Clutch spring constant	8 pN nm^{-1}
F_b	Characteristic clutch rupture force	2 pN

4.9 Biotinylation-based dynamic micropatterns (III)

In order to facilitate the investigation of different ECM components and how they influence cellular responses to substrate geometry, we designed a new method for preparing reversible (dynamic) micropatterns. The technique is based on UV photopatterning of biotinylated PEG-grafted poly-L-lysine (PLL-g-PEG). Please refer to the original publication (III) for a comprehensive list of validation experiments.

4.9.1 Photopatterning of PLL-g-PEG-coated coverslips

Preparation of static micropatterns by UV photopatterning of non-biotinylated PLL-g-PEG has been described previously (Azioune et al., 2009). Here, glass coverslips were cleaned by incubating them in concentrated nitric acid for 5 min under gentle agitation, washed under running water for 3 min, and rinsed 5× with deionized water and 2× with absolute ethanol. Next, the coverslips were air-dried and treated with deep UV light in air (UVO cleaner 342-220 from Jelight Company; low-pressure mercury vapor lamp, λ = 185 nm and 254 nm, 30~33 mW cm^{-2} at 254 nm with distance of ¼") at 5 cm distance for 5 min. The cleaned coverslips were incubated with 0.1 mg ml^{-1} PLL(20)-g[3.5]-PEG(2)/PEG(3.4)-biotin(50%) (SuSoS) (for dynamic micropatterns) or 0.1 mg ml^{-1} PLL(20)-g[3.5]-PEG(2) (for static/conventional micropatterns) in 10 mM HEPES pH 7.4 for 1 h at r.t. The coated coverslips were washed 2× with PBS and once with deionized water.

Quartz/chromium photomasks were acquired from DeltaMask. Prior to every use, the masks were cleaned by rinsing them with deionized water and absolute ethanol, dried using air flow, and treated in the UVO cleaner for 5 min. PLL-g-PEG-coated coverslips were placed on a photomask in drops of deionized water (~5 µl cm^{-2}), with the antifouling surface facing down. The coverslips were then exposed to deep UV light through the photomask for 6 min and carefully detached by covering the mask surface in deionized water. Excess water was blotted away by pressing the corners of the coverslips on lint-free paper and the coverslips were air-dried. Prior to use, the photopatterned coverslips were coated with protein(s) as described below.

4.9.2 Preparation of streptavidin-conjugated ligands

In order to prepare streptavidin-conjugated proteins and peptides, commercial kits from Abnova and Abcam (FastLink and Lightning-Link, respectively) were used according to the manufacturer's instructions. Briefly, 1 µl of modifier reagent was added per 10 µl of the protein/peptide (1 mg ml^{-1} stock). The resulting solution was mixed with the lyophilized material and incubated at r.t. for a minimum of 3 h.

Finally, 1 µl of quencher reagent was added per 10 µl of the protein/peptide. The final conjugate was stored at +4 °C.

4.9.3 Confirming secondary ligand binding

In order to measure the amount of secondary ligand binding to the PLL-g-PEG-biotin-coated coverslips, substrates with linear micropatterns (9 µm wide at 30 µm separation) were prepared as described above. The micropatterns were coated with 225 ng cm^{-2} fibronectin and 75 ng cm^{-2} BSA-Alexa Fluor 555 in PBS for 1 h at r.t., washed 2× with PBS, and incubated with 0, 15, 75 or 225 ng cm^{-2} streptavidin-fibronectin (SA-FN) in growth medium (DMEM/F-12) supplemented with 10% fibronectin-depleted FBS for 15 min at r.t. Next, the coverslips were washed once with medium and once with PBS, blocked for 10 min with 10% horse serum, and prepared into immunofluorescence samples using anti-fibronectin antibody as described below. The samples were imaged using a Marianas spinning disk confocal microscope and data points depicting the average immunofluorescence intensities of non-micropatterned regions were normalized using the areas under the curve representative of each individual experiment. The resulting pooled data were plotted to investigate the relationship between the amount of SA-FN added and the amount of secondary ligand actually attached to the non-irradiated PLL-g-PEG-biotin. In addition, the amount of fibronectin (SA-FN) bound to the non-irradiated PLL-g-PEG-biotin relative to the amount of fibronectin adsorbed to the surrounding micropatterns was visualized using linear intensity profiles.

In order to investigate the rate at which SA-FN binds to the biotinylated PLL-g-PEG in conditions resembling the corresponding live-cell migration experiments, additional coverslips with linear micropatterns were prepared. The coverslips were coated with 750 ng cm^{-2} fibronectin and 75 ng cm^{-2} BSA-Alexa Fluor 555 for 1 h at r.t., followed by blocking with 2% BSA/PBS for 10 min at r.t. The coated coverslips were immersed in U-251MG growth medium and, using the spinning disk confocal microscope, the distribution of SA-FN-FITC in the focal plane next to the glass was recorded every 2 min before and after supplementing the samples with 750 ng cm^{-2} secondary ligand.

4.9.4 Seeding cells on the micropatterns

Before photopatterned coverslips were used in experiments, the micropatterns were coated by incubating them with the indicated amounts and types of substrate molecules for 1 h at r.t. The coated micropatterns were washed with PBS, blocked with 2% BSA/PBS for 30 min at r.t., and washed 2× more with PBS. The coverslips were placed in 24-well plate wells (fixed samples) or assembled into imaging

chambers for live-cell experiments using Attofluor components (Thermo Fisher Scientific). Fibronectin-depleted FBS was used to supplement media in all experiments where substrates other than fibronectin were studied.

Cell suspension and the plates were prewarmed at +37 °C for ~10 min and cells were seeded on the micropatterned coverslips at ~10% confluency. The cells were allowed to adhere and spread on the patterns for approximately 3 h before they were used for experiments (i.e., fixed or taken to a microscope for live-cell imaging). Alternatively, an excess of cells was seeded on each coverslip. After 10–20 min the wells/imaging chambers were tilted and washed carefully with growth medium to remove the unattached cells without allowing the coverslip and remaining cells to dry.

4.10 Tracking cell spreading and migration from dynamic micropatterns (III)

EGFP-centrin-2-expressing U-251MG cells were seeded on 37 μm wide crossbow-shaped micropatterns on PLL-g-PEG-biotin, coated with 750 ng cm^{-2} fibronectin or mAb13 and 75 ng cm^{-2} BSA-Alexa Fluor 555/647. SPY555/650-DNA was used for visualizing the nuclei. After the cells had spread on the micropatterns (~3 h after seeding), imaging was started and the cells were released from confinement to spread and migrate by supplementing the medium with 750 ng cm^{-2} SA-FN. Brightfield images and channels pertaining to centrin-2 and nuclei were captured. Time points from 10 min before to 60 min after the addition of SA-FN were imaged every 5 min, and subsequent time points were imaged every 15 min.

During analysis the images were segmented into nuclei, centrosomes and cell outlines (used for calculating cell areas and centroids), and each feature was tracked separately. Any time points after cells had collided with others to change their direction or had started undergoing apoptosis or mitosis, if present in the data, were excluded from the analysis. The resulting data sets were analyzed to yield metrics about the cells' motility and front-rear polarization (i.e., centrosome orientation relative to the nucleus). For additional details, refer to the original publication (III). The software used for image analysis has been described below.

4.11 Microscopy (I, II, III)

4.11.1 Immunofluorescence sample preparation (I, II, III)

Samples were fixed with warm 4% formaldehyde for 10 min, followed by permeabilization and blocking with 0.3% Triton X-100 in 10% horse serum (Gibco) for 20 min. Primary antibodies were diluted in 10% horse serum and the samples

were incubated with the antibodies overnight at +4 °C. After washing the samples with PBS, secondary antibodies were diluted in PBS and the samples were incubated with the antibodies for 1–2 h at r.t. Samples for the ratiometric analysis of IAC components (I) were prepared by fixing and permeabilizing the specimens with 4% formaldehyde and 0.2% Triton X-100 for 10 min. The samples were quenched with 1 M glycine for 30 min, washed with PBS and incubated with the primary antibodies for 45 min at r.t. Following further washes, the samples were incubated with secondary antibodies for 30 min at r.t.

Where needed, actin and/or nuclei were visualized using different fluorescent counterstains (see section 4.3 and the original publications for details). Samples prepared on coverslips (mainly micropatterns) were also mounted using Mowiol (Merck Millipore) supplemented with 2.5% 1,4-diazabicyclo[2.2.2]octane (DABCO) (Sigma) and allowed to cure overnight at r.t. before imaging.

4.11.2 Light microscopy and image analysis (I, II, III)

Most fluorescent samples were imaged using a Marianas spinning disk confocal microscope with a Yokogawa CSU-W1 scanning unit, controlled by SlideBook 6 software (Intelligent Imaging Innovations). The following objectives were used: 20×/0.8 NA Plan-Apochromat (Zeiss), 40×/1.1 NA W LD C-Apochromat (Zeiss), 63×/1.4 NA O Plan-Apochromat (Zeiss), and 100×/1.4 NA O Plan-Apochromat (Zeiss). The images were acquired using an Orca Flash4.0 sCMOS camera (Hamamatsu Photonics).

Additional specimens were imaged using a Nikon ECLIPSE Ti2-E widefield microscope, controlled by NIS-Elements AR 5.11 software (Nikon). The objectives used were a 10×/0.3 NA CFI Plan Fluor objective (Nikon), for acquiring tile scans of stiffness gradient hydrogels (II); 20×/0.75 NA CFI Plan Apo Lambda (Nikon), for videomicroscopy of cells released from dynamic micropatterns (III); and 40×/0.6 NA CFI S Plan Fluor ELWD ADM (Nikon), for actin retrograde flow measurements (III). The images were acquired using an Orca Flash4.0 sCMOS camera (Hamamatsu Photonics). Live phase-contrast imaging of U-251MG cells on stiffness gradients with linear fibronectin patterns (II) was done using a Nikon ECLIPSE Ti-E microscope, controlled by NIS-Elements AR 4.60 software (Nikon). The objective used was a Plan Fluor 10×/0.30 NA objective (Nikon), and the images were acquired using an Andor Zyla 5.5 sCMOS camera (Andor Technology).

Images for the ratiometric analysis of IAC components (I) were taken using a DeltaVision OMX v4 microscope with a ring TIRF module (GE Healthcare). The images were acquired using a 60×/1.49 NA APO N TIRF oil objective (Olympus) and PCO edge front-illuminated sCMOS camera (PCO). A laser scanning confocal microscope (CLSM, Zeiss LSM 880 AiryScan) with LD LCI Plan-apochromat

40×/1.2 NA objective and super-resolution AiryScan detector was used for imaging TIF adhesions (I). Example images depicting different micropattern shapes (III) were acquired using an EVOS fl microscope (Advanced Microscopy Group), 20×/0.45 NA PlanFluor objective (Advanced Microscopy Group), and ICX285AL CCD camera (Sony).

During live-cell imaging, all samples were maintained in a stage top humidified incubator (Okolab) at +37 °C/5% CO_2. Quantitative analysis of microscopy images was performed using custom Python scripts, ImageJ/Fiji (Schindelin et al., 2012), CellProfiler (Broad Institute), and R (R Core Team) running on RStudio (Rstudio Team). In order to mitigate phototoxicity during extended live-cell imaging, the data depicting actin flow in U-251MG cells were acquired by minimizing total illumination and enhancing the resulting images using the deep learning algorithm content-aware image restoration (Weigert et al., 2018) implemented in the ZeroCostDL4Mic platform (von Chamier et al., 2021). For additional details, see the original publication (III).

4.12 Statistical analysis (I, II, III)

Statistical analyses and plotting were performed using Prism (GraphPad Software) and R running on RStudio. Confidence intervals for means were calculated using bias-corrected and accelerated bootstrap intervals from 10,000 resamples, and confidence intervals for binomial data were calculated using the Wilson score interval (II). Circular correlation coefficients for two paired angles were calculated using the R function cor.circular (III). For simulating paired circular data with a true positive correlation, a sample was drawn from a bivariate von Mises distribution using the function rvmsin (n = 50, kappa1 = 0.8, kappa2 = 0.8, kappa3 = 1, mu1 = 0, mu2 = 0) (III).

For linear regression analyses, any data with standardized residuals >3 were considered outliers. Whenever data were deemed to follow a non-normal distribution (based on Shapiro-Wilk normality test), hypothesis testing was conducted using non-parametric methods. Unless otherwise noted, two-sided *p*-values were reported and values <0.05 were considered statistically significant. The names and/or numbers of individual statistical tests, samples and data points are indicated in the original publications (I, II, III).

5 Results and Discussion

5.1 Fibrillar adhesion composition and growth on mechanically heterogeneous substrates (I)

5.1.1 Fabrication of stiffness gradient hydrogels with fluorescent marker beads

In order to investigate the responsiveness of FBs to substrate stiffness over a comparatively wide range of elastic moduli—reminiscent of different healthy and malignant tissues—we established a method for preparing polyacrylamide hydrogels with different stiffness gradients. Our secondary goal was to overcome some of the limitations of the currently available methodologies, with the aim of making the new hydrogels quick and inexpensive to fabricate, compatible with high-resolution imaging, and easy to adopt by other research groups.

We started by preparing two acrylamide solutions that corresponded to the softest and stiffest regions of the desired gradient (Table 5). The "stiff" solution was supplemented with fluorescent microbeads (0.1 μm, 505/515 nm) as outlined in Materials and Methods. The two solutions were allowed to partially mix and diffuse together on a glass-bottom dish to yield a hydrogel with two continuous regions of high and low bead density, respectively, and a connecting gradient between them (I, Figs. 1a–b, S1a). Fluorescence microscopy was used to confirm the exact orientation of the gradient and the absence of any defects like air bubbles. In the rare case where such defects were observed, the associated gels were promptly discarded.

If an elastic substrate is too thin, cells may be able to sense the underlying rigid support, confounding the experimental results (Buxboim et al., 2010). We measured the thickness of our gradient hydrogels along the length of the gradient using a confocal microscope and found it to be in the range of 100–150 μm (I, Fig. S1b). This was significantly more than the typical tactile length of MSCs but thin enough for low working distance microscopy (Buxboim et al., 2010).

We hypothesized that the density of marker beads in any given region of the gradient would correlate with substrate stiffness, enabling us to visualize the stiffness gradient using a fluorescence microscope. When needed, local substrate stiffness could also be estimated more accurately by counting the beads. To test this, we used

AFM to probe two types of stiffness gradient hydrogels: narrow- (~0.5–22 kPa) and wide-range (~2–60 kPa) gradients (I, Figs. 1c, S1c). In order to correlate the AFM measurements to bead density, the hydrogels were prepared on gridded glass-bottom dishes and a confocal microscope was used to acquire tile scans of the beads across the same graded regions. In all instances, bead density correlated positively with AFM-resolved substrate stiffness (I, Fig. 2a–b). Interestingly, the relationship was linear for the narrow-range gradient gels, but the correlation curve for the wide-range gradients was best described by a logit model: at the two extremes of the gradient, small changes in bead density were associated with comparatively large changes in substrate stiffness. To confirm the reproducibility of these results, we prepared additional wide-range stiffness gradients, imaged them to count the marker beads, and compared the calculated stiffness values to an AFM-derived ground truth. Both values were highly consistent, i.e., all the AFM measurement fell within the 95% confidence interval of the estimated stiffness (I, Fig. S1d).

Finally, we wanted to confirm the applicability of our stiffness gradient hydrogels to biological experiments by monitoring substrate stiffness-dependent morphological changes and YAP subcellular localization in HeLa cells. Cells cultured in the softest (~0.5 kPa) regions of fibronectin-functionalized, narrow-range stiffness gradients were small, round, and presented with mostly cytoplasmic YAP (I, Fig. 2c–f). Upon increasing substrate stiffness, the cells became more spread and irregularly shaped, and YAP became progressively more nuclear (I, Fig. 2c–f). These results were expected (Ladoux et al., 2016; Kirby & Lammerding, 2018) and confirmed that the cells were responding to polyacrylamide stiffness. Taken together, our data indicate that partial mixing of two polymerizing acrylamide solutions can be used to reproducibly generate stiffness gradients, where substrate stiffness can be calculated using local marker bead density as a proxy. Such gradients are fully amenable for cell culture and optical imaging.

5.1.2 Identification of the optimal fibrillar adhesion marker

In order to study FBs on stiffness gradient hydrogels, we first sought to identify the ideal molecular marker for these structures. We cultured human TIFs overnight on fibronectin and determined the localization of selected IAC and ECM components, focusing on known FA- and FB-associated proteins, in a pairwise manner using a ring TIRF module and ratiometric fluorescence analysis. As expected, both tensin-1 and active integrin α5β1 (detected using the SNAKA51 antibody) were found at centrally located elongated IACs that resembled prototypical FBs (I, Fig. 3a). These central IACs co-localized with fibronectin (I, Fig. 3b) but were largely devoid of the FA marker vinculin (I, Fig. S2a). Accordingly, active integrin α5β1 co-localized strongly with fibronectin everywhere in the cell (median Pearson's $r \approx 0.9$) but did

not overlap markedly with phosphorylated paxillin—a marker for FAs (I, Fig. 3c–d). Tensin-1, however, was also enriched at peripheral vinculin-positive FAs (I, Fig. S2b). The co-localization of tensin-1 and fibronectin could not be addressed directly due to the antibodies being raised in the same species. Tensin-3, the other tensin isoform reported to localize at FBs, was also abundant at vinculin-positive FAs (I, Fig. S2c).

To further confirm these findings, we compared tensin-1 distribution to another established FA component, talin-1, and found that both proteins co-localized at peripheral FAs (I, Fig. S3a). In contrast, neither paxillin nor talin-1 were present at the fibronectin-rich central IACs (I, Fig. S3b). Finally, active integrin α5β1 exhibited minimal co-localization with phosphorylated FAK, another protein enriched at FAs (I, Fig. S3c). These data indicate active integrin α5β1 as a more specific marker for FBs than either of the tensins—at least in our system.

5.1.3 Fibrillar adhesions are mechanoresponsive

To address whether FB formation and morphology are dependent on substrate mechanics, we first cultured TIFs overnight on very compliant (~0.5 kPa) and very rigid (~60 kPa) fibronectin-coated hydrogels. As expected, TIFs on the soft hydrogels did not spread much and were mostly round (I, Fig. 4a). Next, we measured the length of FBs—defined as IACs positive for active integrin α5β1 and negative for phosphorylated paxillin—and found that on soft substrate, most of the adhesions appeared small and punctate. Conversely, the cells on stiff substrate displayed elongated, more conventional-looking FBs (I, Fig. 4a–b). To study the mechanosensitive growth of FBs in more detail, we plated TIFs on narrow-range (~0.5–22 kPa) stiffness gradients and confirmed that the length of active integrin α5β1 adhesions correlated positively with substrate stiffness (I, Fig. 4c–d). This increase in adhesion length resembled logarithmic growth: a rapid increase at lower stiffnesses (<7 kPa) was followed by a more gradual increase and finally a plateau at ~10 kPa. The maximum average length of FBs in our system was ~3.5 μm.

Tensins have been shown to maintain integrin β1 activation at FBs (Pankov et al., 2000; Georgiadou et al., 2017). In order to investigate how tensins contribute to FB growth on soft versus stiff substrates, we silenced tensin-1 in TIFs using previously validated (Georgiadou et al., 2017) siRNA oligonucleotides and confirmed the knockdown using quantitative real-time PCR (I, Fig. 5a). Remarkably, tensin-1-depleted cells displayed a ~30% reduction in the length of active integrin α5β1 adhesions across the whole narrow-range stiffness gradient, i.e., at ~0.5–22 kPa (I, Fig. 5b–c). This suggests that tensins support FB formation on both compliant and rigid substrates.

5.1.4 Discussion

Most cellular processes are fundamentally responsive to the biomechanics of the external microenvironment. For example, matrix stiffness can regulate cell survival and proliferation (Yang et al., 2020a), guide differentiation (Engler et al., 2006), and even direct cell migration (DuChez et al., 2019). Several methods have been developed to study cellular responses to mechanically heterogeneous substrates, and they typically involve fabrication of different graded polyacrylamide hydrogels (Isenberg et al., 2009; Tse & Engler, 2010; Vincent et al., 2013; Hartman et al., 2016; Sunyer et al., 2016; Hadden et al., 2017; Zhang et al., 2020). While all of the previously established techniques have their own merits, in practice they are often limited by the need to verify the gradient stiffness, typically via AFM, or the need for other specialized equipment or reagents that make the protocols difficult to adopt by non-specialists.

Here, we established a simple, fast, and cost-effective method for producing stiffness gradient substrates for cell culture applications (I, Fig. 1a). The new technique is based on previously reported protocols that leverage partial mixing of two liquid acrylamide phases prior to their polymerization (Lo et al., 2000; Koser et al., 2016; Hetmanski et al., 2019), and it requires only commercially available reagents, glass bottom dishes and coverslips. For counting the beads and estimating the local substrate rigidity, a confocal microscope is also needed. The full range of available stiffnesses is wide, ~0.5–60 kPa, and spans most physiological and pathological soft tissues (Cox & Erler, 2011). We tested the applicability of our hydrogels to cell culture by plating adhesive HeLa cells on them and observed several prototypical stiffness responses: the cells exhibited substrate stiffness-dependent spreading, elongation and nuclear translocation of YAP (I, Fig. 2c–f).

Besides the ease of fabrication, the main added benefit of our new approach is the inclusion of two AFM-derived calibration curves that directly connect local marker bead density to polyacrylamide stiffness (I, Fig. 2a–b). Estimating substrate mechanics directly from imaging data is efficient and, in theory, allows reproducible implementation of the gradient hydrogels in different laboratories without a need for on-site AFM measurements. This marks a clear improvement over existing methodologies, where similar calibration curves are based on fluorescence intensity—a highly instrument-dependent readout (Koser et al., 2016). However, there are a few important things to consider. First, the relationship between bead density and substrate stiffness was linear only in the narrow-range (~0.5–22 kPa) stiffness gradients (I, Fig. 2a), while the other calibration curve (~2–60 kPa) was better represented by a logit model (I, Fig. 2b). It is currently not clear why this is the case, but the non-linear relationship implies distinct diffusion kinetics between acrylamide and the fluorescent microbeads. This difference may be exacerbated in the wide-range gradients due to the increased acrylamide concentration. To our

knowledge, no other study has reported diffusion-based stiffness gradients with similarly high Young's moduli (i.e., ~60 kPa), and these observations are therefore important to keep in mind for any future applications. Second, even though the stiffness gradients were highly reproducible in our experiments (I, Fig. S1d), we have not conducted an external multi-institute validation of the results. Therefore, verifying the correlation curves on-site using AFM when setting up the technique is still advisable, if precise stiffness estimates across the whole gradient are needed. Finally, owing to the nature of the technique, the slope of the resulting gradient is difficult to control accurately. Thus, in cases where the exact slope of the gradient is considered important for the experiment, other methods may still work better.

FBs are specialized IACs that play a key role in ECM generation and remodeling (Pankov et al., 2000; Georgiadou et al., 2017). Fibronectin fibrillogenesis is known to be responsive to substrate mechanics (Carraher & Schwarzbauer, 2013), but whether the FBs themselves are directly responsive to mechanical cues has not been clear. To study this, we first wanted to select the most appropriate molecular marker for these structures. Even though there is a degree of overlap between the compositions of mature FAs and FBs, active integrin α5β1, tensin-1, and tensin-3 are typically enriched at the FBs (Zamir et al., 1999; Clark et al., 2010). Our results indicated active α5β1 as the most specific FB marker out of the three proteins, based on its high co-localization with fibronectin fibrils and exclusion from peripheral FAs (I, Figs. 3b–d, S3c). Tensin-1 and tensin-3 were present at the centrally located FBs but also clearly enriched at the FAs (I, Figs. 3a, S2b–c, S3a). While this was somewhat expected for tensin-1, tensin-3 has been reported to be mostly absent from FAs in primary human fibroblasts (Clark et al., 2010). Nevertheless, tensin-3 has still been observed at phosphotyrosine-rich FAs in A549 cells (Cui et al., 2004) and was recently reported to co-localize markedly with vinculin and other FA markers in TIFs (Atherton et al., 2022), suggesting that the relative concentration of tensin-3 at different IACs can be somewhat cell type- and context-dependent. It is also worth noting that substrate stiffness could plausibly alter the molecular composition of FBs. However, the fact that active integrin α5β1 foci were still well segregated from phosphorylated paxillin on very soft hydrogels (I, Fig. 4a) suggests that active α5β1 is an appropriate marker for FBs on mechanically graded substrates.

By plating TIFs on ~0.5–22 kPa stiffness gradients, we discovered that the growth of active integrin α5β1 adhesions was dependent on substrate stiffness (I, Fig. 4c). Moreover, tensin-1 facilitated the elongation of α5β1-positive adhesions on both soft and stiff substrates (I, Fig. 5b). Tensins have previously been shown to support integrin activity in human fibroblasts—in a talin-dependent manner—as well as in the myotendinous junctions of *Drosophila* flight muscles (Georgiadou et al., 2017; Green et al., 2018). However, the mechnanistic details of these interactions have been largely unknown.

Here, we found that FB length became maximal and plateaued on substrates of ~7–10 kPa. Interestingly, this is also the stiffness range where FAs become significantly elongated in many cell types and where matrix mechanics become fully supportive of tension-dependent talin unfolding and vinculin recruitment (Elosegui-Artola et al., 2016). This, and the apparent connection between tensin and talin in maintaining integrin activation, suggested that the mechanisms regulating mechanosensitive FA and FB growth may be closely related. Indeed, a recent study confirmed this prediction by showing that tensin-3 binds to talin via its intrinsically disordered region, and this interaction is critical for FB formation and fibrillogenesis (Atherton et al., 2022). Further, FB formation is also dependent on vinculin, and constitutively active full-length vinculin vinT12—which unlocks talin ABS2 and helps retain the rod in unfolded configuration independent of tension (Humphries et al., 2007)—supports partial FB formation even when actomyosin contraction is inhibited. This led the authors to propose a model where tensin is recruited to FAs under increasing force, and a gradual decrease in tension during the transition from FA to FB leads to loss of talin and vinculin. The model is further supported by the observation that FB formation during normal cell spreading requires intracellular contractility, but the maintenance of established FBs does not (Atherton et al., 2022). Surprisingly, Atherton and colleagues also observed that fibronectin fibrillogenesis was increased in U-2OS cells on 5 kPa versus 50 kPa substrates, suggesting that the quantity of assembled fibronectin may not always correlate with the size and number of FBs (Atherton et al., 2022). The reason for this discrepancy is currently not clear, but it may reflect, e.g., mechanosensitive differences in fibronectin expression and an attempt by the cells to adjust the mechanics of the surrounding microenvironment.

The most obvious implication of FB mechanosensitivity relates to enhanced ECM deposition and tentative positive feedback during fibrosis or desmoplasia. However, FBs may also have another unexpected role in cellular mechanoresponses. Nuclear deformation and subsequent mechanosignaling can be sustained in the absence of actomyosin contractility through an FB-mediated connection between the intracellular vimentin cytoskeleton and the ECM (Beedle et al., 2023). This mechanism regulates the timescale of intracellular mechanical adaptations and can potentially influence a number of cell-intrinsic mechanoresponses. Importantly, the authors also observed larger FBs on 30 kPa compared to 5 kPa substrates—another independent confirmation of mechanosensitive FB growth.

Our results and other recent studies paint a picture of FBs as intrinsically mechanosensitive structures that regulate ECM organization but may also play a more direct role in cellular mechanotransduction. Tensins, key regulators of FB formation and function, have been linked to pro- or anti-tumorigenic phenotypes and altered cell migration in many different studies (Rainero et al., 2015; Zhao et al., 2016; Liao & Lo, 2021). Deciphering the potential ECM-related mechanisms and

other, cell-intrinsic responses behind these observations—and how they may be connected to stromal biomechanics—will be an interesting topic for future research. In addition, it will be important to investigate the newly discovered disconnect between substrate stiffness, FB morphology, and fibronectin deposition in more detail (Atherton et al., 2022). Cell migration and cancer invasion are fundamentally linked to ECM composition and architecture, and understanding how these aspects of the stroma are regulated in human tumors remains one of the key topics in cancer research.

5.2 Negative durotaxis—directed migration toward more compliant environments (II)

5.2.1 U-251MG glioma cells undergo negative durotaxis

The commonly observed ability of cells to detect and migrate along stiffness gradients, known as durotaxis, has implications for developmental morphogenesis and cancer invasion. Despite the prior identification of several intracellular structures and molecular players that are involved in durotaxis, including IACs and the actomyosin cytoskeleton, comprehensive mechanistic models of durotaxis are still lacking. In particular, whether cells can migrate preferentially toward more compliant substrates has not been confirmed. Notably, some cell types are known to exhibit specific "stiffness optima", corresponding to some intermediate substrate stiffness that allows the cells to exert maximal traction forces on the substrate (Chan & Odde, 2008; Elosegui-Artola et al., 2016; Bangasser et al., 2017). This raises the interesting possibility that cells could migrate toward softer environments, so long as those are closer to the cell's intrinsic optimum for traction generation than the current substrate.

To test this hypothesis, we cultured U-251MG human glioblastoma cells—previously shown to exert maximal traction on substrates of 5–10 kPa (II, Fig. 1a) (Bangasser et al., 2017)—on fibronectin-functionalized ~0.5–22 kPa (II, Fig. S1a–b) stiffness gradients for 48 h. We found that, over time, the cells had a strong tendency to cluster in regions of intermediate substrate stiffness, suggesting that individual cells were migrating up or down the gradient to reach their stiffness optimum (II, Fig. 1b–c). To exclude cell proliferation as a cause for heterogeneous cell density, we measured the rate of 5-ethynyl-2′-deoxyuridine (EdU) incorporation in cells cultured on isotropic ~0.5, ~10 and ~60 kPa hydrogels. Proliferation was slightly decreased on the ~0.5 kPa substrates compared to the stiffer hydrogels, but there was no difference in EdU incorporation between the ~10 and ~60 kPa substrates (II, Fig. S2a–b). This suggests that the absence of cells in the stiffest regions of the gradient hydrogel was not due to altered cell proliferation. In addition,

we validated our findings by videomicroscopy of U-251MG cells migrating on the stiffness gradients. Cells that were initially located on the softer half of the gradient (<10 kPa) moved somewhat preferentially toward stiffer regions, whereas cells that were initially positioned above their stiffness optimum (>10 kPa) displayed a significant tendency to migrate down the gradient (II, Figs. 1d, S3a–b).

In addition to the continuous stiffness gradients discussed above, we fabricated polyacrylamide hydrogels where the initial acrylamide solution was supplemented with photocleavable crosslinker o-nitrobenzyl bis-acrylate. Using blue light to disrupt only the photosensitive crosslinks, we generated substrates with alternating ~8 kPa and ~15 kPa regions (II, Figs. 1e, S4a–b, S5a–d). In addition, 20-µm-wide fibronectin lines were printed on the hydrogels to facilitate cell movement. When U-251MG cells were cultured on these substrates, the majority of the cells clustered in the softer ~8 kPa regions (II, Figs. 1f–g, S3c–d, Video S1). Moreover, tracking of individual U-251MG cells confirmed that the cells residing at an interface between soft and stiff regions migrated preferentially toward the soft side (II, Figs. 1h, S3e, Video S2). Finally, we ruled out haptotaxis as a cause for directed cell migration in our system by confirming that fibronectin was uniformly distributed on both types of stiffness gradients (II, Figs. S1c, S5e–f). Taken together, these findings demonstrate that U-251MG glioblastoma cells are capable of negative durotaxis, concordant with their substrate stiffness optimum for traction force generation.

5.2.2 U-251MG durotaxis does not correlate with changes in common mechanosignaling pathways

In order to study the molecular mechanisms that regulate durotaxis in U-251MG cells, we first investigated the activation of different IAC-associated signaling pathways on ~0.5, ~8, and ~50 kPa hydrogels. However, we observed no changes in overall FAK, ERK, or myosin light chain 2 (MLC2) phosphorylation on these mechanically distinct substrates (II, Fig. 2a–b). Next, we compared mechanosensitive FA formation in U-251MG cells, capable of negative durotaxis, and MDA-MB-231 breast cancer cells which undergo strictly positive durotaxis in the same stiffness range (DuChez et al., 2019). While the MDA-MB-231 cells formed obvious paxillin-positive FAs on intermediate and stiff (~10 and ~60 kPa) substrates (II, Fig. S6a), the U-251MG cells were mostly devoid of FAs even on the rigid ~60 kPa hydrogels (II, Figs. 2c, S6b). This was despite the fact that phosphorylated MLC2 and key mechanosensitive IAC components talin-1, talin-2, and vinculin were all expressed at comparable levels in both cell types as well as another FA-forming cell line, U-2OS (II, Figs. S6c–d, S16). Nevertheless, U-251MG cells expressed abundant active β1integrin and their spreading on stiff hydrogel was

impeded by the β1 function-blocking mAb13 antibody, confirming that these cells use integrins to interact with fibronectin substrates (II, Fig. S6e–g).

YAP and TAZ are key mechanotransducers that have been linked to FA dynamics and durotaxis (Nardone et al., 2017; Lachowski et al., 2018; Mason et al., 2019). We stained endogenous YAP in U-251MG cells and found that the protein was mostly cytoplasmic or diffusely distributed on ~0.5, ~2, ~10 and ~60 kPa substrates. In contrast, MDA-MB-231 cells exhibited robust substrate stiffness-dependent nuclear localization of YAP (II, Fig. 2d–e). In summary, U-251MG cells display minimal mechanosensitive signaling responses, and none of them appear specific to the 5–10 kPa stiffness range. Thus, these signaling pathways are unlikely to explain the negative durotaxis.

5.2.3 Stochastic molecular clutch simulations recapitulate positive and negative durotaxis

Recently, the molecular clutch model has been used to predict U-251MG migration speed and traction force generation on different soft and stiff substrates (Bangasser et al., 2017). After observing that the cells migrated preferentially toward their stiffness optimum in all of our experimental models (II, Fig. 1a–h), we decided to investigate whether a stochastic computational CMS would be sufficient to recapitulate U-251MG durotaxis in silico (II, Fig. 3a and Materials and Methods). We simulated the spreading and migration of individual cells on isotropic substrates for 1 h (in-simulation) to allow the system to reach a dynamic steady state. Next, the cells were positioned on substrates consisting of alternating 60-μm soft and stiff regions that were joined together by steep (30-μm) stiffness gradients (II, Figs. 3b, S7a–b).

On 10–100 pN nm^{-1} substrates, where the cells' optimal stiffness overlapped with the softer regions (II, Fig. 3c–d), most cells moved to the more compliant areas within the first 12 h of the simulation (II, Fig. 3e–f). When cells were interacting with the graded substrate regions, their protrusions (clutch modules) positioned on the soft substrate exhibited higher average traction forces than the ones interacting with the stiff substrate (II, Fig. S8a–c). The cells also migrated preferentially toward the softer regions (II, Fig. S8d). When the range of the gradient was changed, and the side associated with higher predicted traction forces was the stiffer one, durotaxis was reversed and cells clustered mainly on the stiffer substrate (II, Fig. S9a–c). Finally, when the gradient was chosen so that the difference in predicted traction forces was close to zero, the cells clustered on the stiffer substrate where their migration was slower, suggesting an additional durokinetic effect (II, Fig. S9d). In order to study the tracks of individual cells in quantitative detail, and to minimize the possible confounding effect from durokinesis, we replaced the repeating

substrates with a continuous 10–30 pN nm^{-1} gradient (II, Fig. 3g). Here, too, the majority of cells migrated down the gradient—toward their stiffness optimum—and recapitulated the in vitro behavior of U-251MG cells (II, Fig. 3h–i).

To date, the most compelling experimental evidence for directed cell movement toward softer tissues comes from *Xenopus* retinal ganglion cells, and mechanosensitive growth cone steering may be highly analogous to single-cell durotaxis (Koser et al., 2016). Thus, we applied the molecular clutch model to neural growth cones to see if we could reproduce axonal pathfinding on mechanically graded substrates in silico. The actin-rich growth cones at the distal ends of axons contain many dynamic filopodia of variable orientation and length (II, Fig. S10a). Modeling both individual filopodia (II, Fig. S10b) and semi-circular growth cones with multiple filopodia (II, Fig. S11a), we observed that the actin projections elongated faster and exerted more traction on softer (0.01–0.1 pN nm^{-1}) substrates (II, Figs. S10c–h, S11b). This was consistent with the prevailing notion that most neurons are relatively weak force generators that have low stiffness optima (Chan & Odde, 2008; Betz et al., 2011; Koch et al., 2012). Importantly, gradient slope and range further impacted growth cone mechanoresponses (II, Fig. S11c–e). Growth cone turning toward the soft substrate was impeded when the gradient was too weak (~0.1 pN nm^{-1}/20 μm) or altogether too rigid (>1 pN nm^{-1}) compared to the optimal stiffness.

5.2.4 Inhibiting actomyosin contractility selectively impedes negative durotaxis

According to the molecular clutch model, the optimal substrate stiffness is dictated by multiple parameters. These include the binding and unbinding rates of the clutches as well as the total number of clutches and molecular motors. For example, decreasing the number of motors relative to the available clutches is expected to shift the stiffness optimum up (Bangasser et al., 2013). We confirmed this in our CMS model, where a gradual decrease in motors resulted in a maximum of threefold increase in the optimal stiffness before the system stalled, halting actin dynamics and cell migration (II, Fig. 4a–b). In order to investigate whether actomyosin contractility is similarly connected to the stiffness optimum and durotaxis in U-251MG cells, we plated the cells on ~0.5–22 kPa stiffness gradients and treated them with ROCK1/2 inhibitor H-1152. We observed a significant reduction in total phosphorylated MLC2, increased formation of peripheral actin-rich ruffles, and continued absence of vinculin-positive FAs in the treated cells (II, Figs. 4c–d, S12a). Strikingly, H-1152 treatment also resulted in a dose-dependent increase in the number of cells in the stiffest region of the graded substrate, in contrast to the characteristic accumulation of untreated cells at an intermediate substrate stiffness (II, Fig. 4e–f). We confirmed

these findings by live-cell imaging: as expected, vehicle-treated control cells that were initially positioned on the stiffer half of the gradient (>10 kPa) underwent negative durotaxis, whereas all the H-1152-treated cells were migrating preferentially toward a stiffer environment (II, Figs. 4g, S12b, Video S3). Similar results were obtained when U-251MG cells were treated with an intermediate (5 μM) dose of blebbistatin, a myosin II inhibitor, whereas higher concentrations of the drug inhibited durotaxis and possibly cell migration completely (II, Fig. S12c–d). These results highlight the key role of actomyosin in durotaxis and suggest that altered intracellular contractility can shift the cell-intrinsic stiffness optimum in U-251MG cells. Depending on the stiffness gradient, this can even reverse the direction of durotaxis.

5.2.5 Talin depletion can induce negative durotaxis in MDA-MB-231 cells

Contrary to the distinct stiffness optima observed in many neurons and the U-251MG cells, the traction forces of most adherent cell types increase monotonically as a function of substrate stiffness. One key reason for this is thought to be talin- and vinculin-mediated clutch reinforcement and FA formation. Consequently, inhibiting IAC maturation by downregulating talin can prevent reinforcement, forcing the cells into the biphasic traction regime predicted by the molecular clutch model (II, Fig. 5a) (Elosegui-Artola et al., 2016). We hypothesized that disrupting FA formation in this way could inhibit, or even revert, positive durotaxis. To test this, we performed a double knockdown of talin-1 and talin-2—using two independent sets of siRNA oligos—in MDA-MB-231 cells (II, Figs. 5b, S13a, S17), a cell line reported to undergo positive durotaxis in the 2–18 kPa stiffness range (DuChez et al., 2019). Talin-low cells displayed fewer and smaller FAs (II, Figs. 5c–e, S13b–c) and, importantly, reduced traction forces on the ~22 kPa substrates, where talin is typically expected to facilitate FA formation (II, Figs. 5f–h, S14a) (Elosegui-Artola et al., 2016). When MDA-MB-231 cells were cultured on ~0.5–22 kPa stiffness gradients, control cells clustered at the stiffest end of the gradient. However, talin-low MDA-MB-231 cells phenocopied the U-251MG cells and accumulated in regions of intermediate stiffness (II, Figs. 5i–j, S13d–e). EdU incorporation in MDA-MB-231 cells was only decreased on ~0.5 kPa hydrogels compared to substrates of ~10 kPa and above, with or without talin knockdown (II, Fig. S14b–c). Taken together, these data show that conventional positive durotaxis can be converted to negative by inhibiting talin- and vinculin-mediated clutch reinforcement and FA formation.

5.2.6 Discussion

Metazoan tissues are complex and dynamic, exhibiting both spatial and temporal changes in their molecular composition and physical properties. Gradients of ECM stiffness can guide cell migration during developmental processes and may even contribute to cancer cell movement inside and out of the malignant stroma (Shellard & Mayor, 2021a). Here, we demonstrated for the first time that U-251MG glioblastoma cells are capable of directed migration toward softer environments, termed negative durotaxis—in contrast to the more commonly observed positive durotaxis, i.e., cell migration toward stiffer substrate. We observed negative durotaxis on photoresponsive hydrogels with very steep stiffness gradients and on longer, continuous gradients. On the latter, U-251MG cells exhibited biphasic migration toward regions of intermediate stiffness (~10 kPa).

Strikingly, U-251MG cells exhibited few morphological or signaling responses to the changing substrate stiffness. Most importantly, they presented with very few mature FAs even on rigid (~60 kPa) polyacrylamide substrates, in contrast to many other adherent cell types (II, Fig. 2c). However, U-251MG cells have been previously shown to exert maximal traction forces on substrates of ~5–10 kPa, indicating that the cells can still sense and respond to local substrate mechanics (Bangasser et al., 2017). This apparent contradiction was explained using the molecular clutch model: substrate stiffness influences the rate of force loading on different cytoskeletal and IAC molecules (i.e., the clutch), which directly impacts the lifetimes of the associated chemical bonds. This, in turn, can promote or impede force transmission between the cell and its substrate, regulating mechanosensitive cell spreading and migration (Bangasser et al., 2017). We found that a similar model can sufficiently explain stiffness gradient-dependent positive and negative durotaxis in U-251MG cells (II, Figs. 3a–i, S9a–d). Further, since the optimal stiffness for traction generation is sensitive to the ratio of clutches to motors, reducing intracellular contractility is expected to shift the stiffness optimum up—a prediction we confirmed in vitro by reversing negative durotaxis to positive using ROCK and myosin II inhibitors (II, Fig. 4e–g). These results are also consistent with previous reports indicating that myosin II inhibition does not necessarily impede mechanically directed migration (Puleo et al., 2019). Taken together, our data point to a model where a cell's contractile and adhesive machinery dictates its capacity to exert traction and protrude on mechanically distinct substrates. As a result, cells can migrate up or down stiffness gradients to reach their intrinsic stiffness optimum (II, Fig. S15).

In reality, very few cell types appear capable of negative durotaxis. This is likely to be explained by talin- and vinculin-mediated FA formation, which gives rise to monotonically increasing traction forces. Instead of overloading and dissociating the clutches, increased tension further reinforces the connection between the actin

cytoskeleton and the ECM (Elosegui-Artola et al., 2016). Consequently, biphasic relationships between substrate stiffness and cellular traction forces are rarely observed in wild type cells. We confirmed the impact of clutch reinforcement on positive versus negative durotaxis by silencing talin-1 and talin-2 in MDA-MB-231 cells. As a result, the cells phenocopied the U-251MG cells and clustered in regions of intermediate stiffness on the ~0.5–22 kPa gradients (II, Figs. 5i–j, S13d–e).

While other materials like PDMS are occasionally used for preparing mechanically graded substrates (Breckenridge et al., 2014), polyacrylamide-based stiffness gradients remain the gold standard for studying durotaxis in vitro (Hartman et al., 2016; Sunyer et al., 2016; DuChez et al., 2019; Rong et al., 2021; Yeoman et al., 2021; Guo et al., 2023). Here, we generated polyacrylamide substrates with stiffness gradients using two different approaches: one was based on the photocleavage of o-nitrobenzyl bis-acrylate, an acrylamide crosslinker (II, Fig. S5a), and the other one was based on partial mixing of two acrylamide prepolymer solutions (II, Fig. S1a). Because the ~0.5–22 kPa gradients featured changes in the concentration of the polymer backbone (Table 5), we confirmed that the amount of fibronectin conjugated to the substrate did not differ between the soft and stiff regions (II, Fig. S1c). This excluded haptotaxis as a cause for directed migration. However, polyacrylamide density has also been reported to influence the mechanics of the covalently conjugated ECM molecules. Proteins attached to the softer, more porous polyacrylamide have less “anchoring points” and thus buckle easily under the forces exerted by the cells (Trappmann et al., 2012). This could mean that the cellular phenotypes on the softer substrate result from some combination of lower bulk substrate elasticity and increased yielding of the individual ECM molecules, complicating the interpretation of the results. Nevertheless, the fact that we also observed negative durotaxis on the photoresponsive hydrogels suggests that the phenomenon is not driven by altered ECM conjugation to the underlying substrate.

Many studies have indicated that disrupting FA formation or growth can impede positive durotaxis (Wormer et al., 2014; Puleo et al., 2019; Yip et al., 2021). However, our modeling and in vitro results suggest that positive single-cell durotaxis can readily take place without mature FAs—so long as the cells are migrating on a relatively soft gradient that is below their stiffness optimum. These different observations are surprisingly easy to reconcile. First, the effect of impaired FAs may depend on the range of the stiffness gradient and how it relates to cellular traction forces after the treatment. For example, analyzing U-251MG cell migration on the ~0.5–22 kPa gradients (II, Figs. 1d, 4g [control cells]) without stratifying the cells into two groups based on their stiffness optimum would result in some cells migrating up the gradient and others migrating in the opposite direction—a misleading net effect indicating adurotaxis. Interestingly, inhibiting FA formation in MCF-7 cells on stiff 35 kPa substrates causes the cells to turn away from locally

strained substrate, which could be indicative of negative durotaxis (Puleo et al., 2019). It is likely that such a strong mechanical stimulus is well above the cell-intrinsic optimum without FA-dependent reinforcement. Second, it is also plausible that positive durotaxis is simply more pronounced and robust in the presence of functional, mature FAs. IACs are linked to several positive feedback mechanisms that can reinforce a pre-existing front-rear polarity axis and promote directionally persistent migration. Possible examples include FA-proximal activation of mechanosensitive ion channels (Yao et al., 2022) and polarization of the Golgi and MT array. Indeed, Golgi MTs have already been implicated in the positive durotaxis of human RPE cells (Rong et al., 2021). Whether transient signaling (e.g., Rho GTPase) gradients and polarized actin dynamics can support some degree of Golgi reorientation and anterograde trafficking during negative durotaxis is an interesting open question.

Traction forces between cells and their substrate are fundamental to mesenchymal cell migration, and asymmetric peripheral traction precedes durotaxis in fibroblasts (Trichet et al., 2012; Breckenridge et al., 2014). More recently, this relationship was reported to be causal: cells at an interface between soft and stiff substrates underwent durotaxis only if a cellular-level traction force imbalance between the two sides could be established (Jun et al., 2023). Forces are propagated in cells through the prestressed actin cytoskeleton, a process that is thought to be important for mechanosensing (Hu et al., 2003; Hoffecker et al., 2011). However, there is also ample evidence that cells can probe and respond to substrate mechanics on a local (sub-micron) scale, and FAs pull on the substrate independent of their neighbors (Ghassemi et al., 2012; Plotnikov et al., 2012). This compartmentalization of intracellular forces is likely to be important for durotaxis. In the simplest molecular clutch model of intracellular force transmission—i.e., a 1D contractile actin fiber that is attached to the substrate via identical clutch modules at both ends—the mean forces and actin flow dynamics are evenly balanced. On stiffness gradients, such models naturally produce positive durotaxis due to anisotropic substrate deformation, an effect that is mainly visible in larger cell collectives and depends on active force transmission through cell-cell junctions (Sunyer et al., 2016). In contrast, our model includes multiple protrusions around a central cell body that contains additional clutches, facilitating an asymmetric build-up of forces at the cell periphery (II, Fig. S8a–c) (Fortunato & Sunyer, 2022). Importantly, disruption of the LINC complex in MEFs plated on stiffness gradients does not influence local responses to substrate stiffness, including FA growth, but prevents the imbalance in traction forces at the cellular level and inhibits durotaxis. This suggests that the nucleus serves as a damper to regulate force transmission between the leading and trailing edges of the cell (Jun et al., 2023). Previous studies have also indicated that enucleated cells can undergo normal chemotaxis and haptotaxis, but their migration

velocities on different elastic substrates are significantly altered (Graham et al., 2018). Taken together, our results and the above studies point to a key role of the nucleus in the mechanosensitive regulation of cell motility.

According to the molecular clutch model, the balance between contractile and adhesive forces is one of the key determinants behind cellular responses to substrate mechanics. Recently, Yeoman and colleagues confirmed this notion by studying mechanotypic heterogeneity and durotaxis in breast, lung, and prostate cancer cells (Yeoman et al., 2021). The authors sorted different cancer cell lines into strongly and weakly adherent subpopulations using shear stress and observed striking differences in their behavior on elastic substrates: even though the strongly adherent cells were generally slower and less contractile than the weakly adherent ones, they were also significantly more disposed to undergo positive durotaxis. This was explained by a model where the faster accumulation of forces on the stiff substrate was offset by a decrease in bond lifetimes that was specific for the more contractile cells, resulting in balanced traction forces and absence of durotaxis. Importantly, the authors also modulated durotactic behavior in the different MDA-MB-231 subpopulations in vitro by increasing or decreasing their actomyosin contractility. These observations align well with our own results and make the important additional point that significant mechanotypic differences may arise between cancer cells that have a similar clonal origin—a fact that could also shed light on the migration paradox in human tumors (Yeoman et al., 2021). It is also worth noting that the authors did not observe any differences in cytokine signaling between the weakly and strongly adherent MDA-MB-231 cells. Similarly, the molecular determinants behind the different mechanoresponses in U-251MG and MDA-MB-231 cells in our study (i.e., the lack of FA maturation in the glioma cells despite the expression of both talin and vinculin [II, Fig. S6c–d]) are currently unknown and should be investigated in the future.

We also sought to find out whether our model could explain the mechanosensitive axonal pathfinding of *Xenopus* retinal ganglion cells (Koser et al., 2016; Thompson et al., 2019). Neurons are relatively weak force generators, and individual growth cones exhibit tugging motion and biphasic traction forces characteristic of the molecular clutch model (Chan & Odde, 2008; Betz et al., 2011). Here, our simulations suggested that sufficiently steep and soft stiffness gradients could influence filopodia growth dynamics, resulting in mechanosensitive growth cone turning (II, Figs. S10a–h, S11a–e). There are a few important considerations associated with these results and the *Xenopus* model. First, the in vivo stiffness gradient in the embryonic *Xenopus* brain arises mainly from local differences in cell density and not from altered ECM deposition (Thompson et al., 2019). Nevertheless, the retinal ganglion cells are also sensitive to substrate stiffness on laminin- and fibronectin-coated polyacrylamide hydrogels, indicating that the cells probe tissue

mechanics using integrins and associated adaptor molecules (Koser et al., 2016). Second, normal *Xenopus* retinal ganglion cell elongation in vitro and in vivo is dependent on the mechanosensitive ion channel Piezo1 (Koser et al., 2016). Piezo1 is known to exhibit significant crosstalk with IACs (Yao et al., 2022) and could also plausibly contribute to clutch dynamics in the *Xenopus* retinal ganglion cells. While a molecular clutch-based mechanism may regulate axonal pathfinding in the developing *Xenopus* brain, and possibly in other types of neurons, more research on this hypothesis is needed.

Clusters of carcinoma cells were recently shown to exhibit directionally persistent migration on viscoelastic collagen networks despite lacking any obvious internal polarization (Clark et al., 2022). Interestingly, these cell clusters generate overlapping gradients of collagen alignment, density, and stiffness while they are moving, such that collagen density and stiffness are maximal and alignment is minimal at the rear of the cluster. This ECM anisotropy is critical for the persistent collective migration and gives rise to asymmetric traction forces, suggesting that contact guidance, negative durotaxis, or a combination of both mechanisms may bias protrusion and drive persistent migration in cell clusters (Clark et al., 2022). Negative durotaxis has now also been reported in individual B16-F1 melanoma cells (Huang et al., 2022). These cells were shown to exert maximal traction on ~2 kPa substrates, and their durotaxis was also quantitatively and qualitatively affected by myosin II inhibition and Rho activation. However, the treatments did not appear to influence the B16-F1 stiffness optimum, which makes these results challenging to reconcile with our current model. Nevertheless, the study serves as a promising indication of the existence of negative durotaxis in different cell types.

A growing body of evidence indicates that many eukaryotic cells exhibit a mechanical memory. For example, prolonged culture of human MSCs on stiff (10 kPa) hydrogels leads to a persistent activation of YAP/TAZ and biases the cells toward osteogenic differentiation (Yang et al., 2014). In addition, stiff or soft substrates can lead to relatively rapid (i.e., in the span of days or weeks) and poorly reversible epigenetic adaptations in primary chondrocytes (Scott et al., 2023) and different carcinoma cells (Kaukonen et al., 2016). It is plausible that the prominent FAs and high stiffness optima that are characteristic of many commercial cell lines reflect long-term clonal selection and/or phenotypic adaptation to extremely rigid ($\gg$1 MPa) cell culture plastic. Indeed, primary mouse mammary gland stromal fibroblasts are able to spread and exert high traction forces on compliant (~2 kPa) collagen-coated hydrogels, which was suggested to reflect an adaptation to their native mammary microenvironment (Lerche et al., 2020). It is tempting to speculate that negative durotaxis may be more common in different primary cell populations and possibly in vivo—a hypothesis that should be tested thoroughly in future studies.

In addition to substrate stiffness, the molecular clutch model has successfully recapitulated cellular responses to viscoelastic cues and ligand nanospacing (Oria et al., 2017; Bennett et al., 2018). This raises the intriguing possibility that different mechanical inputs could direct cell migration through a common set of receptors and intracellular adaptor molecules. Indeed, the existence of "viscotaxis", directed cell migration on gradients of substrate viscosity, was recently demonstrated (Shirke et al., 2021). Several research groups have now started to expand the theoretical model of molecular clutch-driven positive and negative durotaxis by incorporating clutch reinforcement and FA formation, polarized Rho GTPase signaling, and viscoelasticity in the same conceptual framework (Shu & Kaplan, 2023; Sáez & Venturini, 2023). Such computational models have already yielded interesting predictions, e.g., that a sufficiently high viscous component abolishes the biphasic relationship between substrate elasticity and directed migration, promoting negative durotaxis (Shu & Kaplan, 2023). Taken together, these results will serve as an important roadmap for future experiments.

In a sense, durotaxis can be seen as one of the most rudimentary forms of gradient sensing: the same intracellular machinery first detects the signal and then transmits the necessary forces to the substrate to drive cell movement (Fortunato & Sunyer, 2022). We demonstrate that this mechanically directed migration can be explained by a relatively simple set of underlying principles that may also regulate cellular responses to other facets of ECM biomechanics. Investigating how cells coordinate responses to such overlapping physical cues should be a key goal for future research. Importantly, our results also illustrate how quantitative changes in intracellular processes, e.g., actomyosin contractility, can lead to qualitative changes in cell migration—up to and including the reversal of durotaxis on a given stiffness gradient. From the perspective of migrastatics and therapeutic targeting of cancer invasion, this poses a problem: it suggests that cancer cells can exhibit surprising, dose-dependent migratory responses to many commonly studied anti-invasive agents.

5.3 Dynamic micropatterns and substrate-specific geometric control of cell front-rear polarity and migration (III)

5.3.1 Binary micropatterning using PLL-g-PEG-biotin and streptavidin-conjugated secondary ligands

Cells are acutely sensitive to the geometry of their local ECM microenvironment, and anisotropic substrates can direct both front-rear polarization and cell migration (Théry et al., 2006; Caballero et al., 2015). In order to investigate the impact of ECM

composition and integrin signaling on the geometric control of cell polarity and movement, and to facilitate research on cell-ECM interactions in general, we established a new accessible method for dynamic micropatterning. We started by cleaning glass coverslips with nitric acid and UVO treatment and coated the cleaned coverslips with 50% biotinylated PLL-g-PEG. Next, deep UV photopatterning was used to convert some of the PEG carbons (C–O–C) to carboxyl groups (COOH), supporting spatially controlled adsorption of ligand molecules to the substrates (III, Figs. 1a, S1a) (Azioune et al., 2009). To functionalize the micropatterns, we incubated them with ECM components (e.g., fibronectin) and fluorescently labeled BSA—an inert protein included at low concentrations to allow micropattern visualization during imaging.

In order to coat the non-patterned regions with a secondary ligand, we incubated the coverslips with varying concentrations of SA-FN. By visualizing the resulting substrates via immunofluorescence, we observed a gradual increase in the amount of bound fibronectin around the micropatterns (III, Fig. 1b–d). Due to the exceptionally high affinity between biotin and streptavidin molecules, the PLL-g-PEG-biotin surfaces coated with streptavidin-conjugated secondary ligands were expected to be very stable. To test this, we incubated PLL-g-PEG-biotin coverslips coated with SA-FN in a humidified incubator, at +37 °C, for up to 6 days. Fibronectin density remained constant across the coated surfaces for the duration of the experiment (III, Fig. S1b–c). In addition, the SA-FN surfaces remained amenable for U-251MG glioma cell adhesion and growth (III, Fig. S1d).

To confirm the specificity of protein coating in both photopatterned and non-patterned substrate regions, we prepared coverslips with thin linear micropatterns and either I) coated them with collagen and no secondary ligand, or II) coated the patterns with fluorescent BSA (non-adhesive) and then incubated the coverslips with streptavidin-conjugated collagen-mimetic peptide (SA-GFOGER). In both cases, the micropatterns were blocked after the initial coating with 2% BSA. Next, we seeded the substrates with MDA-MB-231 cells, allowed them to adhere for 3 h, and fixed the samples. Immunofluorescence microscopy revealed that paxillin-positive IACs were confined specifically to regions that had been coated with integrin ligands, whether inside or outside the photopatterned areas (III, Fig. 1e). Finally, we validated the biocompatibility of PLL-g-PEG-biotin in our system by preparing crossbow-shaped micropatterns on unmodified and biotinylated PLL-g-PEG substrates. After seeding the micropatterns with both U-251MG and U-2OS cells, we observed no morphological differences—including possible changes to the actin cytoskeleton or IACs—between the two PEG moieties (III, Figs. 2a–b, S2a–b). Our results indicate that UV photopatterning of PLL-g-PEG-biotin can be combined with streptavidin-conjugated ECM components to yield binary micropatterns with two kinds of mutually exclusive adhesive surfaces.

5.3.2 PLL-g-PEG-biotin allows a controlled release of cells from the micropatterns

Next, we wanted to find out whether PLL-g-PEG-biotin and streptavidin-conjugated secondary ligands could be used for dynamic micropatterning, i.e., whether we could release the cells from their confinement in a coordinated manner (III, Fig. 2c). We investigated this by growing U-2OS cells on fibronectin-coated micropatterns, supplementing some of the wells with streptavidin-conjugated fibronectin fragment (SA-FNIII 7–10), and fixing the samples after 1 h. Unlike untreated control cells or cells on regular PLL-g-PEG, U2-OS cells grown on micropatterned PLL-g-PEG-biotin and supplemented with SA-FNIII 7–10 had rapidly spread on the substrate around the original micropatterns (III, Fig. 2d). Due to the fast release of the cells and the high affinity of the biotin-streptavidin interaction, we hypothesized that the SA-FN binding to the free PLL-g-PEG-biotin would happen very quickly. To test this, we acquired videos of linear micropatterns on PLL-g-PEG-biotin before and after supplementing the medium with SA-FN conjugated to fluorescein isothiocyanate (FITC). A significant amount of SA-FN-FITC bound to the non-irradiated PLL-g-PEG-biotin almost instantaneously (<2 min), and most of the remaining secondary ligand had disappeared from the medium in ~15 min (III, Fig. S1e–g, Video S1).

To further validate the technique for dynamic micropatterning, we tested its applicability for synchronizing B lymphocyte activation. When B lymphocytes bind antigens, they respond by forming an intricate cell-cell (or cell-ECM) interaction structure called the immune synapse (Kuokkanen et al., 2015). The B cell antigen receptors (BCR) in mouse A20 [D1.3] cells can be activated using anti-IgM antibodies, however, monovalent anti-IgM Fab fragments can only trigger BCR activation if the surrogate antigens are immobilized to a solid support. We sought to use streptavidin-conjugated anti-IgM Fab to direct B lymphocyte activation exclusively to the biotinylated surface, which would allow us to observe immune synapse formation collectively—for multiple cells in parallel—from the very beginning of BCR engagement.

To this end, we prepared small (Ø = 5 μm) round micropatterns on PLL-g-PEG-biotin and coated them with fibronectin. Fibronectin allows B lymphocyte adhesion but does not support activation and immune synapse formation. A20 cells were then seeded on the micropatterns, allowed to adhere, and the medium was supplemented with unconjugated or SA-anti-IgM Fab for 10 min before the cells were fixed. While the cells treated with unconjugated anti-IgM remained round and confined to the fibronectin patterns, the cells supplemented with SA-anti-IgM Fab spread rapidly outward and displayed radial symmetric actin structures characteristic of immune synapses (III, Fig. S3a–c) (Kuokkanen et al., 2015). Taken together, these results show that UV photopatterned PLL-g-PEG-biotin and streptavidin-conjugated ECM

proteins and peptides can be used for dynamic micropatterning. Releasing the micropattern-confined cells happens rapidly and requires the presence of both biotin and streptavidin groups (i.e., all the secondary ligands attach to the substrate via strong non-covalent interactions).

5.3.3 The impact of different ECM components and integrin antibodies on cell front-rear polarity

Additional cues like substrate stiffness can influence cellular responses to local ECM geometry. However, the specific role of ECM composition in the geometric control of front-rear polarity and cell migration is poorly understood. We started investigating this by seeding U-251MG cells on crossbow-shaped micropatterns coated with different physiological integrin ligands, including fibronectin, type I collagen, and laminin-521 (LN-521)—a protein that is found in most human BMs and recognized by a number of different integrin subtypes (Nishiuchi et al., 2006; Yap et al., 2019). The micropatterns were also blocked with 2% BSA, and all comparisons were done using growth medium supplemented with fibronectin-depleted serum (III, Fig. S4a). Front-rear polarization was defined by measuring the orientation of the centrosome, labeled using anti-γ-tubulin or anti-centrin-2 antibodies, relative to the centroid of the nucleus. In addition, paxillin co-localized with the centrosome in U-251MG cells, as reported previously for other cancer cell lines (III, Fig. 3a) (Dubois et al., 2017). As expected, U-251MG cells polarized very consistently on the fibronectin-coated micropatterns, with the centrosomes facing mainly the wide, adhesive edge of the pattern. Front-rear polarization on LN-521 was indistinguishable from fibronectin, but cells on collagen-coated micropatterns polarized less consistently (III, Figs. 3a–b, S4b). This difference was confirmed using the orientation of the trans-Golgi network as a proxy for the front-rear polarity axis (III, Fig. S4c–d).

We wanted to know if the observed differences were due to altered IAC formation on collagen. First, we noted that the U-251MG cells spread equally well on all the different ECM-coated micropatterns, while the number and size of paxillin-positive IACs varied markedly between individual cells. Next, we compared the average basal distribution of paxillin in micropatterned U-251MG cells on each of the different integrin ligands (III, Fig. S5). While the mean paxillin density around the cell periphery did not differ much between fibronectin, LN-521, and collagen, we observed more diffuse paxillin signal throughout the cell on the collagen-coated micropatterns. The relative variation in peripheral paxillin density was also somewhat higher on collagen. This suggests that the spatial distribution of IACs in U-251MG cells is less tightly controlled on collagen versus fibronectin and laminin,

which may contribute to the less consistent front-rear polarization observed in these cells.

Since integrin ligation and clustering are known to elicit distinct—albeit overlapping—responses in many cell types, we wanted to see if these two facets of integrin signaling can be decoupled in the geometric control of cell polarity. We generated additional crossbow-shaped micropatterns coated with bivalent anti-integrin β1 antibodies, mAb13 (recognizes the closed/low-affinity conformation) and 12G10 (extended open/high-affinity conformation) (Su et al., 2016), and seeded U-251MG cells on those. Interestingly, both antibodies were capable of supporting at least partially biased front-rear polarization (III, Figs. 3a–b, S4b). However, the overall intracellular positioning of the centrosomes and nuclei was less uniform than on fibronectin or LN-521, and resembled collagen-coated micropatterns. These results suggest that integrin ligation is not necessary for controlled front-rear polarization on anisotropic micropatterns, but polarization is more consistent on specific physiological integrin ligands.

5.3.4 ECM components and integrin antibodies elicit partially distinct signaling responses

Intrigued by the above differences—and similarities—between ECM components and anti-integrin β1 antibodies, we sought to find out how these different substrates impact common integrin-associated signaling pathways. We plated U-251MG cells on polystyrene surfaces coated with fibronectin, collagen, 12G10, or mAb13, lyzed the cells after 30 min, and analyzed the samples by immunoblotting. The results were contrasted to cells that had been retained in suspension for the same amount of time (negative control) (III, Fig. S6a–c). Surprisingly, we observed minimal differences in AKT phosphorylation (S473) between the different conditions, and ERK phosphorylation (T202/Y204) was markedly decreased only in the negative control. However, FAK phosphorylation (Y397) was maximal on fibronectin and seemed to decrease gradually on collagen, 12G10, mAb13, and finally in the negative control (III, Fig. S6a–b). FAK has also been reported to facilitate front-rear polarization in migrating cells (Maninová et al., 2013; Dubois et al., 2017; Fructuoso et al., 2020). Thus, we treated cells growing on fibronectin-coated, crossbow-shaped micropatterns with a FAK inhibitor, PF-573228, and observed a drastic decrease in both intracellular phosphorylated FAK and front-rear polarization toward the wide edge of the micropattern (III, Fig. 3c–e). The available biological ligands can significantly alter both downstream signaling responses and the capacity of cells to polarize in response to local substrate geometry. In addition, the consistent front-rear polarization of U-251MG cells on fibronectin is dependent on FAK signaling.

5.3.5 Investigation of early spreading and migration events using dynamic micropatterns

Local ECM geometry is known to regulate cell motility. Since front-rear polarity (e.g., MTOC orientation) is considered a key aspect of directed migration, we wanted to investigate how the anisotropic micropatterns coated with different integrin ligands and antibodies influence subsequent cell spreading and migration. First, we confined EGFP-centrin-2-expressing U-251MG cells on fibronectin- or mAb13-coated, crossbow-shaped micropatterns. After the cells had fully occupied the patterns, the medium was supplemented with SA-FN and the cells were tracked over time (III, Figs. 4a, S7a, Video S2). The cells spread rapidly from both types of micropatterns, taking approximately 60 min to reach their final size (III, Fig. 4b). Fibronectin-adhered cells displayed more consistent front-rear polarization prior to their release, as expected, and this coincided with more polarized early spreading and migration away from the patterns (III, Fig. 4c–e). We then continued to track the released cells for up to 4 h, and found that the cells originating from fibronectin-coated patterns migrated with higher directional persistence (III, Fig. S7b–e). Interestingly, however, the total track lengths were slightly longer for the cells released from mAb13, indicating that these cells migrated faster but with less directional persistence (III, Fig. S7e).

In addition to integrin-mediated signaling, another facet of the adhesive and cytoskeletal machinery that has been linked to front-rear polarization is the actin retrograde flow (Gomes et al., 2005; Maiuri et al., 2015). Since cell protrusion and actin flow rate are often inversely coupled, confining cells on micropatterns is expected to promote the rearward flow of actin. However, since the retrograde flow is also practically limited by the physical connection between actin and the ECM (i.e., molecular clutches), we investigated whether fibronectin and mAb13 can differentially regulate actin rearward flow in micropatterned U-251MG cells. We did not observe any significant differences in the actin flow rate between cells on fibronectin- and mAb13-coated, crossbow-shaped micropatterns, suggesting that altered actin dynamics are not a causative factor behind the less consistent front-rear polarization on mAb13 (III, Fig. 4f–g). As expected, releasing the cells on SA-FN resulted in a rapid decrease in the actin flow rate, independent of the original micropattern coating (III, Fig. 4f–g, Video S3). These data indicate that confining cells on micropatterns and restricting their ability to protrude and migrate can markedly promote the retrograde flow of actin. However, the biochemical composition of the substrate is less important—at least in the system reported here.

5.3.6 Early migration correlates poorly with the nucleus-Golgi-centrosome axis

Intrigued by the possible connection between less consistent front-rear polarization (MTOC orientation) and lack of polarized spreading and migration in the mAb13-confined U-251MG cells (III, Fig. 4d–e), we decided to analyze the correlation between centrosome orientation and subsequent cell migration at the single-cell level. We stratified all the cells in (III, Fig. 4c) into two groups according to their centrosome orientation before the SA-FN was added: one group for cells with centrosomes facing the front (i.e., the wide edge of the micropattern) and another for cells with rearward-facing centrosomes (III, Fig. 5a–b, Video S4). Surprisingly, we found that the initial centrosome orientation only weakly predicted the future direction of migration. Specifically, a significant fraction of the cells with forward-facing centrosomes still started migrating toward the narrow end of the micropattern, while many cells with rearward-facing centrosomes started migrating forward. The apparent connection between centrosome orientation and subsequent spreading/migration was somewhat higher for the cells released from mAb13 compared to fibronectin, but many of these cells also migrated in a direction opposite to their initial nucleus-MTOC axis (III, Fig. 5b). To further investigate these unexpected findings, we plotted each centrosome orientation in radians against the exact angular displacement of the same cell 60 min after the release. In addition, we compared the results to a simulated data set representing a true positive circular correlation (III, Fig. S8a–c). However, we did not observe any positive or negative correlation between the initial centrosome orientation and cell migration, except for the fact that both metrics were independently biased toward the wide, adhesive edge of the micropattern.

Despite the common notion that MTOC and MT array orientation are important front-rear polarity cues that help direct mesenchymal cell migration, actin polymerization and cell protrusion can also precede Golgi and centrosome reorientation (Ueda et al., 1997; Chen et al., 2013; Vaidžiulytė et al., 2022). We hypothesized that centrosome orientation toward the leading edge may serve to stabilize the front-rear polarity axis in U-251MG cells after the cells are released on fibronectin, and consistent anterior positioning of the MTOC promotes directionally persistent migration. To investigate this, we calculated the average angle between centrosome orientation (relative to the nucleus) and the corresponding cell movement vector, and plotted the values against the final (4-hour) directionality ratios from the same cells. As expected, we found a clear positive correlation between consistently forward-facing centrosomes and higher directional persistence (III, Fig. 5c–e). This finding may also explain the higher overall persistence in cells leaving fibronectin-coated versus mAb13-coated micropatterns (III, Fig. S7d–e): centrosome orientation is more likely to coincide with the direction of migration

early on if both metrics are biased strongly—but independently—in the same direction. However, we did not observe any consistent correlation between centrosome orientation and cell speed (total track length) (III, Fig. S7f–g), suggesting that migration speed is at least partially uncoupled from persistence when cells are released from spatial confinement.

5.3.7 Discussion

Micropatterning refers to a set of methods that can be used to confine cells on microscale substrates with defined geometries and biochemical compositions (Théry, 2010). Such techniques are often used to investigate the impact of different cell-cell and cell-ECM interactions on cellular functions, including cell survival and movement (Chen et al., 1997; Caballero et al., 2015). Here, we established a new method for preparing dynamic micropatterns on planar cell culture substrates, marking an improvement over previously reported UV photopatterning techniques (III, Fig. 1a) (Azioune et al., 2009; van Dongen et al., 2013). Owing to the use of photomasks, a large number of micropatterned substrates can be prepared easily and in a reasonable amount of time. More importantly, commonly used and commercially available reagents mean that the new method is both inexpensive and highly customizable, i.e., it is compatible with virtually any ECM components or other biomolecules that can be conjugated to streptavidin.

A key feature of the new micropatterning technique is the possibility to release micropattern-confined cells on specific substrate molecules with high temporal resolution. When measuring the rate of SA-FN binding to the PLL-g-PEG-biotin surrounding the micropatterns, we found that a high concentration of secondary ligand had bound to the biotinylated surface in only 2 min (III, Fig. S1e–g). In other experiments, we observed significant cell spreading from the micropatterns almost immediately (in <5 min) after the media had been supplemented with SA-FN (III, Fig. 4f, Video S3). These findings clearly suggest that our method is suitable for studying fast and dynamic cellular processes, such as lymphocyte activation (III, Fig. S3a–c) or IAC formation and turnover. Another important technical consideration relates to the strength of the biotin-streptavidin interaction. We found that both biotin (III, Fig. 2d) and streptavidin (III, Fig. S3a–c) groups are needed for cell spreading, and without either of them the cells remain fully confined on the micropatterns. This means that the spreading and migrating cells are only interacting with secondary ligand molecules that are tightly bound to the underlying substrate, suggesting minimal risk of force-induced delamination that might otherwise confound experimental results (Hu et al., 2018; Sarkar et al., 2020).

Intracellular polarity is sensitive to the geometry of the local microenvironment, but the specific role of ECM composition in this process is poorly understood. We

analyzed U-251MG cell front-rear polarization on anisotropic micropatterns coated with different fibrous ECM proteins and found that both fibronectin and LN-521 supported consistent MTOC orientation toward the wider, more adhesive edge of the micropattern (III, Fig. 3a–b). For fibronectin, these results were expected: the protein has been used for inducing front-rear polarization on micropatterns in several prior studies (Jiang et al., 2005; Théry et al., 2006; Dubois et al., 2017; Lee et al., 2021). In addition, fibronectin is intrinsically linked to cell migration. It is a key ECM component in different models of cancer cell invasion and persistent migration (Attieh et al., 2017; Erdogan et al., 2017) and can facilitate both haptotaxis (Wu et al., 2012) and durotaxis (Hartman et al., 2016). LN-521, on the other hand, is a ubiquitous BM component in postnatal human tissues (Yap et al., 2019). Laminins are widely considered to be important for maintaining apico-basal polarity in epithelial tissues, and their ability to promote front-rear polarization in individual cells may appear counterproductive to this end (Matlin et al., 2017). However, the ability of BM components to promote sustained migration can be useful during processes like wound healing. Accordingly, laminins have been shown to elicit haptotactic responses in various cell types, including cancer cells, non-transformed mesenchymal cells, and possibly even epithelial cells like the Madin-Darby canine kidney (MDCK) cells (McCarthy & Furcht, 1984; Greciano et al., 2012; Wu et al., 2012). Our results further support the notion that laminins can serve as an effective directional cue preceding cell migration, and their specialized role in establishing epithelial organization is dependent on carefully controlled BM assembly and specific intracellular signaling responses (Matlin et al., 2017).

Micropatterns coated with type I collagen were also observed to induce front-rear polarization, but the results were less consistent than on fibronectin or LN-521. While we cannot fully exclude the trivial explanation that this was due to inadequate expression of collagen receptors in the U-251MG cells, several factors suggest otherwise. First, the cells readily attached and spread on collagen (III, Fig. S6a) and they also appeared capable of forming paxillin-positive IACs on the collagen-coated micropatterns (III, Fig. S5). Second, prior studies have demonstrated that type I collagen and fibronectin may play distinct roles in directionally persistent migration. In some models of cancer invasion, fibronectin is specifically needed for directed migration along aligned fibers—collagen alone is not enough (Attieh et al., 2017). Moreover, Cdc42/RhoA signaling at the leading edge of the cell is regulated by different upstream mechanisms in 3D fibronectin and collagen matrices (Kutys & Yamada, 2014). Interestingly, MSCs confined on crossbow-shaped, collagen-coated micropatterns were shown to exhibit substrate stiffness-dependent rearward polarization of myosin IIB, but the same cells failed to position their centrosomes in front of their nuclei irrespective of the micropattern stiffness (Raab & Discher, 2017). Taken together, our data indicate that different physiological integrin ligands

can support different degrees of cell front-rear polarization in response to local substrate geometry. This will be an important additional consideration for future studies on cell polarity and migration.

In order to decouple signaling responses related to integrin clustering from receptor ligation, we coated crossbow-shaped micropatterns with conformation-specific anti-integrin β1 antibodies (Su et al., 2016). We and others have previously employed similar immobilization of integrin antibodies to investigate integrin signaling on isotropic substrates (Artym et al., 2015; Kaukonen et al., 2016). Here, we found that integrin β1 clustering was sufficient to support partial MTOC polarization irrespective of the associated integrin conformer—both active (clone 12G10) and inactive (clone mAb13) states yielded results that were comparable to the collagen-coated micropatterns (III, Fig. 3a–b). Moreover, both antibodies elicited significant downstream signaling responses in the cells (III, Fig. S6b–c). FAK activation was the only response that appeared to correlate with the observed differences in front-rear polarity, and inhibiting FAK in U-251MG cells plated on fibronectin-coated micropatterns impeded their polarization. These findings suggest that the differences in front-rear polarity between the various ECM molecules and antibodies may result from altered FAK signaling, however, previous studies have implicated FAK activation as a prominent cellular response to forced integrin β1 clustering in human fibroblasts (Miyamoto et al., 1995). More studies are needed to confirm the reason for this discrepancy and whether FAK really regulates front-rear polarization on non-fibronectin substrates. Nevertheless, our results highlight the fact that significant front-rear polarization on anisotropic substrates can be achieved through different ECM components or even non-physiological integrin ligation and/or clustering.

By confining U-251MG cells on mAb13-coated instead of fibronectin-coated micropatterns, we observed less consistent initial front front-rear polarization and a decrease in directed cell spreading and migration when the cells were released on fibronectin (III, Fig. 4d–e). However, we found that the initial MTOC orientation was only poorly correlated with future cell migration (III, Figs. 5a–b, S8a–c). Prior reports have suggested a similar disconnect between initial Golgi positioning and direction of migration in non-malignant epithelial and mesenchymal cells confined on micropatterns without a clear front-rear polarity axis (Chen et al., 2013; Vaidžiulytė et al., 2022). Cells protrude preferentially toward corners when confined on square micropatterns (Chen et al., 2013) or seemingly randomly on circular patterns (Vaidžiulytė et al., 2022), but the temporal dynamics in these previous experiments have been relatively slow (cells were released in hours instead of minutes), which makes their interpreration somewhat challenging.

Even if the Golgi is not predictive of cell spreading, it is often reoriented toward the leading edge when a confined cell is released to migrate (III, Fig. 5a) (Chen et

al., 2013; Vaidžiulytė et al., 2022). In RPE cells, this Golgi movement is dependent on Cdc42 and appears critical for persistent migration (Vaidžiulytė et al., 2022). Similarly, our results suggest that successful anterior positioning of the MTOC promotes directionally persistent migration in U-251MG cells (III, Fig. 5d–e). However, we also observed that multiple glioma cells started migrating toward the narrow end of the micropattern—both on fibronectin and on mAb13—even when their own MTOC was oriented in the opposite direction. This implies that the cells are not simply protruding from the edge with more existing IACs, but that instead, another intracellular polarity cue independent of the centrosome and Golgi is 1) (imperfectly and/or dynamically) responsive to integrin-mediated signaling and the geometry of the local microenvironment, 2) only partially correlated with MTOC orientation in confined cells, and 3) ultimately responsible for dictating cell protrusion and migration away from the micropatterns. Rho GTPases like Cdc42 are prime candidates for this role, having been linked to cell protrusion and directed migration on repeating micropattern ratchets (Lee et al., 2021). Taken together, our results show that the commonly studied MTOC orientation is a useful but incomplete proxy for front-rear polarization in single confined cells. Further, our data support a model where anterior positioning of the centrosome and Golgi is controlled by and stabilizes a predefined front-rear polarity axis in migrating normal and cancer cells.

The correlation between Golgi positioning and cell movement is particularly poor in individual Rat2 fibroblasts. However, the same cells—just like many other cell types—consistently orient their Golgi toward the leading edge in wounded monolayers (Uetrecht & Bear, 2009). Interestingly, micropatterned clusters of kidney epithelial cells exhibit collective Golgi polarization that is guided by substrate geometry. This collective front-rear polarity is dependent on intact cell-cell junctions and correlates with directed spreading and migration when the clusters are released from the micropatterns (Costa et al., 2021). Cell-cell interactions are critical for developmental morphogenesis and normal tissue homeostasis (Le & Mayor, 2023). Thus, it is tempting to speculate that intercellular coordination may have a strong general influence on cellular responses to local tissue architecture and geometry.

6 Conclusions

The main purpose of this thesis was to investigate the various biomechanical cues and intracellular responses that govern cell migration, with a specific focus on human cancer cells. The average tumor microenvironment is complex, heterogeneous, and characterized in large part by aberrant ECM deposition and remodeling. Cells can detect and migrate along gradients of different signaling molecules or even tissue stiffness. Alternatively, cancer invasion may be directed by local ECM architecture and topographic cues. However, many of the mechanistic details behind these processes are still poorly understood, which hinders therapeutic targeting of cancer cell motility. In addition, we sought to establish new effective and accessible methodologies for studying dynamic cellular responses to substrate stiffness or confinement in vitro. Our results are expected to be of broad interest to cell biologists, cancer researchers, and biomechanical engineers.

6.1 Fibrillar adhesions are mechanosensitive (I)

We designed a cost-effective technique for preparing polyacrylamide-based stiffness gradients with a wide, physiologically relevant range of available stiffnesses. The method is based on partial diffusion and mixing of two prepolymer solutions, and the stiffness of the resulting substrate can be inferred directly from confocal microscopy data using fluorescent marker beads and AFM-derived calibration curves. By leveraging ratiometric fluorescence analysis, we identified active integrin α5β1 as a more specific marker for ECM-remodeling FBs in human TIFs than the commonly used proteins tensin-1 and tensin-3. In addition, we found that the growth of FBs is directly responsive to substrate mechanics: average FB length increased as a function of substrate stiffness until ~7 kPa, after which it quickly plateaued and reached a maximum of ~3.5 μm in the TIFs. In accordance with previous studies that have indicated tensins as necessary components for FB growth, knockdown of tensin-1 impeded FB elongation similarly on soft and stiff substrates. Taken together, we show that FBs are intrinsically mechanosensitive cellular structures. This may contribute to positive biomechanical feedback and ECM remodeling during aberrant stromal reactions like fibrosis and tumor desmoplasia—an interesting topic for future research.

6.2 Molecular clutch dynamics control positive and negative durotaxis (II)

We investigated the relationship between cellular traction forces and durotaxis, and found that—in addition to the more commonly observed positive durotaxis—U-251MG glioblastoma cells are capable of directed migration toward softer environments (i.e., negative durotaxis). Specifically, the cells move up or down stiffness gradients to reach an optimal stiffness of 5–10 kPa, which allows them to exert maximal traction on their substrate. Positive and negative durotaxis did not coincide with changes in established mechanosensitive signaling pathways, including FAK, ERK, and YAP signaling. Instead, the differences in cellular traction forces and durotactic migration were both explained using the molecular clutch model. Computational simulations recapitulated both U-251MG durotaxis and previously reported axonal pathfinding toward softer tissues. In accordance with the model, partial inhibition of actomyosin contractility impeded negative—but not positive—durotaxis in the U-251MG cells, whereas the normal positive durotaxis of MDA-MB-231 breast cancer cells was partially reversed by silencing both talin isoforms. This prevented normal clutch reinforcement and FA formation, impairing the cells' ability to exert traction on stiffer substrates. Our results shed light on the interplay between actomyosin contractility and cell-ECM adhesion during mechanically directed migration. At the same time, these findings fundamentally challenge some our previous conceptions of durotaxis.

6.3 Substrate anisotropy and composition regulate front-rear polarity and migration (III)

To study the impact of local ECM geometry on dynamic cellular processes—namely, cell polarity and migration—we established a new technique for fabricating dynamic micropatterns. By combining UV photopatterning of biotinylated PLL-g-PEG with streptavidin-conjugated ECM components and biomimetic peptides, cells can be confined on 2D substrates of well-defined shape, size and molecular composition, and later quickly released to spread and migrate on the same or different ligand molecule. The method is fast, scalable, and easy to adopt by other research groups. Using the new micropatterns, we found that the front-rear polarization of U-251MG cells in response to local ECM anisotropy depends on the molecular makeup of the substrate: consistent positioning of the MTOC in front of the nucleus was observed on asymmetric fibronectin- and LN-521-coated micropatterns, while type I collagen and two different anti-integrin β1 antibodies, 12G10 and mAb13, resulted in lower but significant front-rear polarization. In addition, all of the substrates elicited marked integrin-associated signaling responses. Cells released from fibronectin- and mAb13-coated micropatterns on fibronectin exhibited partially distinct migration

phenotypes, where the cells released from fibronectin moved in more directed and persistent manner. However, the initial orientation of the centrosome was only poorly correlated with the direction of subsequent cell spreading and migration. Taken together, we show that ECM composition can directly influence cellular responses to local geometric cues, and that MTOC orientation—a commonly studied facet of cell polarity—represents a useful but incomplete proxy for front-rear polarization in spatially confined cells.

Acknowledgments

This work was carried out at the University of Turku, Faculty of Technology, Department of Life Technologies and at the Turku Bioscience Center. I would like to sincerely thank Prof. Riitta Lahesmaa and Prof. John Eriksson, the current and previous directors of Turku Bioscience, for fostering an inspiring and friendly workplace with excellent scientific facilities. I would also like to thank all the technical and administrative staff at Turku Bioscience for their invaluable help and expertise over the years.

During my doctoral studies, I've had the privilege to work with two outstanding supervisors, Prof. Johanna Ivaska and Dr. Camilo Guzmán. I want to thank Camilo for many excellent pointers and brainstorming during the early days of my PhD projects. Even after you left the lab and our meetings became more sporadic, you've always been willing to lend a hand when needed. I really appreciate your friendly personality and skills as a biophysicist. I am also deeply grateful to my other supervisor, Johanna, for guiding me through my whole PhD journey. You are an inspiring scientist and a great mentor, and I can't even begin to list the many things I've learned from you. Thank you for having me in your lab, and I hope that we can cross paths again in the future. I would also like to thank the members of my advisory committee, Prof. Varpu Marjomäki and Docent Saara Ollila, for all their support and guidance during my PhD work.

I conducted my doctoral studies in the University of Turku Doctoral Programme in Molecular Life Sciences and the Doctoral Programme in Technology. I would like to thank director Prof. Eevi Rintamäki and all the coordinators of both doctoral programs for keeping things running smoothly and for supporting the student community. I am also grateful to research director Prof. Jyrki Heino for accepting me as a doctoral candidate at the Department of Life Technologies.

I would like to express my gratitude to the two pre-examiners of this thesis, Dr. Anna Taubenberger and Docent Teemu Ihalainen. Your insightful suggestions and advice were much appreciated. I am also thankful to Prof. Adam Engler for accepting the invitation to be my opponent. I am looking forward to discussing cancer mechanobiology with you.

I have been lucky to work with many excellent collaborators and co-authors. I would especially like to thank Prof. David Odde from the University of Minnesota for hosting me during my research visit and teaching me the ins and outs of the molecular clutch. You are a gentleman and a scholar. I am also grateful to Benjamin Fuller, Bo Cheng, Camilo Guzmán, Feng Xu, Ghaidan Shamsan, Guy Genin, Hellyeh Hamidi, Jay Hou, Jesse Kasim, Jonna Alanko, Karla Saukkonen, Keun-Young Park, Maria Georgiadou, Mark Distefano, Markku Saari, Mathilde Mathieu, Min Lin, Mohsen Mahmoodi, Nuria Barber-Pérez, Pieta Mattila, Sara Hernández-Pérez, and Tian Jian Lu for their expertise. It has been a great pleasure working with you all. I've also crossed paths with many other talented scientists and colleagues at Turku Bioscience and elsewhere, and their help has often been invaluable. While there are too many names to list here, you know who you are. Thank you for everything.

I would like to express my gratitude to all my current and past colleagues at the Ivaska lab. Thank you, Aki, Alisa, Camilo, David, Elisa, Ella-Maria, Emmi, Emmy, Eva, Gautier, Guillaume, Hanna, Hellyeh, Hussein, Ilkka, Iman, Inés, James, Jaroslav, Jasmin, Jenni, Johanna J., Johanna L., Jonna, Karla, Kerstin, Loane, Maria G., Maria R., Maria T., Markku, Martina, Mathilde, Max, Megan, Meri, Michal, Michalis, Mika, Mitro, Nicolas, Niklas, Nuria, Omkar, Paulina, Petra, Pranshu, Rafael, Riina, Siiri, Taru, Valentijn, and Veli-Matti. You are all amazingly talented, helpful, and kind people, and I wouldn't be writing this thesis without you. I've really enjoyed your company over the years, both in and outside the lab. I would like to extend a special thank you to our skilled technicians, Jenni and Petra, for all their help and support. I am also deeply grateful to our coordinator Hellyeh. You are one of the most helpful—and efficient—people I know.

I owe my deepest gratitude to my family. Doing science takes time, which often means long days and weekends at the bench. Thank you for always supporting me and having my back, even when it means that I can't spend as much time with you as I would like. And just as importantly, thank you for making me the person I am today. I am also grateful to all my friends, old and new, for their continued support and friendship. You keep reminding me of the things that are important in life.

This work has been financially supported by the University of Turku Doctoral Programme in Molecular Life Sciences, the Finnish Cultural Foundation, the Orion Research Foundation, the K. Albin Johansson Foundation, and the Company of Biologists/Journal of Cell Science.

Turku, March 2024

Aleksi Isomursu

References

Abercrombie M. 1970. Contact inhibition in tissue culture. In Vitro. **6**: 128–142.

Abercrombie M. 1980. The Croonian Lecture, 1978 - The crawling movement of metazoan cells. Proc. R. Soc. Lond. B Biol. Sci. **207**: 129–147.

Abercrombie M., Heaysman J.E.M. & Pegrum S.M. 1970. The locomotion of fibroblasts in culture I. Movements of the leading edge. Exp. Cell Res. **59**: 393–398.

Acerbi I., Cassereau L., Dean I., Shi Q., Au A., Park C., Chen Y.Y., Liphardt J., Hwang E.S. & Weaver V.M. 2015. Human breast cancer invasion and aggression correlates with ECM stiffening and immune cell infiltration. Integr. Biol. **7**: 1120–1134.

Albert P.J. & Schwarz U.S. 2016. Modeling cell shape and dynamics on micropatterns. Cell Adhes. Migr. **10**: 516–528.

Alghamdi R.A., Exposito-Rodriguez M., Mullineaux P.M., Brooke G.N. & Laissue P.P. 2021. Assessing Phototoxicity in a Mammalian Cell Line: How Low Levels of Blue Light Affect Motility in PC3 Cells. Front. Cell Dev. Biol. **9**: 738786.

Alibert C., Goud B. & Manneville J.-B. 2017. Are cancer cells really softer than normal cells?. Biol. Cell. **109**: 167–189.

Anderson S.M., Kelly M. & Odde D.J. 2023. Glioblastoma cells use an integrin- and CD44-mediated motor-clutch mode of migration in brain tissue. bioRxiv. 2023.10.23.563458.

Angulo-Urarte A., van der Wal T. & Huveneers S. 2020. Cell-cell junctions as sensors and transducers of mechanical forces. Biochim. Biophys. Acta BBA - Biomembr. **1862**: 183316.

Artym V.V., Swatkoski S., Matsumoto K., Campbell C.B., Petrie R.J., Dimitriadis E.K., Li X., Mueller S.C., Bugge T.H., Gucek M. & Yamada K.M. 2015. Dense fibrillar collagen is a potent inducer of invadopodia via a specific signaling network. J. Cell Biol. **208**: 331–350.

Atherton P., Konstantinou R., Neo S.P., Wang E., Balloi E., Ptushkina M., Bennett H., Clark K., Gunaratne J., Critchley D., Barsukov I., Manser E. & Ballestrem C. 2022. Tensin3 interaction with talin drives the formation of fibronectin-associated fibrillar adhesions. J. Cell Biol. **221**: e202107022.

Atherton P., Stutchbury B., Wang D.-Y., Jethwa D., Tsang R., Meiler-Rodriguez E., Wang P., Bate N., Zent R., Barsukov I.L., Goult B.T., Critchley D.R. & Ballestrem C. 2015. Vinculin controls talin engagement with the actomyosin machinery. Nat. Commun. **6**: 1–12.

Attieh Y., Clark A.G., Grass C., Richon S., Pocard M., Mariani P., Elkhatib N., Betz T., Gurchenkov B. & Vignjevic D.M. 2017. Cancer-associated fibroblasts lead tumor invasion through integrin-β3–dependent fibronectin assembly. J. Cell Biol. **216**: 3509–3520.

Austen K., Ringer P., Mehlich A., Chrostek-Grashoff A., Kluger C., Klingner C., Sabass B., Zent R., Rief M. & Grashoff C. 2015. Extracellular rigidity sensing by talin isoform-specific mechanical linkages. Nat. Cell Biol. **17**: 1597–1606.

Azioune A., Storch M., Bornens M., Théry M. & Piel M. 2009. Simple and rapid process for single cell micro-patterning. Lab. Chip. **9**: 1640–1642.

Bachir A.I., Zareno J., Moissoglu K., Plow E.F., Gratton E. & Horwitz A.R. 2014. Integrin-Associated Complexes Form Hierarchically with Variable Stoichiometry in Nascent Adhesions. Curr. Biol. **24**: 1845–1853.

Baker A.-M., Bird D., Lang G., Cox T.R. & Erler J.T. 2013. Lysyl oxidase enzymatic function increases stiffness to drive colorectal cancer progression through FAK. Oncogene. **32**: 1863–1868.

Balcioglu H.E., van Hoorn H., Donato D.M., Schmidt T. & Danen E.H.J. 2015. The integrin expression profile modulates orientation and dynamics of force transmission at cell–matrix adhesions. J. Cell Sci. **128**: 1316–1326.

Bangasser B.L. & Odde D.J. 2013. Master equation-based analysis of a motor-clutch model for cell traction force. Cell. Mol. Bioeng. **6**: 449–459.

Bangasser B.L., Rosenfeld S.S. & Odde D.J. 2013. Determinants of maximal force transmission in a motor-clutch model of cell traction in a compliant microenvironment. Biophys. J. **105**: 581–592.

Bangasser B.L., Shamsan G.A., Chan C.E., Opoku K.N., Tüzel E., Schlichtmann B.W., Kasim J.A., Fuller B.J., McCullough B.R., Rosenfeld S.S. & Odde D.J. 2017. Shifting the optimal stiffness for cell migration. Nat. Commun. **8**: 1–10.

Barbazan J., Pérez-González C., Gómez-González M., Dedenon M., Richon S., Latorre E., Serra M., Mariani P., Descroix S., Sens P., Trepat X. & Vignjevic D.M. 2023. Cancer-associated fibroblasts actively compress cancer cells and modulate mechanotransduction. Nat. Commun. **14**: 6966.

Barrasa-Fano J., Shapeti A., Jorge-Peñas Á., Barzegari M., Sanz-Herrera J.A. & Van Oosterwyck H. 2021. TFMLAB: A MATLAB toolbox for 4D traction force microscopy. SoftwareX. **15**: 100723.

Barriga E.H., Franze K., Charras G. & Mayor R. 2018. Tissue stiffening coordinates morphogenesis by triggering collective cell migration in vivo. Nature. **554**: 523–527.

Beaver J.A., Kluetz P.G. & Pazdur R. 2018. Metastasis-free Survival — A New End Point in Prostate Cancer Trials. N. Engl. J. Med. **378**: 2458–2460.

Beedle A.E.M., Jaganathan A., Albajar-Sigalés A., Yavitt F.M., Bera K., Andreu I., Granero-Moya I., Zalvidea D., Kechagia Z., Wiche G., Trepat X., Ivaska J., Anseth K.S., Shenoy V.B. & Roca-Cusachs P. 2023. Fibrillar adhesion dynamics govern the timescales of nuclear mechano-response via the vimentin cytoskeleton. bioRxiv. 2023.11.08.566191.

Bell G.I. 1978. Models for the specific adhesion of cells to cells. Science. **200**: 618–627.

Bennett M., Cantini M., Reboud J., Cooper J.M., Roca-Cusachs P. & Salmeron-Sanchez M. 2018. Molecular clutch drives cell response to surface viscosity. Proc. Natl. Acad. Sci. U. S. A. **115**: 1192–1197.

Betz T., Koch D., Lu Y.-B., Franze K. & Käs J.A. 2011. Growth cones as soft and weak force generators. Proc. Natl. Acad. Sci. U. S. A. **108**: 13420–13425.

Bisaria A., Hayer A., Garbett D., Cohen D. & Meyer T. 2020. Membrane-proximal F-actin restricts local membrane protrusions and directs cell migration. Science. **368**: 1205–1210.

Bischofs I.B. & Schwarz U.S. 2003. Cell organization in soft media due to active mechanosensing. Proc. Natl. Acad. Sci. U. S. A. **100**: 9274–9279.

Bissell M.J. & Hines W.C. 2011. Why don't we get more cancer? A proposed role of the microenvironment in restraining cancer progression. Nat. Med. **17**: 320–329.

Bledzka K., Bialkowska K., Sossey-Alaoui K., Vaynberg J., Pluskota E., Qin J. & Plow E.F. 2016. Kindlin-2 directly binds actin and regulates integrin outside-in signaling. J. Cell Biol. **213**: 97–108.

Bodescu M.A., Aretz J., Grison M., Rief M. & Fässler R. 2023. Kindlin stabilizes the talin·integrin bond under mechanical load by generating an ideal bond. Proc. Natl. Acad. Sci. **120**: e2218116120.

Bolado-Carrancio A., Rukhlenko O.S., Nikonova E., Tsyganov M.A., Wheeler A., Garcia-Munoz A., Kolch W., von Kriegsheim A. & Kholodenko B.N. 2020. Periodic propagating waves coordinate RhoGTPase network dynamics at the leading and trailing edges during cell migration. eLife. **9**: e58165.

Bouchet B.P., Gough R.E., Ammon Y.-C., van de Willige D., Post H., Jacquemet G., Altelaar A.M., Heck A.J., Goult B.T. & Akhmanova A. 2016. Talin-KANK1 interaction controls the recruitment of cortical microtubule stabilizing complexes to focal adhesions. eLife. **5**: e18124.

Bouvard D., Pouwels J., De Franceschi N. & Ivaska J. 2013. Integrin inactivators: balancing cellular functions in vitro and in vivo. Nat. Rev. Mol. Cell Biol. **14**: 430–442.

Boyd N.F., Guo H., Martin L.J., Sun L., Stone J., Fishell E., Jong R.A., Hislop G., Chiarelli A., Minkin S. & Yaffe M.J. 2007. Mammographic Density and the Risk and Detection of Breast Cancer. N. Engl. J. Med. **356**: 227–236.

Breckenridge M.T., Desai R.A., Yang M.T., Fu J. & Chen C.S. 2014. Substrates with Engineered Step Changes in Rigidity Induce Traction Force Polarity and Durotaxis. Cell. Mol. Bioeng. **7**: 26–34.

Bunch T.A. 2010. Integrin αIIbβ3 Activation in Chinese Hamster Ovary Cells and Platelets Increases Clustering Rather than Affinity. J. Biol. Chem. **285**: 1841–1849.

Burute M., Prioux M., Blin G., Truchet S., Letort G., Tseng Q., Bessy T., Lowell S., Young J., Filhol O. & Théry M. 2017. Polarity Reversal by Centrosome Repositioning Primes Cell Scattering during Epithelial-to-Mesenchymal Transition. Dev. Cell. **40**: 168–184.

Buxboim A., Rajagopal K., Brown A.E.X. & Discher D.E. 2010. How deeply cells feel: methods for thin gels. J. Phys. Condens. Matter. **22**: 194116.

Caballero D., Comelles J., Piel M., Voituriez R. & Riveline D. 2015. Ratchetaxis: Long-Range Directed Cell Migration by Local Cues. Trends Cell Biol. **25**: 815–827.

Caballero D., Palacios L., Freitas P.P. & Samitier J. 2017. An Interplay between Matrix Anisotropy and Actomyosin Contractility Regulates 3D-Directed Cell Migration. Adv. Funct. Mater. **27**: 1702322.

Caballero D., Voituriez R. & Riveline D. 2014. Protrusion Fluctuations Direct Cell Motion. Biophys. J. **107**: 34–42.

Caliari S.R. & Burdick J.A. 2016. A practical guide to hydrogels for cell culture. Nat. Methods. **13**: 405–414.

Calvo F., Ege N., Grande-Garcia A., Hooper S., Jenkins R.P., Chaudhry S.I., Harrington K., Williamson P., Moeendarbary E., Charras G. & Sahai E. 2013. Mechanotransduction and YAP-dependent matrix remodelling is required for the generation and maintenance of cancer-associated fibroblasts. Nat. Cell Biol. **15**: 637–646.

Campanale J.P., Sun T.Y. & Montell D.J. 2017. Development and dynamics of cell polarity at a glance. J. Cell Sci. **130**: 1201.

Campàs O., Mammoto T., Hasso S., Sperling R.A., O'Connell D., Bischof A.G., Maas R., Weitz D.A., Mahadevan L. & Ingber D.E. 2014. Quantifying cell-generated mechanical forces within living embryonic tissues. Nat. Methods. **11**: 183–189.

Campbell I.D. & Humphries M.J. 2011. Integrin Structure, Activation, and Interactions. Cold Spring Harb. Perspect. Biol. **3**: a004994.

Carisey A., Tsang R., Greiner A.M., Nijenhuis N., Heath N., Nazgiewicz A., Kemkemer R., Derby B., Spatz J. & Ballestrem C. 2013. Vinculin Regulates the Recruitment and Release of Core Focal Adhesion Proteins in a Force-Dependent Manner. Curr. Biol. **23**: 271–281.

Carraher C.L. & Schwarzbauer J.E. 2013. Regulation of Matrix Assembly through Rigidity-dependent Fibronectin Conformational Changes. J. Biol. Chem. **288**: 14805–14814.

Case L.B. & Waterman C.M. 2015. Integration of actin dynamics and cell adhesion by a three-dimensional, mechanosensitive molecular clutch. Nat. Cell Biol. **17**: 955–963.

Caspani E.M., Echevarria D., Rottner K. & Small J.V. 2006. Live imaging of glioblastoma cells in brain tissue shows requirement of actin bundles for migration. Neuron Glia Biol. **2**: 105–114.

Chabin-Brion K., Marceiller J., Perez F., Settegrana C., Drechou A., Durand G. & Poüs C. 2001. The Golgi Complex Is a Microtubule-organizing Organelle. Mol. Biol. Cell. **12**: 2047–2060.

von Chamier L., Laine R.F., Jukkala J., Spahn C., Krentzel D., Nehme E., Lerche M., Hernández-Pérez S., Mattila P.K., Karinou E., Holden S., Solak A.C., Krull A., Buchholz T.-O., Jones M.L., Royer L.A., Leterrier C., Shechtman Y., Jug F., Heilemann M., Jacquemet G. & Henriques R. 2021. Democratising deep learning for microscopy with ZeroCostDL4Mic. Nat. Commun. **12**: 2276.

Chan C.E. & Odde D.J. 2008. Traction Dynamics of Filopodia on Compliant Substrates. Science. **322**: 1687–1691.

Chang W.-C., Chang C.-F., Li Y.-H., Yang C.-Y., Su R.-Y., Lin C.-K. & Chen Y.-W. 2019. A histopathological evaluation and potential prognostic implications of oral squamous cell carcinoma with adverse features. Oral Oncol. **95**: 65–73.

Changede R., Xu X., Margadant F. & Sheetz M.P. 2015. Nascent Integrin Adhesions Form on All Matrix Rigidities after Integrin Activation. Dev. Cell. **35**: 614–621.

Chastney M.R., Conway J.R.W. & Ivaska J. 2021. Integrin adhesion complexes. Curr. Biol. **31**: R536–R542.

Chastney M.R., Lawless C., Humphries J.D., Warwood S., Jones M.C., Knight D., Jorgensen C. & Humphries M.J. 2020. Topological features of integrin adhesion complexes revealed by multiplexed proximity biotinylation. J. Cell Biol. **219**: e202003038.

Chaudhuri O., Cooper-White J., Janmey P.A., Mooney D.J. & Shenoy V.B. 2020. Effects of extracellular matrix viscoelasticity on cellular behaviour. Nature. **584**: 535–546.

Chaudhuri O., Koshy S.T., Branco da Cunha C., Shin J.-W., Verbeke C.S., Allison K.H. & Mooney D.J. 2014. Extracellular matrix stiffness and composition jointly regulate the induction of malignant phenotypes in mammary epithelium. Nat. Mater. **13**: 970–978.

Chauhan V.P., Martin J.D., Liu H., Lacorre D.A., Jain S.R., Kozin S.V., Stylianopoulos T., Mousa A.S., Han X., Adstamongkonkul P., Popović Z., Huang P., Bawendi M.G., Boucher Y. & Jain R.K. 2013. Angiotensin inhibition enhances drug delivery and potentiates chemotherapy by decompressing tumour blood vessels. Nat. Commun. **4**: 2516.

Chen B., Kumar G., Co C.C. & Ho C.-C. 2013. Geometric Control of Cell Migration. Sci. Rep. **3**: 2827.

Chen C.S., Mrksich M., Huang S., Whitesides G.M. & Ingber D.E. 1997. Geometric control of cell life and death. Science. **276**: 1425–1428.

Chen W., Lou J., Evans E.A. & Zhu C. 2012. Observing force-regulated conformational changes and ligand dissociation from a single integrin on cells. J. Cell Biol. **199**: 497–512.

Chen W., Lou J., Hsin J., Schulten K., Harvey S.C. & Zhu C. 2011. Molecular Dynamics Simulations of Forced Unbending of Integrin αVβ3. PLOS Comput. Biol. **7**: e1001086.

Chen Y., Lee H., Tong H., Schwartz M. & Zhu C. 2017. Force regulated conformational change of integrin αVβ3. Matrix Biol. **60–61**: 70–85.

Cheng H.-W., Hsiao C.-T., Chen Y.-Q., Huang C.-M., Chan S.-I., Chiou A. & Kuo J.-C. 2019. Centrosome guides spatial activation of Rac to control cell polarization and directed cell migration. Life Sci. Alliance. **2**: e201800135.

Choi C.K., Vicente-Manzanares M., Zareno J., Whitmore L.A., Mogilner A. & Horwitz A.R. 2008. Actin and α-actinin orchestrate the assembly and maturation of nascent adhesions in a myosin II motor-independent manner. Nat. Cell Biol. **10**: 1039–1050.

Choi C.K., Zareno J., Digman M.A., Gratton E. & Horwitz A.R. 2011. Cross-Correlated Fluctuation Analysis Reveals Phosphorylation-Regulated Paxillin-FAK Complexes in Nascent Adhesions. Biophys. J. **100**: 583–592.

Choi Y.I., Duke-Cohan J.S., Chen W., Liu B., Rossy J., Tabarin T., Ju L., Gui J., Gaus K., Zhu C. & Reinherz E.L. 2014. Dynamic control of β1 integrin adhesion by the plexinD1-sema3E axis. Proc. Natl. Acad. Sci. U. S. A. **111**: 379–384.

Chung C.Y. & Erickson H.P. 1997. Glycosaminoglycans modulate fibronectin matrix assembly and are essential for matrix incorporation of tenascin-C. J. Cell Sci. **110**: 1413–1419.

Clark A.G., Maitra A., Jacques C., Bergert M., Pérez-González C., Simon A., Lederer L., Diz-Muñoz A., Trepat X., Voituriez R. & Vignjevic D.M. 2022. Self-generated gradients steer collective migration on viscoelastic collagen networks. Nat. Mater. **21**: 1200–1210.

Clark A.G. & Vignjevic D.M. 2015. Modes of cancer cell invasion and the role of the microenvironment. Curr. Opin. Cell Biol. **36**: 13–22.

Clark K., Howe J.D., Pullar C.E., Green J.A., Artym V.V., Yamada K.M. & Critchley D.R. 2010. Tensin 2 modulates cell contractility in 3D collagen gels through the RhoGAP DLC1. J. Cell. Biochem. **109**: 808–817.

Clark K., Pankov R., Travis M.A., Askari J.A., Mould A.P., Craig S.E., Newham P., Yamada K.M. & Humphries M.J. 2005. A specific α5β1-integrin conformation promotes directional integrin translocation and fibronectin matrix formation. J. Cell Sci. **118**: 291–300.

Cóndor M., Steinwachs J., Mark C., García-Aznar J. m. & Fabry B. 2017. Traction Force Microscopy in 3-Dimensional Extracellular Matrix Networks. Curr. Protoc. Cell Biol. **75**: 10.22.1-10.22.20.

Conklin M.W., Eickhoff J.C., Riching K.M., Pehlke C.A., Eliceiri K.W., Provenzano P.P., Friedl A. & Keely P.J. 2011. Aligned Collagen Is a Prognostic Signature for Survival in Human Breast Carcinoma. Am. J. Pathol. **178**: 1221–1232.

Cormier A., Campbell M.G., Ito S., Wu S., Lou J., Marks J., Baron J.L., Nishimura S.L. & Cheng Y. 2018. Cryo-EM structure of the αvβ8 integrin reveals a mechanism for stabilizing integrin extension. Nat. Struct. Mol. Biol. **25**: 698–704.

Costa P., Blowes L.M., Laly A.C. & Connelly J.T. 2021. Regulation of collective cell polarity and migration using dynamically adhesive micropatterned substrates. Acta Biomater. **126**: 291–300.

Costa P., Gautrot J.E. & Connelly J.T. 2014. Directing cell migration using micropatterned and dynamically adhesive polymer brushes. Acta Biomater. **10**: 2415–2422.

Cox E.A., Sastry S.K. & Huttenlocher A. 2001. Integrin-mediated Adhesion Regulates Cell Polarity and Membrane Protrusion through the Rho Family of GTPases. Mol. Biol. Cell. **12**: 265–277.

Cox T.R. & Erler J.T. 2011. Remodeling and homeostasis of the extracellular matrix: implications for fibrotic diseases and cancer. Dis. Model. Mech. **4**: 165–178.

Crowley E. & Horwitz A.F. 1995. Tyrosine phosphorylation and cytoskeletal tension regulate the release of fibroblast adhesions. J. Cell Biol. **131**: 525–537.

Cui Y., Liao Y.-C. & Lo S.H. 2004. Epidermal Growth Factor Modulates Tyrosine Phosphorylation of a Novel Tensin Family Member, Tensin31. Mol. Cancer Res. **2**: 225–232.

Cukierman E., Pankov R., Stevens D.R. & Yamada K.M. 2001. Taking Cell-Matrix Adhesions to the Third Dimension. Science. **294**: 1708–1712.

Das A., Fischer R.S., Pan D. & Waterman C.M. 2016. YAP Nuclear Localization in the Absence of Cell-Cell Contact Is Mediated by a Filamentous Actin-dependent, Myosin II- and Phospho-YAP-independent Pathway during Extracellular Matrix Mechanosensing. J. Biol. Chem. **291**: 6096–6110.

Davis L.E., Shalin S.C. & Tackett A.J. 2019. Current state of melanoma diagnosis and treatment. Cancer Biol. Ther. **20**: 1366–1379.

Dillekås H., Rogers M.S. & Straume O. 2019. Are 90% of deaths from cancer caused by metastases?. Cancer Med. **8**: 5574–5576.

Dokukina I.V. & Gracheva M.E. 2010. A Model of Fibroblast Motility on Substrates with Different Rigidities. Biophys. J. **98**: 2794–2803.

Dong J.-M., Tay F.P.-L., Swa H.L.-F., Gunaratne J., Leung T., Burke B. & Manser E. 2016. Proximity biotinylation provides insight into the molecular composition of focal adhesions at the nanometer scale. Sci. Signal. **9**: rs4–rs4.

van Dongen S.F.M., Maiuri P., Marie E., Tribet C. & Piel M. 2013. Triggering Cell Adhesion, Migration or Shape Change with a Dynamic Surface Coating. Adv. Mater. **25**: 1687–1691.

Doyle A.D., Sykora D.J., Pacheco G.G., Kutys M.L. & Yamada K.M. 2021. 3D mesenchymal cell migration is driven by anterior cellular contraction that generates an extracellular matrix prestrain. Dev. Cell. **56**: 826-841.e4.

Doyle A.D. & Yamada K.M. 2016. Mechanosensing via cell-matrix adhesions in 3D microenvironments. Exp. Cell Res. **343**: 60–66.

Dubois F., Alpha K. & Turner C.E. 2017. Paxillin regulates cell polarization and anterograde vesicle trafficking during cell migration. Mol. Biol. Cell. **28**: 3815–3831.

DuChez B.J., Doyle A.D., Dimitriadis E.K. & Yamada K.M. 2019. Durotaxis by Human Cancer Cells. Biophys. J. **116**: 670–683.

Ehrengruber M.U., Geiser T. & Deranleau D.A. 1994. Activation of human neutrophils by C3a and C5A. Comparison of the effects on shape changes, chemotaxis, secretion, and respiratory burst. FEBS Lett. **346**: 181–184.

Elosegui-Artola A., Bazellières E., Allen M.D., Andreu I., Oria R., Sunyer R., Gomm J.J., Marshall J.F., Jones J.L., Trepat X. & Roca-Cusachs P. 2014. Rigidity sensing and adaptation through regulation of integrin types. Nat. Mater. **13**: 631–637.

Elosegui-Artola A., Oria R., Chen Y., Kosmalska A., Pérez-González C., Castro N., Zhu C., Trepat X. & Roca-Cusachs P. 2016. Mechanical regulation of a molecular clutch defines force transmission and transduction in response to matrix rigidity. Nat. Cell Biol. **18**: 540–548.

Elosegui-Artola A., Trepat X. & Roca-Cusachs P. 2018. Control of Mechanotransduction by Molecular Clutch Dynamics. Trends Cell Biol. **28**: 356–367.

Engler A.J., Sen S., Sweeney H.L. & Discher D.E. 2006. Matrix Elasticity Directs Stem Cell Lineage Specification. Cell. **126**: 677–689.

Erdogan B., Ao M., White L.M., Means A.L., Brewer B.M., Yang L., Washington M.K., Shi C., Franco O.E., Weaver A.M., Hayward S.W., Li D. & Webb D.J. 2017. Cancer-associated fibroblasts promote directional cancer cell migration by aligning fibronectin. J. Cell Biol. **216**: 3799–3816.

Etienne-Manneville S. & Hall A. 2001. Integrin-Mediated Activation of Cdc42 Controls Cell Polarity in Migrating Astrocytes through PKCζ. Cell. **106**: 489–498.

Etienne-Manneville S., Manneville J.-B., Nicholls S., Ferenczi M.A. & Hall A. 2005. Cdc42 and Par6–PKCζ regulate the spatially localized association of Dlg1 and APC to control cell polarization. J. Cell Biol. **170**: 895–901.

Feng J., Levine H., Mao X. & Sander L.M. 2019. Cell motility, contact guidance, and durotaxis. Soft Matter. **15**: 4856–4864.

Ferlay J., Colombet M., Soerjomataram I., Parkin D.M., Piñeros M., Znaor A. & Bray F. 2021. Cancer statistics for the year 2020: An overview. Int. J. Cancer. **149**: 778–789.

Fernández-Sánchez M.E., Barbier S., Whitehead J., Béalle G., Michel A., Latorre-Ossa H., Rey C., Fouassier L., Claperon A., Brullé L., Girard E., Servant N., Rio-Frio T., Marie H., Lesieur S., Housset C., Gennisson J.-L., Tanter M., Ménager C., Fre S., Robine S. & Farge E. 2015. Mechanical induction of the tumorigenic β-catenin pathway by tumour growth pressure. Nature. **523**: 92–95.

Filleron T., Le Guellec S., Chevreau C., Cabarrou B., Lesluyes T., Lodin S., Massoubre A., Mounier M., Poublanc M., Chibon F. & Valentin T. 2020. Value of peri-operative chemotherapy in patients with CINSARC high-risk localized grade 1 or 2 soft tissue sarcoma: study protocol of the target selection phase III CHIC-STS trial. BMC Cancer. **20**: 716.

Fortunato I.C. & Sunyer R. 2022. The Forces behind Directed Cell Migration. Biophysica. **2**: 548–563.

Foster C.T., Gualdrini F. & Treisman R. 2017. Mutual dependence of the MRTF-SRF and YAP-TEAD pathways in cancer-associated fibroblasts is indirect and mediated by cytoskeletal dynamics. Genes Dev. **31**: 2361–2375.

Frantz C., Stewart K.M. & Weaver V.M. 2010. The extracellular matrix at a glance. J. Cell Sci. **123**: 4195–4200.

Franze K. 2020. Integrating Chemistry and Mechanics: The Forces Driving Axon Growth. Annu. Rev. Cell Dev. Biol. **36**: 61–83.

Friedl P. & Alexander S. 2011. Cancer Invasion and the Microenvironment: Plasticity and Reciprocity. Cell. **147**: 992–1009.

Friedl P. & Bröker E.-B. 2000. T Cell Migration in Three-dimensional Extracellular Matrix: Guidance by Polarity and Sensations. Dev. Immunol. **7**: 249–266.

Friedl P. & Wolf K. 2009. Proteolytic interstitial cell migration: a five-step process. Cancer Metastasis Rev. **28**: 129–135.

Friedland J.C., Lee M.H. & Boettiger D. 2009. Mechanically Activated Integrin Switch Controls α5β1 Function. Science. **323**: 642–644.

Fructuoso M., Legrand M., Mousson A., Steffan T., Vauchelles R., De Mey J., Sick E., Rondé P. & Dujardin D. 2020. FAK regulates dynein localisation and cell polarity in migrating mouse fibroblasts. Biol. Cell. **112**: 53–72.

Funamoto S., Meili R., Lee S., Parry L. & Firtel R.A. 2002. Spatial and Temporal Regulation of 3-Phosphoinositides by PI 3-Kinase and PTEN Mediates Chemotaxis. Cell. **109**: 611–623.

Gaggioli C., Hooper S., Hidalgo-Carcedo C., Grosse R., Marshall J.F., Harrington K. & Sahai E. 2007. Fibroblast-led collective invasion of carcinoma cells with differing roles for RhoGTPases in leading and following cells. Nat. Cell Biol. **9**: 1392–1400.

Galbraith C.G., Yamada K.M. & Sheetz M.P. 2002. The relationship between force and focal complex development. J. Cell Biol. **159**: 695–705.

Gan Z., Ding L., Burckhardt C.J., Lowery J., Zaritsky A., Sitterley K., Mota A., Costigliola N., Starker C.G., Voytas D.F., Tytell J., Goldman R.D. & Danuser G. 2016. Vimentin Intermediate Filaments Template Microtubule Networks to Enhance Persistence in Cell Polarity and Directed Migration. Cell Syst. **3**: 252-263.e8.

Gandalovičová A., Rosel D., Fernandes M., Veselý P., Heneberg P., Čermák V., Petruželka L., Kumar S., Sanz-Moreno V. & Brábek J. 2017. Migrastatics—Anti-metastatic and Anti-invasion Drugs: Promises and Challenges. Trends Cancer. **3**: 391–406.

Gardel M.L., Sabass B., Ji L., Danuser G., Schwarz U.S. & Waterman C.M. 2008. Traction stress in focal adhesions correlates biphasically with actin retrograde flow speed. J. Cell Biol. **183**: 999–1005.

Gensbittel V., Kräter M., Harlepp S., Busnelli I., Guck J. & Goetz J.G. 2021. Mechanical Adaptability of Tumor Cells in Metastasis. Dev. Cell. **56**: 164–179.

Georgiadou M., Lilja J., Jacquemet G., Guzmán C., Rafaeva M., Alibert C., Yan Y., Sahgal P., Lerche M., Manneville J.-B., Mäkelä T.P. & Ivaska J. 2017. AMPK negatively regulates tensin-dependent integrin activity. J. Cell Biol. **216**: 1107–1121.

Gerstberger S., Jiang Q. & Ganesh K. 2023. Metastasis. Cell. **186**: 1564–1579.

Ghassemi S., Meacci G., Liu S., Gondarenko A.A., Mathur A., Roca-Cusachs P., Sheetz M.P. & Hone J. 2012. Cells test substrate rigidity by local contractions on submicrometer pillars. Proc. Natl. Acad. Sci. U. S. A. **109**: 5328–5333.

Ghibaudo M., Saez A., Trichet L., Xayaphoummine A., Browaeys J., Silberzan P., Buguin A. & Ladoux B. 2008. Traction forces and rigidity sensing regulate cell functions. Soft Matter. **4**: 1836–1843.

Giese A., Loo M.A., Tran N., Haskett D., Coons S.W. & Berens M.E. 1996. Dichotomy of astrocytoma migration and proliferation. Int. J. Cancer. **67**: 275–282.

Gillespie D.T. 1977. Exact stochastic simulation of coupled chemical reactions. J. Phys. Chem. **81**: 2340–2361.

Gillis N.K. & McLeod H.L. 2016. The pharmacogenomics of drug resistance to protein kinase inhibitors. Drug Resist. Updat. **28**: 28–42.

Glentis A., Oertle P., Mariani P., Chikina A., El Marjou F., Attieh Y., Zaccarini F., Lae M., Loew D., Dingli F., Sirven P., Schoumacher M., Gurchenkov B.G., Plodinec M. & Vignjevic D.M. 2017. Cancer-associated fibroblasts induce metalloprotease-independent cancer cell invasion of the basement membrane. Nat. Commun. **8**: 924.

Goetz J.G., Minguet S., Navarro-Lérida I., Lazcano J.J., Samaniego R., Calvo E., Tello M., Osteso-Ibáñez T., Pellinen T., Echarri A., Cerezo A., Klein-Szanto A.J.P., Garcia R., Keely P.J., Sánchez-Mateos P., Cukierman E. & Del Pozo M.A. 2011. Biomechanical Remodeling of the Microenvironment by Stromal Caveolin-1 Favors Tumor Invasion and Metastasis. Cell. **146**: 148–163.

Gomes E.R., Jani S. & Gundersen G.G. 2005. Nuclear Movement Regulated by Cdc42, MRCK, Myosin, and Actin Flow Establishes MTOC Polarization in Migrating Cells. Cell. **121**: 451–463.

Gopal S., Veracini L., Grall D., Butori C., Schaub S., Audebert S., Camoin L., Baudelet E., Radwanska A., Beghelli-de la Forest Divonne S., Violette S.M., Weinreb P.H., Rekima S., Ilie M., Sudaka A., Hofman P. & Van Obberghen-Schilling E. 2017. Fibronectin-guided migration of carcinoma collectives. Nat. Commun. **8**: 14105.

Goreczny G.J., Forsythe I.J. & Turner C.E. 2018. Hic-5 regulates fibrillar adhesion formation to control tumor extracellular matrix remodeling through interaction with tensin1. Oncogene. **37**: 1699–1713.

Gotlieb A.I., May L.M., Subrahmanyan L. & Kalnins V.I. 1981. Distribution of microtubule organizing centers in migrating sheets of endothelial cells. J. Cell Biol. **91**: 589–594.

Gough R.E. & Goult B.T. 2018. The tale of two talins – two isoforms to fine-tune integrin signalling. Febs Lett. **592**: 2108.

Goult B.T., Yan J. & Schwartz M.A. 2018. Talin as a mechanosensitive signaling hub. J. Cell Biol. **217**: 3776–3784.

Graham D.M., Andersen T., Sharek L., Uzer G., Rothenberg K., Hoffman B.D., Rubin J., Balland M., Bear J.E. & Burridge K. 2018. Enucleated cells reveal differential roles of the nucleus in cell migration, polarity, and mechanotransduction. J. Cell Biol. **217**: 895–914.

Greciano P.G., Moyano J.V., Buschmann M.M., Tang J., Lu Y., Rudnicki J., Manninen A. & Matlin K.S. 2012. Laminin 511 partners with laminin 332 to mediate directional migration of Madin–Darby canine kidney epithelial cells. Mol. Biol. Cell. **23**: 121–136.

Green H.J., Griffiths A.G., Ylänne J. & Brown N.H. 2018. Novel functions for integrin-associated proteins revealed by analysis of myofibril attachment in Drosophila. eLife. **7**: e35783.

Gregor M., Osmanagic-Myers S., Burgstaller G., Wolfram M., Fischer I., Walko G., Resch G.P., Jörgl A., Herrmann H. & Wiche G. 2014. Mechanosensing through focal adhesion-anchored intermediate filaments. FASEB J. **28**: 715–729.

Gritsenko P.G., Ilina O. & Friedl P. 2012. Interstitial guidance of cancer invasion. J. Pathol. **226**: 185–199.

Gulvady A.C., Dubois F., Deakin N.O., Goreczny G.J. & Turner C.E. 2018. Hic-5 expression is a major indicator of cancer cell morphology, migration, and plasticity in three-dimensional matrices. Mol. Biol. Cell. **29**: 1704–1717.

Gundem G., Van Loo P., Kremeyer B., Alexandrov L.B., Tubio J.M.C., Papaemmanuil E., Brewer D.S., Kallio H.M.L., Högnäs G., Annala M., Kivinummi K., Goody V., Latimer C., O'Meara S., Dawson K.J., Isaacs W., Emmert-Buck M.R., Nykter M., Foster C., Kote-Jarai Z., Easton D., Whitaker H.C., Neal D.E., Cooper C.S., Eeles R.A., Visakorpi T., Campbell P.J., McDermott U., Wedge D.C. & Bova G.S. 2015. The evolutionary history of lethal metastatic prostate cancer. Nature. **520**: 353–357.

Guo T., Jiang C., Yang S.-Z., Zhu Y., He C., Carter A.B., Antony V.B., Peng H. & Zhou Y. 2023. Mitochondrial fission and bioenergetics mediate human lung fibroblast durotaxis. JCI Insight. **8**: e157348.

Guo W. & Wang Y. 2007. Retrograde Fluxes of Focal Adhesion Proteins in Response to Cell Migration and Mechanical Signals. Mol. Biol. Cell. **18**: 4519–4527.

Hadden W.J., Young J.L., Holle A.W., McFetridge M.L., Kim D.Y., Wijesinghe P., Taylor-Weiner H., Wen J.H., Lee A.R., Bieback K., Vo B.-N., Sampson D.D., Kennedy B.F., Spatz J.P., Engler A.J. & Choi Y.S. 2017. Stem cell migration and mechanotransduction on linear stiffness gradient hydrogels. Proc. Natl. Acad. Sci. U. S. A. **114**: 5647–5652.

Hakanpää L., Abouelezz A., Lenaerts A.-S., Culfa S., Algie M., Bärlund J., Katajisto P., McMahon H. & Almeida-Souza L. 2023. Reticular adhesions are assembled at flat clathrin lattices and opposed by active integrin α5β1. J. Cell Biol. **222**: e202303107.

Hakeem R.M., Subramanian B.C., Hockenberry M.A., King Z.T., Butler M.T., Legant W.R. & Bear J.E. 2023. A Photopolymerized Hydrogel System with Dual Stiffness Gradients Reveals Distinct Actomyosin-Based Mechano-Responses in Fibroblast Durotaxis. ACS Nano. **17**: 197–211.

Hamidi H. & Ivaska J. 2018. Every step of the way: integrins in cancer progression and metastasis. Nat. Rev. Cancer. **18**: 533–548.

Han S.J., Oak Y., Groisman A. & Danuser G. 2015. Traction microscopy to identify force modulation in sub-resolution adhesions. Nat. Methods. **12**: 653–656.

Hanahan D. & Weinberg R.A. 2011. Hallmarks of Cancer: The Next Generation. Cell. **144**: 646–674.

Hao H., Niu J., Xue B., Su Q.P., Liu M., Yang J., Qin J., Zhao S., Wu C. & Sun Y. 2020. Golgi-associated microtubules are fast cargo tracks and required for persistent cell migration. EMBO Rep. **21**: e48385.

Harada T., Swift J., Irianto J., Shin J.-W., Spinler K.R., Athirasala A., Diegmiller R., Dingal P.C.D.P., Ivanovska I.L. & Discher D.E. 2014. Nuclear lamin stiffness is a barrier to 3D migration, but softness can limit survival. J. Cell Biol. **204**: 669–682.

Harland B., Walcott S. & Sun S.X. 2011. Adhesion dynamics and durotaxis in migrating cells. Phys. Biol. **8**: 015011.

Hartman C.D., Isenberg B.C., Chua S.G. & Wong J.Y. 2016. Vascular smooth muscle cell durotaxis depends on extracellular matrix composition. Proc. Natl. Acad. Sci. U. S. A. **113**: 11190–11195.

Harunaga J.S. & Yamada K.M. 2011. Cell-matrix adhesions in 3D. Matrix Biol. **30**: 363–368.

Haugh J.M., Codazzi F., Teruel M. & Meyer T. 2000. Spatial Sensing in Fibroblasts Mediated by 3′ Phosphoinositides. J. Cell Biol. **151**: 1269–1280.

van Helvert S., Storm C. & Friedl P. 2018. Mechanoreciprocity in cell migration. Nat. Cell Biol. **20**: 8–20.

Hetmanski J.H.R., de Belly H., Busnelli I., Waring T., Nair R.V., Sokleva V., Dobre O., Cameron A., Gauthier N., Lamaze C., Swift J., del Campo A., Starborg T., Zech T., Goetz J.G., Paluch E.K., Schwartz J.-M. & Caswell P.T. 2019. Membrane Tension Orchestrates Rear Retraction in Matrix-Directed Cell Migration. Dev. Cell. **51**: 460-475.e10.

Hoffecker I.T., Guo W. & Wang Y. 2011. Assessing the spatial resolution of cellular rigidity sensing using a micropatterned hydrogel–photoresist composite. Lab. Chip. **11**: 3538–3544.

Hons M., Kopf A., Hauschild R., Leithner A., Gaertner F., Abe J., Renkawitz J., Stein J.V. & Sixt M. 2018. Chemokines and integrins independently tune actin flow and substrate friction during intranodal migration of T cells. Nat. Immunol. **19**: 606–616.

Horton E.R., Byron A., Askari J.A., Ng D.H.J., Millon-Frémillon A., Robertson J., Koper E.J., Paul N.R., Warwood S., Knight D., Humphries J.D. & Humphries M.J. 2015. Definition of a consensus integrin adhesome and its dynamics during adhesion complex assembly and disassembly. Nat. Cell Biol. **17**: 1577–1587.

Horton E.R., Humphries J.D., James J., Jones M.C., Askari J.A. & Humphries M.J. 2016. The integrin adhesome network at a glance. J. Cell Sci. **129**: 4159–4163.

Hosseini H., Obradović M.M.S., Hoffmann M., Harper K.L., Sosa M.S., Werner-Klein M., Nanduri L.K., Werno C., Ehrl C., Maneck M., Patwary N., Haunschild G., Gužvić M., Reimelt C., Grauvogl M., Eichner N., Weber F., Hartkopf A.D., Taran F.-A., Brucker S.Y., Fehm T., Rack B., Buchholz S., Spang R., Meister G., Aguirre-Ghiso J.A. & Klein C.A. 2016. Early dissemination seeds metastasis in breast cancer. Nature. **540**: 552–558.

Hou J.C., Shamsan G.A., Anderson S.M., McMahon M.M., Tyler L.P., Castle B.T., Heussner R.K., Provenzano P.P., Keefe D.F., Barocas V.H. & Odde D.J. 2019. Modeling distributed forces within cell adhesions of varying size on continuous substrates. Cytoskeleton. **76**: 571–585.

Hu K., Ji L., Applegate K.T., Danuser G. & Waterman-Storer C.M. 2007. Differential Transmission of Actin Motion Within Focal Adhesions. Science. **315**: 111–115.

Hu S., Chen J., Fabry B., Numaguchi Y., Gouldstone A., Ingber D.E., Fredberg J.J., Butler J.P. & Wang N. 2003. Intracellular stress tomography reveals stress focusing and structural anisotropy in cytoskeleton of living cells. Am. J. Physiol.-Cell Physiol. **285**: C1082–C1090.

Hu S., Chen T.-H., Zhao Y., Wang Z. & Lam R.H.W. 2018. Protein–Substrate Adhesion in Microcontact Printing Regulates Cell Behavior. Langmuir. **34**: 1750–1759.

Hu S., Tee Y.-H., Kabla A., Zaidel-Bar R., Bershadsky A. & Hersen P. 2015. Structured illumination microscopy reveals focal adhesions are composed of linear subunits. Cytoskeleton. **72**: 235–245.

Huang D.L., Bax N.A., Buckley C.D., Weis W.I. & Dunn A.R. 2017. Vinculin forms a directionally asymmetric catch bond with F-actin. Science. **357**: 703–706.

Huang Y., Su J., Liu J., Yi X., Zhou F., Zhang J., Wang J., Meng X., Si L. & Wu C. 2022. YAP Activation in Promoting Negative Durotaxis and Acral Melanoma Progression. Cells. **11**: 3543.

Huang Y.-J., Hoffmann G., Wheeler B., Schiapparelli P., Quinones-Hinojosa A. & Searson P. 2016. Cellular microenvironment modulates the galvanotaxis of brain tumor initiating cells. Sci. Rep. **6**: 21583.

Humphries J.D., Chastney M.R., Askari J.A. & Humphries M.J. 2019. Signal transduction via integrin adhesion complexes. Curr. Opin. Cell Biol. **56**: 14–21.

Humphries J.D., Wang P., Streuli C., Geiger B., Humphries M.J. & Ballestrem C. 2007. Vinculin controls focal adhesion formation by direct interactions with talin and actin. J. Cell Biol. **179**: 1043–1057.

Hurtado L., Caballero C., Gavilan M.P., Cardenas J., Bornens M. & Rios R.M. 2011. Disconnecting the Golgi ribbon from the centrosome prevents directional cell migration and ciliogenesis. J. Cell Biol. **193**: 917–933.

Hynes R.O. 2002. Integrins: Bidirectional, Allosteric Signaling Machines. Cell. **110**: 673–687.

Isenberg B.C., DiMilla P.A., Walker M., Kim S. & Wong J.Y. 2009. Vascular Smooth Muscle Cell Durotaxis Depends on Substrate Stiffness Gradient Strength. Biophys. J. **97**: 1313–1322.

Iskratsch T., Wolfenson H. & Sheetz M.P. 2014. Appreciating force and shape — the rise of mechanotransduction in cell biology. Nat. Rev. Mol. Cell Biol. **15**: 825–833.

Isomursu A., Lerche M., Taskinen M.E., Ivaska J. & Peuhu E. 2019. Integrin signaling and mechanotransduction in regulation of somatic stem cells. Exp. Cell Res. **378**: 217–225.

Iwanicki M.P., Vomastek T., Tilghman R.W., Martin K.H., Banerjee J., Wedegaertner P.B. & Parsons J.T. 2008. FAK, PDZ-RhoGEF and ROCKII cooperate to regulate adhesion movement and trailing-edge retraction in fibroblasts. J. Cell Sci. **121**: 895–905.

Jacquemet G., Hamidi H. & Ivaska J. 2015. Filopodia in cell adhesion, 3D migration and cancer cell invasion. Curr. Opin. Cell Biol. **36**: 23–31.

Jacquemet G., Stubb A., Saup R., Miihkinen M., Kremneva E., Hamidi H. & Ivaska J. 2019. Filopodome Mapping Identifies p130Cas as a Mechanosensitive Regulator of Filopodia Stability. Curr. Biol. CB. **29**: 202-216.e7.

Jain R.K. & Baxter L.T. 1988. Mechanisms of heterogeneous distribution of monoclonal antibodies and other macromolecules in tumors: significance of elevated interstitial pressure. Cancer Res. **48**: 7022–7032.

Jiang X., Bruzewicz D.A., Wong A.P., Piel M. & Whitesides G.M. 2005. Directing cell migration with asymmetric micropatterns. Proc. Natl. Acad. Sci. U. S. A. **102**: 975–978.

Jimenez A.J., Schaeffer A., Pascalis C.D., Letort G., Vianay B., Bornens M., Piel M., Blanchoin L. & Théry M. 2021. Acto-myosin network geometry defines centrosome position. Curr. Biol. **31**: 1206-1220.e5.

Jiu Y., Lehtimäki J., Tojkander S., Cheng F., Jäälinoja H., Liu X., Varjosalo M., Eriksson J.E. & Lappalainen P. 2015. Bidirectional Interplay between Vimentin Intermediate Filaments and Contractile Actin Stress Fibers. Cell Rep. **11**: 1511–1518.

Jo M.H., Li J., Jaumouillé V., Hao Y., Coppola J., Yan J., Waterman C.M., Springer T.A. & Ha T. 2022. Single-molecule characterization of subtype-specific β1 integrin mechanics. Nat. Commun. **13**: 7471.

Jun M., Lee Y.L., Zhou T., Maric M., Burke B., Park S., Low B.C. & Chiam K.-H. 2023. Subcellular Force Imbalance in Actin Bundles Induces Nuclear Repositioning and Durotaxis. ACS Appl. Mater. Interfaces. **15**: 43387–43402.

Kalli M., Li R., Mills G.B., Stylianopoulos T. & Zervantonakis I.K. 2022. Mechanical Stress Signaling in Pancreatic Cancer Cells Triggers p38 MAPK- and JNK-Dependent Cytoskeleton Remodeling and Promotes Cell Migration via Rac1/cdc42/Myosin II. Mol. Cancer Res. **20**: 485–497.

Kalli M., Voutouri C., Minia A., Pliaka V., Fotis C., Alexopoulos L.G. & Stylianopoulos T. 2019. Mechanical Compression Regulates Brain Cancer Cell Migration Through MEK1/Erk1 Pathway Activation and GDF15 Expression. Front. Oncol. **9**: 992.

Kameritsch P. & Renkawitz J. 2020. Principles of Leukocyte Migration Strategies. Trends Cell Biol. **30**: 818–832.

Kanchanawong P. & Calderwood D.A. 2023. Organization, dynamics and mechanoregulation of integrin-mediated cell–ECM adhesions. Nat. Rev. Mol. Cell Biol. **24**: 142–161.

Kanchanawong P., Shtengel G., Pasapera A.M., Ramko E.B., Davidson M.W., Hess H.F. & Waterman C.M. 2010. Nanoscale architecture of integrin-based cell adhesions. Nature. **468**: 580–584.

Kaukonen R., Mai A., Georgiadou M., Saari M., De Franceschi N., Betz T., Sihto H., Ventelä S., Elo L., Jokitalo E., Westermarck J., Kellokumpu-Lehtinen P.-L., Joensuu H., Grenman R. & Ivaska J. 2016. Normal stroma suppresses cancer cell proliferation via mechanosensitive regulation of JMJD1a-mediated transcription. Nat. Commun. **7**: 12237.

Kechagia J.Z., Ivaska J. & Roca-Cusachs P. 2019. Integrins as biomechanical sensors of the microenvironment. Nat. Rev. Mol. Cell Biol. **20**: 457–473.

Kechagia Z., Sáez P., Gómez-González M., Canales B., Viswanadha S., Zamarbide M., Andreu I., Koorman T., Beedle A.E.M., Elosegui-Artola A., Derksen P.W.B., Trepat X., Arroyo M. & Roca-Cusachs P. 2023. The laminin–keratin link shields the nucleus from mechanical deformation and signalling. Nat. Mater. **22**: 1409–1420.

Kim D.-H., Han K., Gupta K., Kwon K.W., Suh K.-Y. & Levchenko A. 2009a. Mechanosensitivity of fibroblast cell shape and movement to anisotropic substratum topography gradients. Biomaterials. **30**: 5433–5444.

Kim D.-H., Provenzano P.P., Smith C.L. & Levchenko A. 2012. Matrix nanotopography as a regulator of cell function. J. Cell Biol. **197**: 351–360.

Kim M., Carman C.V., Yang W., Salas A. & Springer T.A. 2004. The primacy of affinity over clustering in regulation of adhesiveness of the integrin αLβ2. J. Cell Biol. **167**: 1241–1253.

Kim M.-C., Silberberg Y.R., Abeyaratne R., Kamm R.D. & Asada H.H. 2018. Computational modeling of three-dimensional ECM-rigidity sensing to guide directed cell migration. Proc. Natl. Acad. Sci. U. S. A. **115**: E390–E399.

Kim M.-Y., Oskarsson T., Acharyya S., Nguyen D.X., Zhang X.H.-F., Norton L. & Massagué J. 2009b. Tumor Self-Seeding by Circulating Cancer Cells. Cell. **139**: 1315–1326.

Kirby T.J. & Lammerding J. 2018. Emerging views of the nucleus as a cellular mechanosensor. Nat. Cell Biol. **20**: 373–381.

Klank R.L., Decker Grunke S.A., Bangasser B.L., Forster C.L., Price M.A., Odde T.J., SantaCruz K.S., Rosenfeld S.S., Canoll P., Turley E.A., McCarthy J.B., Ohlfest J.R. & Odde D.J. 2017. Biphasic Dependence of Glioma Survival and Cell Migration on CD44 Expression Level. Cell Rep. **18**: 23–31.

Ko Y.-G., Co C.C. & Ho C.-C. 2013. Directing cell migration in continuous microchannels by topographical amplification of natural directional persistence. Biomaterials. **34**: 353–360.

Koch D., Rosoff W.J., Jiang J., Geller H.M. & Urbach J.S. 2012. Strength in the Periphery: Growth Cone Biomechanics and Substrate Rigidity Response in Peripheral and Central Nervous System Neurons. Biophys. J. **102**: 452–460.

Kong F., García A.J., Mould A.P., Humphries M.J. & Zhu C. 2009. Demonstration of catch bonds between an integrin and its ligand. J. Cell Biol. **185**: 1275–1284.

Koser D.E., Thompson A.J., Foster S.K., Dwivedy A., Pillai E.K., Sheridan G.K., Svoboda H., Viana M., Costa L. da F., Guck J., Holt C.E. & Franze K. 2016. Mechanosensing is critical for axon growth in the developing brain. Nat. Neurosci. **19**: 1592–1598.

Krieg M., Fläschner G., Alsteens D., Gaub B.M., Roos W.H., Wuite G.J.L., Gaub H.E., Gerber C., Dufrêne Y.F. & Müller D.J. 2019. Atomic force microscopy-based mechanobiology. Nat. Rev. Phys. **1**: 41–57.

Kuipers A.J., Middelbeek J., Vrenken K., Pérez-González C., Poelmans G., Klarenbeek J., Jalink K., Trepat X. & van Leeuwen F.N. 2018. TRPM7 controls mesenchymal features of breast cancer cells by tensional regulation of SOX4. Biochim. Biophys. Acta Mol. Basis Dis. **1864**: 2409–2419.

Kumar G., Co C.C. & Ho C.-C. 2011. Steering cell migration using microarray amplification of natural directional persistence. Langmuir ACS J. Surf. Colloids. **27**: 3803–3807.

Kümper S., Mardakheh F.K., McCarthy A., Yeo M., Stamp G.W., Paul A., Worboys J., Sadok A., Jørgensen C., Guichard S. & Marshall C.J. 2016. Rho-associated kinase (ROCK) function is essential for cell cycle progression, senescence and tumorigenesis. eLife. **5**: e12203.

Kuo J.-C., Han X., Hsiao C.-T., Yates III J.R. & Waterman C.M. 2011. Analysis of the myosin-II-responsive focal adhesion proteome reveals a role for β-Pix in negative regulation of focal adhesion maturation. Nat. Cell Biol. **13**: 383–393.

Kuokkanen E., Šuštar V. & Mattila P.K. 2015. Molecular Control of B Cell Activation and Immunological Synapse Formation. Traffic. **16**: 311–326.

Kupfer A., Louvard D. & Singer S.J. 1982. Polarization of the Golgi apparatus and the microtubule-organizing center in cultured fibroblasts at the edge of an experimental wound. Proc. Natl. Acad. Sci. U. S. A. **79**: 2603–2607.

Kutys M.L. & Yamada K.M. 2014. An extracellular matrix-specific GEF-GAP interaction regulates Rho GTPase crosstalk for 3D collagen migration. Nat. Cell Biol. **16**: 909–917.

Labernadie A., Kato T., Brugués A., Serra-Picamal X., Derzsi S., Arwert E., Weston A., González-Tarragó V., Elosegui-Artola A., Albertazzi L., Alcaraz J., Roca-Cusachs P., Sahai E. & Trepat X. 2017. A mechanically active heterotypic E-cadherin/N-cadherin adhesion enables fibroblasts to drive cancer cell invasion. Nat. Cell Biol. **19**: 224–237.

Lachowski D., Cortes E., Robinson B., Rice A., Rombouts K. & Del Río Hernández A.E. 2018. FAK controls the mechanical activation of YAP, a transcriptional regulator required for durotaxis. FASEB J. Off. Publ. Fed. Am. Soc. Exp. Biol. **32**: 1099–1107.

Ladoux B., Mège R.-M. & Trepat X. 2016. Front-Rear Polarization by Mechanical Cues: From Single Cells to Tissues. Trends Cell Biol. **26**: 420–433.

Lambert A.W., Pattabiraman D.R. & Weinberg R.A. 2017. Emerging Biological Principles of Metastasis. Cell. **168**: 670–691.

Lauffenburger D.A. & Horwitz A.F. 1996. Cell Migration: A Physically Integrated Molecular Process. Cell. **84**: 359–369.

Lawson C.D. & Ridley A.J. 2018. Rho GTPase signaling complexes in cell migration and invasion. J. Cell Biol. **217**: 447–457.

Le H.A. & Mayor R. 2023. Cell-matrix and cell-cell interaction mechanics in guiding migration. Biochem. Soc. Trans. **51**: 1733–1745.

Leduc C. & Etienne-Manneville S. 2017. Regulation of microtubule-associated motors drives intermediate filament network polarization. J. Cell Biol. **216**: 1689–1703.

Lee G., Han S.-B. & Kim D.-H. 2021. Cell-ECM contact-guided intracellular polarization is mediated via lamin A/C dependent nucleus-cytoskeletal connection. Biomaterials. **268**: 120548.

Lee J.W. & Juliano R. l. 2000. α5β1 Integrin Protects Intestinal Epithelial Cells from Apoptosis through a Phosphatidylinositol 3-Kinase and Protein Kinase B–dependent Pathway. Mol. Biol. Cell. **11**: 1973–1987.

Lee J.Y., Chang J.K., Dominguez A.A., Lee H., Nam S., Chang J., Varma S., Qi L.S., West R.B. & Chaudhuri O. 2019. YAP-independent mechanotransduction drives breast cancer progression. Nat. Commun. **10**: 1–9.

Lee M. & Vasioukhin V. 2008. Cell polarity and cancer – cell and tissue polarity as a non-canonical tumor suppressor. J. Cell Sci. **121**: 1141–1150.

Legerstee K., Abraham T.E., van Cappellen W.A., Nigg A.L., Slotman J.A. & Houtsmuller A.B. 2021. Growth factor dependent changes in nanoscale architecture of focal adhesions. Sci. Rep. **11**: 2315.

Lehmann S., Boekhorst V. te, Odenthal J., Bianchi R., Helvert S. van, Ikenberg K., Ilina O., Stoma S., Xandry J., Jiang L., Grenman R., Rudin M. & Friedl P. 2017. Hypoxia Induces a HIF-1-Dependent Transition from Collective-to-Amoeboid Dissemination in Epithelial Cancer Cells. Curr. Biol. **27**: 392–400.

Lerche M., Elosegui-Artola A., Kechagia J.Z., Guzmán C., Georgiadou M., Andreu I., Gullberg D., Roca-Cusachs P., Peuhu E. & Ivaska J. 2020. Integrin Binding Dynamics Modulate Ligand-Specific Mechanosensing in Mammary Gland Fibroblasts. iScience. **23**: 100907.

Lerche M., Mathieu M., Malerød L., Pedersen N.M., Hamidi H., Chastney M., Bruininks B.M.H., Kaptan S., Jacquemet G., Vattulainen I., Roca-Cusachs P., Brech A., Perez F., Boncompain G.,

Miserey S. & Ivaska J. 2022. Regulation of cell dynamics by rapid transport of integrins through the biosynthetic pathway. bioRxiv. 2022.07.12.498931.

Li H., Deng Y., Sun K., Yang H., Liu J., Wang M., Zhang Z., Lin J., Wu C., Wei Z. & Yu C. 2017. Structural basis of kindlin-mediated integrin recognition and activation. Proc. Natl. Acad. Sci. U. S. A. **114**: 9349–9354.

Li J. & Springer T.A. 2017. Integrin extension enables ultrasensitive regulation by cytoskeletal force. Proc. Natl. Acad. Sci. U. S. A. **114**: 4685–4690.

Li J., Yan J. & Springer T.A. 2021. Low-affinity integrin states have faster ligand-binding kinetics than the high-affinity state. eLife. **10**: e73359.

Liang D., Shi S., Xu J., Zhang B., Qin Y., Ji S., Xu W., Liu J., Liu L., Liu C., Long J., Ni Q. & Yu X. 2016. New insights into perineural invasion of pancreatic cancer: More than pain. Biochim. Biophys. Acta BBA - Rev. Cancer. **1865**: 111–122.

Liao Y.-C. & Lo S.H. 2021. Tensins - emerging insights into their domain functions, biological roles and disease relevance. J. Cell Sci. **134**: jcs254029.

Liebig C., Ayala G., Wilks J.A., Berger D.H. & Albo D. 2009. Perineural invasion in cancer. Cancer. **115**: 3379–3391.

Lin C.-H. & Forscher P. 1995. Growth cone advance is inversely proportional to retrograde F-actin flow. Neuron. **14**: 763–771.

Linder S., Cervero P., Eddy R. & Condeelis J. 2023. Mechanisms and roles of podosomes and invadopodia. Nat. Rev. Mol. Cell Biol. **24**: 86–106.

Liu J., Wang Y., Goh W.I., Goh H., Baird M.A., Ruehland S., Teo S., Bate N., Critchley D.R., Davidson M.W. & Kanchanawong P. 2015a. Talin determines the nanoscale architecture of focal adhesions. Proc. Natl. Acad. Sci. U. S. A. **112**: E4864-4873.

Liu Y.-J., Le Berre M., Lautenschlaeger F., Maiuri P., Callan-Jones A., Heuzé M., Takaki T., Voituriez R. & Piel M. 2015b. Confinement and Low Adhesion Induce Fast Amoeboid Migration of Slow Mesenchymal Cells. Cell. **160**: 659–672.

Lo C.M., Wang H.B., Dembo M. & Wang Y.L. 2000. Cell movement is guided by the rigidity of the substrate. Biophys. J. **79**: 144–152.

Lock J.G., Jones M.C., Askari J.A., Gong X., Oddone A., Olofsson H., Göransson S., Lakadamyali M., Humphries M.J. & Strömblad S. 2018. Reticular adhesions are a distinct class of cell-matrix adhesions that mediate attachment during mitosis. Nat. Cell Biol. **20**: 1290–1302.

Lomonaco S.L., Finniss S., Xiang C., Lee H.K., Jiang W., Lemke N., Rempel S.A., Mikkelsen T. & Brodie C. 2011. Cilengitide induces autophagy-mediated cell death in glioma cells. Neuro-Oncol. **13**: 857–865.

Lu F., Zhu L., Bromberger T., Yang J., Yang Q., Liu J., Plow E.F., Moser M. & Qin J. 2022. Mechanism of integrin activation by talin and its cooperation with kindlin. Nat. Commun. **13**: 2362.

Lu J., Doyle A.D., Shinsato Y., Wang S., Bodendorfer M.A., Zheng M. & Yamada K.M. 2020. Basement Membrane Regulates Fibronectin Organization Using Sliding Focal Adhesions Driven by a Contractile Winch. Dev. Cell. **52**: 631-646.e4.

Lugassy C., Kleinman H.K., Vermeulen P.B. & Barnhill R.L. 2020. Angiotropism, pericytic mimicry and extravascular migratory metastasis: an embryogenesis-derived program of tumor spread. Angiogenesis. **23**: 27–41.

Machacek M., Hodgson L., Welch C., Elliott H., Pertz O., Nalbant P., Abell A., Johnson G.L., Hahn K.M. & Danuser G. 2009. Coordination of Rho GTPase activities during cell protrusion. Nature. **461**: 99–103.

Mahmud G., Campbell C.J., Bishop K.J.M., Komarova Y.A., Chaga O., Soh S., Huda S., Kandere-Grzybowska K. & Grzybowski B.A. 2009. Directing cell motions on micropatterned ratchets. Nat. Phys. **5**: 606–612.

Maiques O., Fanshawe B., Crosas-Molist E., Rodriguez-Hernandez I., Volpe A., Cantelli G., Boehme L., Orgaz J.L., Mardakheh F.K., Sanz-Moreno V. & Fruhwirth G.O. 2021. A preclinical pipeline

to evaluate migrastatics as therapeutic agents in metastatic melanoma. Br. J. Cancer. **125**: 699–713.

Maiuri P., Rupprecht J.-F., Wieser S., Ruprecht V., Bénichou O., Carpi N., Coppey M., De Beco S., Gov N., Heisenberg C.-P., Lage Crespo C., Lautenschlaeger F., Le Berre M., Lennon-Dumenil A.-M., Raab M., Thiam H.-R., Piel M., Sixt M. & Voituriez R. 2015. Actin Flows Mediate a Universal Coupling between Cell Speed and Cell Persistence. Cell. **161**: 374–386.

Malik R., Luong T., Cao X., Han B., Shah N., Franco-Barraza J., Han L., Shenoy V.B., Lelkes P.I. & Cukierman E. 2019. Rigidity controls human desmoplastic matrix anisotropy to enable pancreatic cancer cell spread via extracellular signal-regulated kinase 2. Matrix Biol. J. Int. Soc. Matrix Biol. **81**: 50–69.

Maninová M., Klímová Z., Parsons J.T., Weber M.J., Iwanicki M.P. & Vomastek T. 2013. The Reorientation of Cell Nucleus Promotes the Establishment of Front–Rear Polarity in Migrating Fibroblasts. J. Mol. Biol. **425**: 2039–2055.

Margaron Y., Nagai T., Guyon L., Kurzawa L., Morel A.-P., Pinheiro A., Blanchoin L., Reyal F., Puisieux A. & Théry M. 2019. Biophysical properties of intermediate states of EMT outperform both epithelial and mesenchymal states. bioRxiv. 797654.

Martin K., Reimann A., Fritz R.D., Ryu H., Jeon N.L. & Pertz O. 2016. Spatio-temporal co-ordination of RhoA, Rac1 and Cdc42 activation during prototypical edge protrusion and retraction dynamics. Sci. Rep. **6**: 21901.

Martin M., Veloso A., Wu J., Katrukha E.A. & Akhmanova A. 2018. Control of endothelial cell polarity and sprouting angiogenesis by non-centrosomal microtubules. eLife. **7**: e33864.

Mason D.E., Collins J.M., Dawahare J.H., Nguyen T.D., Lin Y., Voytik-Harbin S.L., Zorlutuna P., Yoder M.C. & Boerckel J.D. 2019. YAP and TAZ limit cytoskeletal and focal adhesion maturation to enable persistent cell motility. J. Cell Biol. **218**: 1369–1389.

Matlin K.S., Myllymäki S.-M. & Manninen A. 2017. Laminins in Epithelial Cell Polarization: Old Questions in Search of New Answers. Cold Spring Harb. Perspect. Biol. **9**: a027920.

Matsuoka S. & Ueda M. 2018. Mutual inhibition between PTEN and PIP3 generates bistability for polarity in motile cells. Nat. Commun. **9**: 4481.

Matthews H.K., Ganguli S., Plak K., Taubenberger A.V., Win Z., Williamson M., Piel M., Guck J. & Baum B. 2020. Oncogenic Signaling Alters Cell Shape and Mechanics to Facilitate Cell Division under Confinement. Dev. Cell. **52**: 563-573.e3.

Mayor R. & Etienne-Manneville S. 2016. The front and rear of collective cell migration. Nat. Rev. Mol. Cell Biol. **17**: 97–109.

Mayorca-Guiliani A.E., Madsen C.D., Cox T.R., Horton E.R., Venning F.A. & Erler J.T. 2017. ISDoT: in situ decellularization of tissues for high-resolution imaging and proteomic analysis of native extracellular matrix. Nat. Med. **23**: 890–898.

McCarthy J.B. & Furcht L.T. 1984. Laminin and fibronectin promote the haptotactic migration of B16 mouse melanoma cells in vitro. J. Cell Biol. **98**: 1474–1480.

McCleverty C.J., Lin D.C. & Liddington R.C. 2007. Structure of the PTB domain of tensin1 and a model for its recruitment to fibrillar adhesions. Protein Sci. **16**: 1223–1229.

McDonald J.A., Kelley D.G. & Broekelmann T.J. 1982. Role of fibronectin in collagen deposition: Fab' to the gelatin-binding domain of fibronectin inhibits both fibronectin and collagen organization in fibroblast extracellular matrix. J. Cell Biol. **92**: 485–492.

McLeod R., Kumar R., Papadatos-Pastos D., Mateo J., Brown J.S., Garces A.H.I., Ruddle R., Decordova S., Jueliger S., Ferraldeschi R., Maiques O., Sanz-Moreno V., Jones P., Traub S., Halbert G., Mellor S., Swales K.E., Raynaud F.I., Garrett M.D. & Banerji U. 2020. First-in-Human Study of AT13148, a Dual ROCK-AKT Inhibitor in Patients with Solid Tumors. Clin. Cancer Res. **26**: 4777–4784.

Meiring J.C.M., Shneyer B.I. & Akhmanova A. 2020. Generation and regulation of microtubule network asymmetry to drive cell polarity. Curr. Opin. Cell Biol. **62**: 86–95.

Miller P.M., Folkmann A.W., Maia A.R.R., Efimova N., Efimov A. & Kaverina I. 2009. Golgi-derived CLASP-dependent microtubules control Golgi organization and polarized trafficking in motile cells. Nat. Cell Biol. **11**: 1069–1080.

Miroshnikova Y.A., Mouw J.K., Barnes J.M., Pickup M.W., Lakins J.N., Kim Y., Lobo K., Persson A.I., Reis G.F., McKnight T.R., Holland E.C., Phillips J.J. & Weaver V.M. 2016. Tissue mechanics promote IDH1-dependent HIF1α-tenascin C feedback to regulate glioblastoma aggression. Nat. Cell Biol. **18**: 1336–1345.

Missirlis D., Haraszti T., Scheele C. v. C., Wiegand T., Diaz C., Neubauer S., Rechenmacher F., Kessler H. & Spatz J.P. 2016. Substrate engagement of integrins α5β1 and αvβ3 is necessary, but not sufficient, for high directional persistence in migration on fibronectin. Sci. Rep. **6**: 23258.

Missirlis D. & Spatz J.P. 2014. Combined Effects of PEG Hydrogel Elasticity and Cell-Adhesive Coating on Fibroblast Adhesion and Persistent Migration. Biomacromolecules. **15**: 195–205.

Mitchison T. & Kirschner M. 1988. Cytoskeletal dynamics and nerve growth. Neuron. **1**: 761–772.

Miyamoto S., Akiyama S.K. & Yamada K.M. 1995. Synergistic roles for receptor occupancy and aggregation in integrin transmembrane function. Science. **267**: 883–885.

Miyazaki N., Iwasaki K. & Takagi J. 2018. A systematic survey of conformational states in β1 and β4 integrins using negative-stain electron microscopy. J. Cell Sci. **131**: jcs216754.

Musiime M., Chang J., Hansen U., Kadler K.E., Zeltz C. & Gullberg D. 2021. Collagen Assembly at the Cell Surface: Dogmas Revisited. Cells. **10**: 662.

Nakajima K., Zhu K., Sun Y.-H., Hegyi B., Zeng Q., Murphy C.J., Small J.V., Chen-Izu Y., Izumiya Y., Penninger J.M. & Zhao M. 2015. KCNJ15/Kir4.2 couples with polyamines to sense weak extracellular electric fields in galvanotaxis. Nat. Commun. **6**: 8532.

Nardone G., Cruz J.O.-D.L., Vrbsky J., Martini C., Pribyl J., Skládal P., Pešl M., Caluori G., Pagliari S., Martino F., Maceckova Z., Hajduch M., Sanz-Garcia A., Pugno N.M., Stokin G.B. & Forte G. 2017. YAP regulates cell mechanics by controlling focal adhesion assembly. Nat. Commun. **8**: 1–13.

Newman D., Young L.E., Waring T., Brown L., Wolanska K.I., MacDonald E., Charles-Orszag A., Goult B.T., Caswell P.T., Sakuma T., Yamamoto T., Machesky L.M., Morgan M.R. & Zech T. 2023. 3D matrix adhesion feedback controls nuclear force coupling to drive invasive cell migration. Cell Rep. **42**: 113554.

Nia H.T., Liu H., Seano G., Datta M., Jones D., Rahbari N., Incio J., Chauhan V.P., Jung K., Martin J.D., Askoxylakis V., Padera T.P., Fukumura D., Boucher Y., Hornicek F.J., Grodzinsky A.J., Baish J.W., Munn L.L. & Jain R.K. 2016. Solid stress and elastic energy as measures of tumour mechanopathology. Nat. Biomed. Eng. **1**: 1–11.

Nia H.T., Munn L.L. & Jain R.K. 2020. Physical traits of cancer. Science. **370**: eaaz0868.

Nishida N., Xie C., Shimaoka M., Cheng Y., Walz T. & Springer T.A. 2006. Activation of Leukocyte β2 Integrins by Conversion from Bent to Extended Conformations. Immunity. **25**: 583–594.

Nishiuchi R., Takagi J., Hayashi M., Ido H., Yagi Y., Sanzen N., Tsuji T., Yamada M. & Sekiguchi K. 2006. Ligand-binding specificities of laminin-binding integrins: a comprehensive survey of laminin-integrin interactions using recombinant alpha3beta1, alpha6beta1, alpha7beta1 and alpha6beta4 integrins. Matrix Biol. J. Int. Soc. Matrix Biol. **25**: 189–197.

Novikova E.A., Raab M., Discher D.E. & Storm C. 2017. Persistence-Driven Durotaxis: Generic, Directed Motility in Rigidity Gradients. Phys. Rev. Lett. **118**: 078103.

Oakes P.W., Patel D.C., Morin N.A., Zitterbart D.P., Fabry B., Reichner J.S. & Tang J.X. 2009. Neutrophil morphology and migration are affected by substrate elasticity. Blood. **114**: 1387–1395.

Oria R., Wiegand T., Escribano J., Elosegui-Artola A., Uriarte J.J., Moreno-Pulido C., Platzman I., Delcanale P., Albertazzi L., Navajas D., Trepat X., García-Aznar J.M., Cavalcanti-Adam E.A. & Roca-Cusachs P. 2017. Force loading explains spatial sensing of ligands by cells. Nature. **552**: 219–224.

Oudin M.J., Jonas O., Kosciuk T., Broye L.C., Guido B.C., Wyckoff J., Riquelme D., Lamar J.M., Asokan S.B., Whittaker C., Ma D., Langer R., Cima M.J., Wisinski K.B., Hynes R.O.,

Lauffenburger D.A., Keely P.J., Bear J.E. & Gertler F.B. 2016. Tumor Cell-Driven Extracellular Matrix Remodeling Drives Haptotaxis during Metastatic Progression. Cancer Discov. **6**: 516–531.

Owen L.M., Adhikari A.S., Patel M., Grimmer P., Leijnse N., Kim M.C., Notbohm J., Franck C. & Dunn A.R. 2017. A cytoskeletal clutch mediates cellular force transmission in a soft, three-dimensional extracellular matrix. Mol. Biol. Cell. **28**: 1959–1974.

Pàez-Ribes M., Allen E., Hudock J., Takeda T., Okuyama H., Viñals F., Inoue M., Bergers G., Hanahan D. & Casanovas O. 2009. Antiangiogenic therapy elicits malignant progression of tumors to increased local invasion and distant metastasis. Cancer Cell. **15**: 220–231.

Pallarès M.E., Pi-Jaumà I., Fortunato I.C., Grazu V., Gómez-González M., Roca-Cusachs P., de la Fuente J.M., Alert R., Sunyer R., Casademunt J. & Trepat X. 2023. Stiffness-dependent active wetting enables optimal collective cell durotaxis. Nat. Phys. **19**: 279–289.

Pankov R., Cukierman E., Katz B.Z., Matsumoto K., Lin D.C., Lin S., Hahn C. & Yamada K.M. 2000. Integrin dynamics and matrix assembly: tensin-dependent translocation of alpha(5)beta(1) integrins promotes early fibronectin fibrillogenesis. J. Cell Biol. **148**: 1075–1090.

Papavassiliou K.A., Basdra E.K. & Papavassiliou A.G. 2023. The emerging promise of tumour mechanobiology in cancer treatment. Eur. J. Cancer Oxf. Engl. 1990. **190**: 112938.

Pardo-Pastor C., Rubio-Moscardo F., Vogel-González M., Serra S.A., Afthinos A., Mrkonjic S., Destaing O., Abenza J.F., Fernández-Fernández J.M., Trepat X., Albiges-Rizo C., Konstantopoulos K. & Valverde M.A. 2018. Piezo2 channel regulates RhoA and actin cytoskeleton to promote cell mechanobiological responses. Proc. Natl. Acad. Sci. U. S. A. **115**: 1925–1930.

Park J., Kim D.-H., Kim H.-N., Wang C.J., Kwak M.K., Hur E., Suh K.-Y., An S.S. & Levchenko A. 2016. Directed migration of cancer cells guided by the graded texture of the underlying matrix. Nat. Mater. **15**: 792–801.

Park J., Kim D.-H. & Levchenko A. 2018. Topotaxis: A New Mechanism of Directed Cell Migration in Topographic ECM Gradients. Biophys. J. **114**: 1257–1263.

Parker K.K., Brock A.L., Brangwynne C., Mannix R.J., Wang N., Ostuni E., Geisse N.A., Adams J.C., Whitesides G.M. & Ingber D.E. 2002. Directional control of lamellipodia extension by constraining cell shape and orienting cell tractional forces. FASEB J. **16**: 1195–1204.

Paszek M.J., Boettiger D., Weaver V.M. & Hammer D.A. 2009. Integrin Clustering Is Driven by Mechanical Resistance from the Glycocalyx and the Substrate. PLOS Comput. Biol. **5**: e1000604.

Paszek M.J., DuFort C.C., Rossier O., Bainer R., Mouw J.K., Godula K., Hudak J.E., Lakins J.N., Wijekoon A.C., Cassereau L., Rubashkin M.G., Magbanua M.J., Thorn K.S., Davidson M.W., Rugo H.S., Park J.W., Hammer D.A., Giannone G., Bertozzi C.R. & Weaver V.M. 2014. The cancer glycocalyx mechanically primes integrin-mediated growth and survival. Nature. **511**: 319–325.

Paszek M.J., Zahir N., Johnson K.R., Lakins J.N., Rozenberg G.I., Gefen A., Reinhart-King C.A., Margulies S.S., Dembo M., Boettiger D., Hammer D.A. & Weaver V.M. 2005. Tensional homeostasis and the malignant phenotype. Cancer Cell. **8**: 241–254.

Peglion F. & Etienne-Manneville S. 2023. Cell polarity changes in cancer initiation and progression. J. Cell Biol. **223**: e202308069.

Pelham R.J. & Wang Y. 1997. Cell locomotion and focal adhesions are regulated by substrate flexibility. Proc. Natl. Acad. Sci. U. S. A. **94**: 13661–13665.

Perl A., Reinhoudt D.N. & Huskens J. 2009. Microcontact Printing: Limitations and Achievements. Adv. Mater. **21**: 2257–2268.

Pertz O., Hodgson L., Klemke R.L. & Hahn K.M. 2006. Spatiotemporal dynamics of RhoA activity in migrating cells. Nature. **440**: 1069–1072.

Petrie R.J., Gavara N., Chadwick R.S. & Yamada K.M. 2012. Nonpolarized signaling reveals two distinct modes of 3D cell migration. J. Cell Biol. **197**: 439–455.

Petrie R.J., Harlin H.M., Korsak L.I.T. & Yamada K.M. 2017. Activating the nuclear piston mechanism of 3D migration in tumor cells. J. Cell Biol. **216**: 93–100.

Petrie R.J., Koo H. & Yamada K.M. 2014. Generation of compartmentalized pressure by a nuclear piston governs cell motility in a 3D matrix. Science. **345**: 1062–1065.

Peuhu E., Jacquemet G., Scheele C.L.G.J., Isomursu A., Laisne M.-C., Koskinen L.M., Paatero I., Thol K., Georgiadou M., Guzmán C., Koskinen S., Laiho A., Elo L.L., Boström P., Hartiala P., van Rheenen J. & Ivaska J. 2022. MYO10-filopodia support basement membranes at pre-invasive tumor boundaries. Dev. Cell. **57**: 2350-2364.e7.

Peussa H., Fedele C., Tran H., Marttinen M., Fadjukov J., Mäntylä E., Priimägi A., Nymark S. & Ihalainen T.O. 2023. Light-Induced Nanoscale Deformation in Azobenzene Thin Film Triggers Rapid Intracellular Ca2+ Increase via Mechanosensitive Cation Channels. Adv. Sci. **10**: 2206190.

Plodinec M., Loparic M., Monnier C.A., Obermann E.C., Zanetti-Dallenbach R., Oertle P., Hyotyla J.T., Aebi U., Bentires-Alj M., Lim R.Y.H. & Schoenenberger C.-A. 2012. The nanomechanical signature of breast cancer. Nat. Nanotechnol. **7**: 757–765.

Plotnikov S.V., Pasapera A.M., Sabass B. & Waterman C.M. 2012. Force fluctuations within focal adhesions mediate ECM-rigidity sensing to guide directed cell migration. Cell. **151**: 1513–1527.

Polacheck W.J., Charest J.L. & Kamm R.D. 2011. Interstitial flow influences direction of tumor cell migration through competing mechanisms. Proc. Natl. Acad. Sci. U. S. A. **108**: 11115–11120.

Pouthas F., Girard P., Lecaudey V., Ly T.B.N., Gilmour D., Boulin C., Pepperkok R. & Reynaud E.G. 2008. In migrating cells, the Golgi complex and the position of the centrosome depend on geometrical constraints of the substratum. J. Cell Sci. **121**: 2406–2414.

Prentice-Mott H.V., Chang C.-H., Mahadevan L., Mitchison T.J., Irimia D. & Shah J.V. 2013. Biased migration of confined neutrophil-like cells in asymmetric hydraulic environments. Proc. Natl. Acad. Sci. U. S. A. **110**: 21006–21011.

Provenzano P.P., Eliceiri K.W., Campbell J.M., Inman D.R., White J.G. & Keely P.J. 2006. Collagen reorganization at the tumor-stromal interface facilitates local invasion. BMC Med. **4**: 38.

Provenzano P.P., Inman D.R., Eliceiri K.W., Knittel J.G., Yan L., Rueden C.T., White J.G. & Keely P.J. 2008. Collagen density promotes mammary tumor initiation and progression. BMC Med. **6**: 11.

Puklin-Faucher E. & Vogel V. 2009. Integrin activation dynamics between the RGD-binding site and the headpiece hinge. J. Biol. Chem. **284**: 36557–36568.

Puleo J.I., Parker S.S., Roman M.R., Watson A.W., Eliato K.R., Peng L., Saboda K., Roe D.J., Ros R., Gertler F.B. & Mouneimne G. 2019. Mechanosensing during directed cell migration requires dynamic actin polymerization at focal adhesions. J. Cell Biol. **218**: 4215–4235.

Qazi H., Palomino R., Shi Z.-D., Munn L.L. & Tarbell J.M. 2013. Cancer cell glycocalyx mediates mechanotransduction and flow-regulated invasion. Integr. Biol. **5**: 1334–1343.

Qazi H., Shi Z.-D. & Tarbell J.M. 2011. Fluid Shear Stress Regulates the Invasive Potential of Glioma Cells via Modulation of Migratory Activity and Matrix Metalloproteinase Expression. PLOS ONE. **6**: e20348.

Raab M. & Discher D.E. 2017. Matrix rigidity regulates the microtubule network polarization in migration. Cytoskelet. Hoboken. **74**: 114–124.

Raab M., Swift J., Dingal P.C.D.P., Shah P., Shin J.-W. & Discher D.E. 2012. Crawling from soft to stiff matrix polarizes the cytoskeleton and phosphoregulates myosin-II heavy chain. J. Cell Biol. **199**: 669–683.

Rafiq N.B.M., Nishimura Y., Plotnikov S.V., Thiagarajan V., Zhang Z., Shi S., Natarajan M., Viasnoff V., Kanchanawong P., Jones G.E. & Bershadsky A.D. 2019. A mechano-signalling network linking microtubules, myosin IIA filaments and integrin-based adhesions. Nat. Mater. **18**: 638–649.

Raghavan S., Desai R.A., Kwon Y., Mrksich M. & Chen C.S. 2010. Micropatterned Dynamically Adhesive Substrates for Cell Migration. Langmuir. **26**: 17733–17738.

Rahikainen R., von Essen M., Schaefer M., Qi L., Azizi L., Kelly C., Ihalainen T.O., Wehrle-Haller B., Bastmeyer M., Huang C. & Hytönen V.P. 2017. Mechanical stability of talin rod controls cell migration and substrate sensing. Sci. Rep. **7**: 3571.

Rainero E., Howe J.D., Caswell P.T., Jamieson N.B., Anderson K., Critchley D.R., Machesky L. & Norman J.C. 2015. Ligand-Occupied Integrin Internalization Links Nutrient Signaling to Invasive Migration. Cell Rep. **10**: 398–413.

Rakshit S. & Sivasankar S. 2014. Biomechanics of cell adhesion: how force regulates the lifetime of adhesive bonds at the single molecule level. Phys. Chem. Chem. Phys. **16**: 2211–2223.

Raudenská M., Petrláková K., Juriňáková T., Leischner Fialová J., Fojtů M., Jakubek M., Rösel D., Brábek J. & Masařík M. 2023. Engine shutdown: migrastatic strategies and prevention of metastases. Trends Cancer. **9**: 293–308.

Renkawitz J., Kopf A., Stopp J., de Vries I., Driscoll M.K., Merrin J., Hauschild R., Welf E.S., Danuser G., Fiolka R. & Sixt M. 2019. Nuclear positioning facilitates amoeboid migration along the path of least resistance. Nature. **568**: 546–550.

Rens E.G. & Merks R.M.H. 2020. Cell Shape and Durotaxis Explained from Cell-Extracellular Matrix Forces and Focal Adhesion Dynamics. iScience. **23**: 101488.

Reuten R., Zendehroud S., Nicolau M., Fleischhauer L., Laitala A., Kiderlen S., Nikodemus D., Wullkopf L., Nielsen S.R., McNeilly S., Prein C., Rafaeva M., Schoof E.M., Furtwängler B., Porse B.T., Kim H., Won K.J., Sudhop S., Zornhagen K.W., Suhr F., Maniati E., Pearce O.M.T., Koch M., Oddershede L.B., Van Agtmael T., Madsen C.D., Mayorca-Guiliani A.E., Bloch W., Netz R.R., Clausen-Schaumann H. & Erler J.T. 2021. Basement membrane stiffness determines metastases formation. Nat. Mater. **20**: 892–903.

Reversat A., Gaertner F., Merrin J., Stopp J., Tasciyan S., Aguilera J., de Vries I., Hauschild R., Hons M., Piel M., Callan-Jones A., Voituriez R. & Sixt M. 2020. Cellular locomotion using environmental topography. Nature. **582**: 582–585.

Rhim A.D., Mirek E.T., Aiello N.M., Maitra A., Bailey J.M., McCallister F., Reichert M., Beatty G.L., Rustgi A.K., Vonderheide Robert.H., Leach S.D. & Stanger B.Z. 2012. EMT and dissemination precede pancreatic tumor formation. Cell. **148**: 349–361.

Rice A.J., Cortes E., Lachowski D., Cheung B.C.H., Karim S.A., Morton J.P. & del Río Hernández A. 2017. Matrix stiffness induces epithelial–mesenchymal transition and promotes chemoresistance in pancreatic cancer cells. Oncogenesis. **6**: e352–e352.

del Rio A., Perez-Jimenez R., Liu R., Roca-Cusachs P., Fernandez J.M. & Sheetz M.P. 2009. Stretching Single Talin Rod Molecules Activates Vinculin Binding. Science. **323**: 638–641.

Robitaille M.C., Kim C., Christodoulides J.A., Calhoun P.J., Kang W., Liu J., Byers J.M. & Raphael M.P. 2024. Topographical depth reveals contact guidance mechanism distinct from focal adhesion confinement. Cytoskelet. Hoboken. .

Roca-Cusachs P., Conte V. & Trepat X. 2017. Quantifying forces in cell biology. Nat. Cell Biol. **19**: 742–751.

Roca-Cusachs P., Gauthier N.C., del Rio A. & Sheetz M.P. 2009. Clustering of α5β1 integrins determines adhesion strength whereas αvβ3 and talin enable mechanotransduction. Proc. Natl. Acad. Sci. U. S. A. **106**: 16245–16250.

Rodriguez N.M., Desai R.A., Trappmann B., Baker B.M. & Chen C.S. 2014. Micropatterned Multicolor Dynamically Adhesive Substrates to Control Cell Adhesion and Multicellular Organization. Langmuir. **30**: 1327–1335.

Rolli C.G., Nakayama H., Yamaguchi K., Spatz J.P., Kemkemer R. & Nakanishi J. 2012. Switchable adhesive substrates: Revealing geometry dependence in collective cell behavior. Biomaterials. **33**: 2409–2418.

Rong Y., Yang W., Hao H., Wang W., Lin S., Shi P., Huang Y., Li B., Sun Y., Liu Z. & Wu C. 2021. The Golgi microtubules regulate single cell durotaxis. EMBO Rep. **22**: e51094.

Rossier O., Octeau V., Sibarita J.-B., Leduc C., Tessier B., Nair D., Gatterdam V., Destaing O., Albigès-Rizo C., Tampé R., Cognet L., Choquet D., Lounis B. & Giannone G. 2012. Integrins β1 and β3 exhibit distinct dynamic nanoscale organizations inside focal adhesions. Nat. Cell Biol. **14**: 1057–1067.

Roussos E.T., Condeelis J.S. & Patsialou A. 2011. Chemotaxis in cancer. Nat. Rev. Cancer. **11**: 573–587.

Sabatier L., Chen D., Fagotto-Kaufmann C., Hubmacher D., McKee M.D., Annis D.S., Mosher D.F. & Reinhardt D.P. 2009. Fibrillin Assembly Requires Fibronectin. Mol. Biol. Cell. **20**: 846–858.

Sáez P. & Venturini C. 2023. Positive, negative and controlled durotaxis. Soft Matter. **19**: 2993–3001.

Sahai E. & Marshall C.J. 2003. Differing modes of tumour cell invasion have distinct requirements for Rho/ROCK signalling and extracellular proteolysis. Nat. Cell Biol. **5**: 711–719.

Saito K., Mori M., Kambara N. & Ohta Y. 2021. FilGAP, a GAP protein for Rac, regulates front-rear polarity and tumor cell migration through the ECM. FASEB J. Off. Publ. Fed. Am. Soc. Exp. Biol. **35**: e21508.

Salierno M.J., García A.J. & del Campo A. 2013. Photo-Activatable Surfaces for Cell Migration Assays. Adv. Funct. Mater. **23**: 5974–5980.

Sarkar A., LeVine D.N., Kuzmina N., Zhao Y. & Wang X. 2020. Cell Migration Driven by Self-Generated Integrin Ligand Gradient on Ligand-Labile Surfaces. Curr. Biol. CB. **30**: 4022-4032.e5.

Saunders J.T. & Schwarzbauer J.E. 2019. Fibronectin matrix as a scaffold for procollagen proteinase binding and collagen processing. Mol. Biol. Cell. **30**: 2218–2226.

Sawada Y., Tamada M., Dubin-Thaler B.J., Cherniavskaya O., Sakai R., Tanaka S. & Sheetz M.P. 2006. Force Sensing by Mechanical Extension of the Src Family Kinase Substrate p130Cas. Cell. **127**: 1015–1026.

Schiller H.B., Hermann M.-R., Polleux J., Vignaud T., Zanivan S., Friedel C.C., Sun Z., Raducanu A., Gottschalk K.-E., Théry M., Mann M. & Fässler R. 2013. β1- and αv-class integrins cooperate to regulate myosin II during rigidity sensing of fibronectin-based microenvironments. Nat. Cell Biol. **15**: 625–636.

Schindelin J., Arganda-Carreras I., Frise E., Kaynig V., Longair M., Pietzsch T., Preibisch S., Rueden C., Saalfeld S., Schmid B., Tinevez J.-Y., White D.J., Hartenstein V., Eliceiri K., Tomancak P. & Cardona A. 2012. Fiji: an open-source platform for biological-image analysis. Nat. Methods. **9**: 676–682.

Schmitt M.S., Colen J., Sala S., Devany J., Seetharaman S., Caillier A., Gardel M.L., Oakes P.W. & Vitelli V. 2024. Machine learning interpretable models of cell mechanics from protein images. Cell. **187**: 481-494.e24.

Schoenherr C., Frame M.C. & Byron A. 2018. Trafficking of Adhesion and Growth Factor Receptors and Their Effector Kinases. Annu. Rev. Cell Dev. Biol. **34**: 29–58.

Schumacher S., Dedden D., Nunez R.V., Matoba K., Takagi J., Biertümpfel C. & Mizuno N. 2021. Structural insights into integrin α5β1 opening by fibronectin ligand. Sci. Adv. **7**: eabe9716.

Scott A.K., Casas E., Schneider S.E., Swearingen A.R., Van Den Elzen C.L., Seelbinder B., Barthold J.E., Kugel J.F., Stern J.L., Foster K.J., Emery N.C., Brumbaugh J. & Neu C.P. 2023. Mechanical memory stored through epigenetic remodeling reduces cell therapeutic potential. Biophys. J. **122**: 1428–1444.

Seddiki R., Narayana G.H.N.S., Strale P.-O., Balcioglu H.E., Peyret G., Yao M., Le A.P., Teck Lim C., Yan J., Ladoux B. & Mège R.M. 2018. Force-dependent binding of vinculin to α-catenin regulates cell–cell contact stability and collective cell behavior. Mol. Biol. Cell. **29**: 380–388.

Seetharaman S. & Etienne-Manneville S. 2018. Integrin diversity brings specificity in mechanotransduction. Biol. Cell. **110**: 49–64.

Seetharaman S. & Etienne-Manneville S. 2020. Cytoskeletal Crosstalk in Cell Migration. Trends Cell Biol. **30**: 720–735.

Seetharaman S., Vianay B., Roca V., Farrugia A.J., De Pascalis C., Boëda B., Dingli F., Loew D., Vassilopoulos S., Bershadsky A., Théry M. & Etienne-Manneville S. 2022. Microtubules tune mechanosensitive cell responses. Nat. Mater. **21**: 366–377.

Seker-Polat F., Pinarbasi Degirmenci N., Solaroglu I. & Bagci-Onder T. 2022. Tumor Cell Infiltration into the Brain in Glioblastoma: From Mechanisms to Clinical Perspectives. Cancers. **14**: 443.

SenGupta S., Parent C.A. & Bear J.E. 2021. The principles of directed cell migration. Nat. Rev. Mol. Cell Biol. **22**: 529–547.

Shatkin G., Yeoman B., Birmingham K., Katira P. & Engler A.J. 2020. Computational models of migration modes improve our understanding of metastasis. APL Bioeng. **4**: 041505.

Shellard A. & Mayor R. 2021a. Durotaxis: The Hard Path from In Vitro to In Vivo. Dev. Cell. **56**: 227–239.

Shellard A. & Mayor R. 2021b. Collective durotaxis along a self-generated stiffness gradient in vivo. Nature. **600**: 690–694.

Shirke P.U., Goswami H., Kumar V., Shah D., Beri S., Das S., Bellare J., Mayor S., Venkatesh K.V., Seth J.R. & Majumder A. 2021. "Viscotaxis"- directed migration of mesenchymal stem cells in response to loss modulus gradient. Acta Biomater. **135**: 356–367.

Short S.M., Boyer J.L. & Juliano R.L. 2000. Integrins Regulate the Linkage between Upstream and Downstream Events in G Protein-coupled Receptor Signaling to Mitogen-activated Protein Kinase *. J. Biol. Chem. **275**: 12970–12977.

Shu W. & Kaplan C.N. 2023. A multiscale whole-cell theory for mechanosensitive migration on viscoelastic substrates. Biophys. J. **122**: 114–129.

Singh P., Carraher C. & Schwarzbauer J.E. 2010. Assembly of Fibronectin Extracellular Matrix. Annu. Rev. Cell Dev. Biol. **26**: 397–419.

Singh S.P., Schwartz M.P., Lee J.Y., Fairbanks B.D. & Anseth K.S. 2014. A peptide functionalized poly(ethylene glycol) (PEG) hydrogel for investigating the influence of biochemical and biophysical matrix properties on tumor cell migration. Biomater. Sci. **2**: 1024–1034.

Smith M.L., Gourdon D., Little W.C., Kubow K.E., Eguiluz R.A., Luna-Morris S. & Vogel V. 2007. Force-Induced Unfolding of Fibronectin in the Extracellular Matrix of Living Cells. PLOS Biol. **5**: e268.

Solomon J., Raškova M., Rösel D., Brábek J. & Gil-Henn H. 2021. Are We Ready for Migrastatics?. Cells. **10**: 1845.

Song J.W. & Munn L.L. 2011. Fluid forces control endothelial sprouting. Proc. Natl. Acad. Sci. U. S. A. **108**: 15342–15347.

Sorrentino S., Conesa J.J., Cuervo A., Melero R., Martins B., Fernandez-Gimenez E., de Isidro-Gomez F.P., de la Morena J., Studt J.-D., Sorzano C.O.S., Eibauer M., Carazo J.M. & Medalia O. 2021. Structural analysis of receptors and actin polarity in platelet protrusions. Proc. Natl. Acad. Sci. U. S. A. **118**: e2105004118.

Spiess M., Hernandez-Varas P., Oddone A., Olofsson H., Blom H., Waithe D., Lock J.G., Lakadamyali M. & Strömblad S. 2018. Active and inactive β1 integrins segregate into distinct nanoclusters in focal adhesions. J. Cell Biol. **217**: 1929–1940.

Spooner B.S., Yamada K.M. & Wessells N.K. 1971. MICROFILAMENTS AND CELL LOCOMOTION. J. Cell Biol. **49**: 595–613.

Srinivasan S., Wang F., Glavas S., Ott A., Hofmann F., Aktories K., Kalman D. & Bourne H.R. 2003. Rac and Cdc42 play distinct roles in regulating PI(3,4,5)P3 and polarity during neutrophil chemotaxis. J. Cell Biol. **160**: 375–385.

Stehbens S.J., Paszek M., Pemble H., Ettinger A., Gierke S. & Wittmann T. 2014. CLASPs link focal-adhesion-associated microtubule capture to localized exocytosis and adhesion site turnover. Nat. Cell Biol. **16**: 558–570.

Stehn J.R., Haass N.K., Bonello T., Desouza M., Kottyan G., Treutlein H., Zeng J., Nascimento P.R.B.B., Sequeira V.B., Butler T.L., Allanson M., Fath T., Hill T.A., McCluskey A., Schevzov G., Palmer S.J., Hardeman E.C., Winlaw D., Reeve V.E., Dixon I., Weninger W., Cripe T.P. & Gunning P.W. 2013. A Novel Class of Anticancer Compounds Targets the Actin Cytoskeleton in Tumor Cells. Cancer Res. **73**: 5169–5182.

Strale P.-O., Azioune A., Bugnicourt G., Lecomte Y., Chahid M. & Studer V. 2016. Multiprotein Printing by Light-Induced Molecular Adsorption. Adv. Mater. **28**: 2024–2029.

Ström P., Nordström T., Delahunt B., Samaratunga H., Grönberg H., Egevad L. & Eklund M. 2020. Prognostic value of perineural invasion in prostate needle biopsies: a population-based study of patients treated by radical prostatectomy. J. Clin. Pathol. **73**: 630–635.

Stubb A., Guzmán C., Närvä E., Aaron J., Chew T.-L., Saari M., Miihkinen M., Jacquemet G. & Ivaska J. 2019. Superresolution architecture of cornerstone focal adhesions in human pluripotent stem cells. Nat. Commun. **10**: 4756.

Stupp R., Hegi M.E., Gorlia T., Erridge S.C., Perry J., Hong Y.-K., Aldape K.D., Lhermitte B., Pietsch T., Grujicic D., Steinbach J.P., Wick W., Tarnawski R., Nam D.-H., Hau P., Weyerbrock A., Taphoorn M.J.B., Shen C.-C., Rao N., Thurzo L., Herrlinger U., Gupta T., Kortmann R.-D., Adamska K., McBain C., Brandes A.A., Tonn J.C., Schnell O., Wiegel T., Kim C.-Y., Nabors L.B., Reardon D.A., van den Bent M.J., Hicking C., Markivskyy A., Picard M. & Weller M. 2014. Cilengitide combined with standard treatment for patients with newly diagnosed glioblastoma with methylated MGMT promoter (CENTRIC EORTC 26071-22072 study): a multicentre, randomised, open-label, phase 3 trial. Lancet Oncol. **15**: 1100–1108.

Stutchbury B., Atherton P., Tsang R., Wang D.-Y. & Ballestrem C. 2017. Distinct focal adhesion protein modules control different aspects of mechanotransduction. J. Cell Sci. **130**: 1612–1624.

Su Y., Xia W., Li J., Walz T., Humphries M.J., Vestweber D., Cabañas C., Lu C. & Springer T.A. 2016. Relating conformation to function in integrin α5β1. Proc. Natl. Acad. Sci. U. S. A. **113**: E3872–E3881.

Sugimura K., Lenne P.-F. & Graner F. 2016. Measuring forces and stresses in situ in living tissues. Development. **143**: 186–196.

Sulzmaier F.J., Jean C. & Schlaepfer D.D. 2014. FAK in cancer: mechanistic findings and clinical applications. Nat. Rev. Cancer. **14**: 598–610.

Sun Z., Guo S.S. & Fässler R. 2016. Integrin-mediated mechanotransduction. J. Cell Biol. **215**: 445–456.

Sundararaman A., Fukushima Y., Norman J.C., Uemura A. & Mellor H. 2020. RhoJ Regulates α5β1 Integrin Trafficking to Control Fibronectin Remodeling during Angiogenesis. Curr. Biol. **30**: 2146-2155.e5.

Sunyer R., Conte V., Escribano J., Elosegui-Artola A., Labernadie A., Valon L., Navajas D., Garcia-Aznar J.M., Munoz J.J., Roca-Cusachs P. & Trepat X. 2016. Collective cell durotaxis emerges from long-range intercellular force transmission. Science. **353**: 1157–1161.

Swartz M.A. & Lund A.W. 2012. Lymphatic and interstitial flow in the tumour microenvironment: linking mechanobiology with immunity. Nat. Rev. Cancer. **12**: 210–219.

Tabdanov E.D., Puram V., Zhovmer A. & Provenzano P.P. 2018. Microtubule-Actomyosin Mechanical Cooperation during Contact Guidance Sensing. Cell Rep. **25**: 328-338.e5.

Tabdanov E.D., Rodríguez-Merced N.J., Cartagena-Rivera A.X., Puram V.V., Callaway M.K., Ensminger E.A., Pomeroy E.J., Yamamoto K., Lahr W.S., Webber B.R., Moriarity B.S., Zhovmer A.S. & Provenzano P.P. 2021. Engineering T cells to enhance 3D migration through structurally and mechanically complex tumor microenvironments. Nat. Commun. **12**: 2815.

Takagi J., Petre B.M., Walz T. & Springer T.A. 2002. Global Conformational Rearrangements in Integrin Extracellular Domains in Outside-In and Inside-Out Signaling. Cell. **110**: 599–611.

Tang M., Liu Q., Yang X., Chen L., Yu J., Qi X. & Wang Y. 2019. Perineural invasion as a prognostic risk factor in patients with early cervical cancer. Oncol. Lett. **17**: 1101–1107.

Tao A., LaCroix A.S., Shoyer T.C., Venkatraman V., Xu K.L., Feiger B. & Hoffman B.D. 2023. Identifying constitutive and context-specific molecular-tension-sensitive protein recruitment within focal adhesions. Dev. Cell. **58**: 522-534.e7.

Taubenberger A.V., Bray L.J., Haller B., Shaposhnykov A., Binner M., Freudenberg U., Guck J. & Werner C. 2016. 3D extracellular matrix interactions modulate tumour cell growth, invasion and angiogenesis in engineered tumour microenvironments. Acta Biomater. **36**: 73–85.

Theodosiou M., Widmaier M., Böttcher R.T., Rognoni E., Veelders M., Bharadwaj M., Lambacher A., Austen K., Müller D.J., Zent R. & Fässler R. 2016. Kindlin-2 cooperates with talin to activate integrins and induces cell spreading by directly binding paxillin. eLife. **5**: e10130.

Théry M. 2010. Micropatterning as a tool to decipher cell morphogenesis and functions. J. Cell Sci. **123**: 4201–4213.

Théry M., Racine V., Piel M., Pépin A., Dimitrov A., Chen Y., Sibarita J.-B. & Bornens M. 2006. Anisotropy of cell adhesive microenvironment governs cell internal organization and orientation of polarity. Proc. Natl. Acad. Sci. **103**: 19771–19776.

Thomas L.A. & Yamada K.M. 1992. Contact stimulation of cell migration. J. Cell Sci. **103**: 1211–1214.

Thompson A.J., Pillai E.K., Dimov I.B., Foster S.K., Holt C.E. & Franze K. 2019. Rapid changes in tissue mechanics regulate cell behaviour in the developing embryonic brain. eLife. **8**: e39356.

Tiwari S., Askari J.A., Humphries M.J. & Bulleid N.J. 2011. Divalent cations regulate the folding and activation status of integrins during their intracellular trafficking. J. Cell Sci. **124**: 1672–1680.

Tozluoğlu M., Tournier A.L., Jenkins R.P., Hooper S., Bates P.A. & Sahai E. 2013. Matrix geometry determines optimal cancer cell migration strategy and modulates response to interventions. Nat. Cell Biol. **15**: 751–762.

Trappmann B., Baker B.M., Polacheck W.J., Choi C.K., Burdick J.A. & Chen C.S. 2017. Matrix degradability controls multicellularity of 3D cell migration. Nat. Commun. **8**: 371.

Trappmann B., Gautrot J.E., Connelly J.T., Strange D.G.T., Li Y., Oyen M.L., Cohen Stuart M.A., Boehm H., Li B., Vogel V., Spatz J.P., Watt F.M. & Huck W.T.S. 2012. Extracellular-matrix tethering regulates stem-cell fate. Nat. Mater. **11**: 642–649.

Trichet L., Le Digabel J., Hawkins R.J., Vedula S.R.K., Gupta M., Ribrault C., Hersen P., Voituriez R. & Ladoux B. 2012. Evidence of a large-scale mechanosensing mechanism for cellular adaptation to substrate stiffness. Proc. Natl. Acad. Sci. U. S. A. **109**: 6933–6938.

Tse J.M., Cheng G., Tyrrell J.A., Wilcox-Adelman S.A., Boucher Y., Jain R.K. & Munn L.L. 2012. Mechanical compression drives cancer cells toward invasive phenotype. Proc. Natl. Acad. Sci. U. S. A. **109**: 911–916.

Tse J.R. & Engler A.J. 2010. Preparation of Hydrogel Substrates with Tunable Mechanical Properties. Curr. Protoc. Cell Biol. **47**: 10.16.1-10.16.16.

Tse J.R. & Engler A.J. 2011. Stiffness Gradients Mimicking In Vivo Tissue Variation Regulate Mesenchymal Stem Cell Fate. PLOS ONE. **6**: e15978.

Tsuda Y., Kikuchi A., Yamato M., Nakao A., Sakurai Y., Umezu M. & Okano T. 2005. The use of patterned dual thermoresponsive surfaces for the collective recovery as co-cultured cell sheets. Biomaterials. **26**: 1885–1893.

Ueda M., Gräf R., MacWilliams H.K., Schliwa M. & Euteneuer U. 1997. Centrosome positioning and directionality of cell movements. Proc. Natl. Acad. Sci. U. S. A. **94**: 9674–9678.

Uetrecht A.C. & Bear J.E. 2009. Golgi polarity does not correlate with speed or persistence of freely migrating fibroblasts. Eur. J. Cell Biol. **88**: 711–717.

Vaidžiulytė K., Macé A.-S., Battistella A., Beng W., Schauer K. & Coppey M. 2022. Persistent cell migration emerges from a coupling between protrusion dynamics and polarized trafficking. eLife. **11**: e69229.

Vartiainen M.K., Guettler S., Larijani B. & Treisman R. 2007. Nuclear Actin Regulates Dynamic Subcellular Localization and Activity of the SRF Cofactor MAL. Science. **316**: 1749–1752.

Velling T., Risteli J., Wennerberg K., Mosher D.F. & Johansson S. 2002. Polymerization of Type I and III Collagens Is Dependent On Fibronectin and Enhanced By Integrins α11β1and α2β1. J. Biol. Chem. **277**: 37377–37381.

Vicente-Manzanares M., Koach M.A., Whitmore L., Lamers M.L. & Horwitz A.F. 2008. Segregation and activation of myosin IIB creates a rear in migrating cells. J. Cell Biol. **183**: 543–554.

Vicente-Manzanares M., Zareno J., Whitmore L., Choi C.K. & Horwitz A.F. 2007. Regulation of protrusion, adhesion dynamics, and polarity by myosins IIA and IIB in migrating cells. J. Cell Biol. **176**: 573–580.

Vignaud T., Galland R., Tseng Q., Blanchoin L., Colombelli J. & Théry M. 2012. Reprogramming cell shape with laser nano-patterning. J. Cell Sci. **125**: 2134–2140.

Vincent L.G., Choi Y.S., Alonso-Latorre B., Álamo J.C. del & Engler A.J. 2013. Mesenchymal stem cell durotaxis depends on substrate stiffness gradient strength. Biotechnol. J. **8**: 472–484.

Vishwakarma M., Di Russo J., Probst D., Schwarz U.S., Das T. & Spatz J.P. 2018. Mechanical interactions among followers determine the emergence of leaders in migrating epithelial cell collectives. Nat. Commun. **9**: 3469.

Voorneveld P.W., Kodach L.L., Jacobs R.J., Liv N., Zonnevylle A.C., Hoogenboom J.P., Biemond I., Verspaget H.W., Hommes D.W., de Rooij K., van Noesel C.J.M., Morreau H., van Wezel T., Offerhaus G.J.A., van den Brink G.R., Peppelenbosch M.P., ten Dijke P. & Hardwick J.C.H. 2014. Loss of SMAD4 Alters BMP Signaling to Promote Colorectal Cancer Cell Metastasis via Activation of Rho and ROCK. Gastroenterology. **147**: 196-208.e13.

Waclaw B., Bozic I., Pittman M.E., Hruban R.H., Vogelstein B. & Nowak M.A. 2015. A spatial model predicts that dispersal and cell turnover limit intratumour heterogeneity. Nature. **525**: 261–264.

Wang H.B., Dembo M., Hanks S.K. & Wang Y. 2001. Focal adhesion kinase is involved in mechanosensing during fibroblast migration. Proc. Natl. Acad. Sci. U. S. A. **98**: 11295–11300.

Wang W.Y., Davidson C.D., Lin D. & Baker B.M. 2019. Actomyosin contractility-dependent matrix stretch and recoil induces rapid cell migration. Nat. Commun. **10**: 1186.

Wang Y., Stear J.H., Swain A., Xu X., Bryce N.S., Carnell M., Alieva I.B., Dugina V.B., Cripe T.P., Stehn J., Hardeman E.C. & Gunning P.W. 2020. Drug Targeting the Actin Cytoskeleton Potentiates the Cytotoxicity of Low Dose Vincristine by Abrogating Actin-Mediated Repair of Spindle Defects. Mol. Cancer Res. **18**: 1074–1087.

Wang Y., Zhang C., Yang W., Shao S., Xu X., Sun Y., Li P., Liang L. & Wu C. 2021. LIMD1 phase separation contributes to cellular mechanics and durotaxis by regulating focal adhesion dynamics in response to force. Dev. Cell. **56**: 1313-1325.e7.

Wang Y.L. 1985. Exchange of actin subunits at the leading edge of living fibroblasts: possible role of treadmilling. J. Cell Biol. **101**: 597–602.

Wedlich-Soldner R., Altschuler S., Wu L. & Li R. 2003. Spontaneous Cell Polarization Through Actomyosin-Based Delivery of the Cdc42 GTPase. Science. **299**: 1231–1235.

Weigert M., Schmidt U., Boothe T., Müller A., Dibrov A., Jain A., Wilhelm B., Schmidt D., Broaddus C., Culley S., Rocha-Martins M., Segovia-Miranda F., Norden C., Henriques R., Zerial M., Solimena M., Rink J., Tomancak P., Royer L., Jug F. & Myers E.W. 2018. Content-aware image restoration: pushing the limits of fluorescence microscopy. Nat. Methods. **15**: 1090–1097.

Whitlock B.B., Gardai S., Fadok V., Bratton D. & Henson P.M. 2000. Differential Roles for αMβ2 Integrin Clustering or Activation in the Control of Apoptosis via Regulation of Akt and ERK Survival Mechanisms. J. Cell Biol. **151**: 1305–1320.

Wisdom K.M., Adebowale K., Chang J., Lee J.Y., Nam S., Desai R., Rossen N.S., Rafat M., West R.B., Hodgson L. & Chaudhuri O. 2018. Matrix mechanical plasticity regulates cancer cell migration through confining microenvironments. Nat. Commun. **9**: 4144.

Wolf K., Mazo I., Leung H., Engelke K., von Andrian U.H., Deryugina E.I., Strongin A.Y., Bröcker E.-B. & Friedl P. 2003. Compensation mechanism in tumor cell migration: mesenchymal-amoeboid transition after blocking of pericellular proteolysis. J. Cell Biol. **160**: 267–277.

Wolf K.J., Shukla P., Springer K., Lee S., Coombes J.D., Choy C.J., Kenny S.J., Xu K. & Kumar S. 2020. A mode of cell adhesion and migration facilitated by CD44-dependent microtentacles. Proc. Natl. Acad. Sci. U. S. A. **117**: 11432–11443.

Wolfenson H., Bershadsky A., Henis Y.I. & Geiger B. 2011. Actomyosin-generated tension controls the molecular kinetics of focal adhesions. J. Cell Sci. **124**: 1425–1432.

Wolfenson H., Meacci G., Liu S., Stachowiak M.R., Iskratsch T., Ghassemi S., Roca-Cusachs P., O'Shaughnessy B., Hone J. & Sheetz M.P. 2016. Tropomyosin controls sarcomere-like contractions for rigidity sensing and suppressing growth on soft matrices. Nat. Cell Biol. **18**: 33–42.

Wong V.K., Ganeshan D., Jensen C.T. & Devine C.E. 2021. Imaging and Management of Bladder Cancer. Cancers. **13**: 1396.

Wormer D.B., Davis K.A., Henderson J.H. & Turner C.E. 2014. The focal adhesion-localized CdGAP regulates matrix rigidity sensing and durotaxis. PloS One. **9**: e91815.

Wu C., Asokan S.B., Berginski M.E., Haynes E.M., Sharpless N.E., Griffith J.D., Gomez S.M. & Bear J.E. 2012. Arp2/3 Is Critical for Lamellipodia and Response to Extracellular Matrix Cues but Is Dispensable for Chemotaxis. Cell. **148**: 973–987.

Wu C., Hughes P.E., Ginsberg M.H. & McDonald J.A. 1996. Identification of a new biological function for the integrin alpha v beta 3: initiation of fibronectin matrix assembly. Cell Adhes. Commun. **4**: 149–158.

Wu J., de Heus C., Liu Q., Bouchet B.P., Noordstra I., Jiang K., Hua S., Martin M., Yang C., Grigoriev I., Katrukha E.A., Altelaar A.F.M., Hoogenraad C.C., Qi R.Z., Klumperman J. & Akhmanova A. 2016. Molecular Pathway of Microtubule Organization at the Golgi Apparatus. Dev. Cell. **39**: 44–60.

Xiao Z., Todd L., Huang L., Noguera-Ortega E., Lu Z., Huang L., Kopp M., Li Y., Pattada N., Zhong W., Guo W., Scholler J., Liousia M., Assenmacher C.-A., June C.H., Albelda S.M. & Puré E. 2023. Desmoplastic stroma restricts T cell extravasation and mediates immune exclusion and immunosuppression in solid tumors. Nat. Commun. **14**: 5110.

Xing M., Peterman M.C., Davis R.L., Oegema K., Shiau A.K. & Field S.J. 2016. GOLPH3 drives cell migration by promoting Golgi reorientation and directional trafficking to the leading edge. Mol. Biol. Cell. **27**: 3828–3840.

Xiong J.-P., Stehle T., Diefenbach B., Zhang R., Dunker R., Scott D.L., Joachimiak A., Goodman S.L. & Arnaout M.A. 2001. Crystal Structure of the Extracellular Segment of Integrin αVβ3. Science. **294**: 339–345.

Yamada K.M. & Sixt M. 2019. Mechanisms of 3D cell migration. Nat. Rev. Mol. Cell Biol. **20**: 738–752.

Yamashiro S., Rutkowski D.M., Lynch K.A., Liu Y., Vavylonis D. & Watanabe N. 2023. Force transmission by retrograde actin flow-induced dynamic molecular stretching of Talin. Nat. Commun. **14**: 8468.

Yang B., Wolfenson H., Chung V.Y., Nakazawa N., Liu S., Hu J., Huang R.Y.-J. & Sheetz M.P. 2020a. Stopping transformed cancer cell growth by rigidity sensing. Nat. Mater. **19**: 239–250.

Yang C., Tibbitt M.W., Basta L. & Anseth K.S. 2014. Mechanical memory and dosing influence stem cell fate. Nat. Mater. **13**: 645–652.

Yang S. & Plotnikov S.V. 2021. Mechanosensitive Regulation of Fibrosis. Cells. **10**: 994.

Yang Y., Xie K. & Jiang H. 2020b. Durotaxis Index of 3T3 Fibroblast Cells Scales with Stiff-to-Soft Membrane Tension Polarity. Biophys. J. **119**: 1427–1438.

Yao M., Tijore A., Cheng D., Li J.V., Hariharan A., Martinac B., Tran Van Nhieu G., Cox C.D. & Sheetz M. 2022. Force- and cell state–dependent recruitment of Piezo1 drives focal adhesion dynamics and calcium entry. Sci. Adv. **8**: eabo1461.

Yap L., Tay H.G., Nguyen M.T.X., Tjin M.S. & Tryggvason K. 2019. Laminins in Cellular Differentiation. Trends Cell Biol. **29**: 987–1000.

Ye F., Petrich B.G., Anekal P., Lefort C.T., Kasirer-Friede A., Shattil S.J., Ruppert R., Moser M., Fässler R. & Ginsberg M.H. 2013. The Mechanism of Kindlin-Mediated Activation of Integrin αIIbβ3. Curr. Biol. **23**: 2288–2295.

Yeoman B., Shatkin G., Beri P., Banisadr A., Katira P. & Engler A.J. 2021. Adhesion strength and contractility enable metastatic cells to become adurotactic. Cell Rep. **34**: 108816.

Yip A.K., Zhang S., Chong L.H., Cheruba E., Woon J.Y.X., Chua T.X., Goh C.J.H., Yang H., Tay C.Y., Koh C.-G. & Chiam K.-H. 2021. Zyxin Is Involved in Fibroblast Rigidity Sensing and Durotaxis. Front. Cell Dev. Biol. **9**: 735298.

Yoshioka K., Foletta V., Bernard O. & Itoh K. 2003. A role for LIM kinase in cancer invasion. Proc. Natl. Acad. Sci. U. S. A. **100**: 7247–7252.

Yu C., Rafiq N.B.M., Cao F., Zhou Y., Krishnasamy A., Biswas K.H., Ravasio A., Chen Z., Wang Y.-H., Kawauchi K., Jones G.E. & Sheetz M.P. 2015. Integrin-beta3 clusters recruit clathrin-mediated endocytic machinery in the absence of traction force. Nat. Commun. **6**: 8672.

Yu G., Feng J., Man H. & Levine H. 2017. Phenomenological modeling of durotaxis. Phys. Rev. E. **96**: 010402.

Zaidel-Bar R., Ballestrem C., Kam Z. & Geiger B. 2003. Early molecular events in the assembly of matrix adhesions at the leading edge of migrating cells. J. Cell Sci. **116**: 4605–4613.

Zamir E., Katz B.-Z., Aota S., Yamada K.M., Geiger B. & Kam Z. 1999. Molecular diversity of cell-matrix adhesions. J. Cell Sci. **112**: 1655–1669.

Zamir E., Katz M., Posen Y., Erez N., Yamada K.M., Katz B.-Z., Lin S., Lin D.C., Bershadsky A., Kam Z. & Geiger B. 2000. Dynamics and segregation of cell–matrix adhesions in cultured fibroblasts. Nat. Cell Biol. **2**: 191–196.

Zancla A., Mozetic P., Orsini M., Forte G. & Rainer A. 2022. A primer to traction force microscopy. J. Biol. Chem. **298**: 101867.

Zanotelli M.R., Zhang J. & Reinhart-King C.A. 2021. Mechanoresponsive metabolism in cancer cell migration and metastasis. Cell Metab. **33**: 1307–1321.

Zhang H., Lin F., Huang J. & Xiong C. 2020. Anisotropic stiffness gradient-regulated mechanical guidance drives directional migration of cancer cells. Acta Biomater. **106**: 181–192.

Zhang J., Goliwas K.F., Wang W., Taufalele P.V., Bordeleau F. & Reinhart-King C.A. 2019. Energetic regulation of coordinated leader-follower dynamics during collective invasion of breast cancer cells. Proc. Natl. Acad. Sci. U. S. A. **116**: 7867–7872.

Zhang J. & Wang Y. 2017. Centrosome defines the rear of cells during mesenchymal migration. Mol. Biol. Cell. **28**: 3240–3251.

Zhang K. & Chen J. 2012. The regulation of integrin function by divalent cations. Cell Adhes. Migr. **6**: 20–29.

Zhao Z., Tan S.H., Machiyama H., Kawauchi K., Araki K., Hirata H. & Sawada Y. 2016. Association between tensin 1 and p130Cas at focal adhesions links actin inward flux to cell migration. Biol. Open. **5**: 499–506.

Zhong C., Chrzanowska-Wodnicka M., Brown J., Shaub A., Belkin A.M. & Burridge K. 1998. Rho-mediated Contractility Exposes a Cryptic Site in Fibronectin and Induces Fibronectin Matrix Assembly. J. Cell Biol. **141**: 539–551.

Zhu J., Luo B.-H., Xiao T., Zhang C., Nishida N. & Springer T.A. 2008. Structure of a complete integrin ectodomain in a physiologic resting state and activation and deactivation by applied forces. Mol. Cell. **32**: 849–861.

Zhu M., Tao H., Samani M., Luo M., Wang X., Hopyan S. & Sun Y. 2020. Spatial mapping of tissue properties in vivo reveals a 3D stiffness gradient in the mouse limb bud. Proc. Natl. Acad. Sci. U. S. A. **117**: 4781–4791.

TURUN
YLIOPISTO
UNIVERSITY
OF TURKU

Painosalama, Turku, Finland 2024

ISBN 978-951-29-9672-8 (PRINT)
ISBN 978-951-29-9673-5 (PDF)
ISSN 2736-9390 (Print)
ISSN 2736-9684 (Online)